Fluctuations of a Greenlandic tidewater glacier from the Little Ice Age to present:

Reconstruction and modelling of
Kangiata Nunaata Sermia, SW Greenland

James M. Lea

M.A. (Cantab.), M.Sc. (London)

A thesis presented for the degree of Doctor of Philosophy
at the University of Aberdeen

April, 2014

Author's Declaration

I declare that this thesis has been composed by myself, and has not formed a part of any previous application for a degree. The work herein has been undertaken by myself, with any contributions from others in the form of data, or other significant input, being explicitly stated and acknowledged at the beginning of each chapter. All sources of information used are specifically acknowledged and referenced.

Signed: Date:

James M. Lea

Acknowledgements

Firstly, I would like to thank my principal supervisor, Doug Mair, for his help and guidance in making sure I stayed even roughly on the right track over the last 3 and a bit years. This project was the result of his initial idea, so I am extremely grateful to him for giving me the opportunity to work on one of the more unpronounceable, but also one of the more interesting glaciers in Greenland. In combination with Brice Rea, both have provided me with endless encouragement and constructive criticism that has, to say the least, helped to significantly improve the work presented in this thesis.

Special thanks must also go to Faezeh Nick for perhaps the initially unenviable task of supervising me on the numerical modelling side of things. Given that I started off this Ph.D. having never coded anything in my life, it would be an understatement to say that I am significantly indebted to Faezeh for all the time and help that she has given me with this part of the project. The reassurance and encouragement that she has offered throughout has been a consistent source of motivation.

I would also like to thank Ed Schofield for his supervision and helping to substantially improve my knowledge and appreciation of the Norse archaeology in Greenland, while I am also grateful to Pete Nienow for the useful discussions had at various points over the course of the project.

Considerable thanks are due to Dirk van As for all his help and encouragement, in addition to letting me tag along with him and Faezeh for my first experience of Greenlandic fieldwork in 2011; Cris Simonetti for his willingness to throw himself into the more physically arduous fieldwork in 2013, and helping make the time spent out there enjoyable despite the aches and pains that resulted; Michael Rosing for transporting us out into the field, and introducing me to ptarmigan schnapps; Christian Koch Madsen for helping me track down obscure sources in the Danish National Museum Archives with the benefit of relatively little reference information; Anker Weidick for providing a wealth of source information and the benefit of his considerable experience of Greenlandic glaciology; Kurt Kjær and Niels Korsgaard for generously providing digital elevation model data for the area; and Mathieu Morlighem for agreeing to generate the subglacial topography reconstruction of KNS.

In addition to those mentioned above, this work would not have been possible without the help, generosity and friendship of too many people to mention. However, amongst those in Aberdeen I would particularly like to thank: David Ashmore, Paul Coghill, Jonathan Dick, Véro Forbes, Craig Frew, Ardern Hulme-Beaman, Toby Irving, Mike Kennedy, Paul Ledger, Laura McHardie, Ellen McManus, Dawn Mooney and Richard Morris for always being keen for a procrastinating coffee or a pint at The Machar once the clock struck 5. Their company since I arrived in Aberdeen has not only helped maintain at least a modicum of sanity, but also made my time here thoroughly enjoyable.

Last, but far from least, I would like to thank my mum, dad and sister for supporting me over the past few years through thick and thin. This would not have been possible without them.

Abstract

Fluctuations of a Greenlandic tidewater glacier from the Little Ice Age to present: reconstruction and modelling of Kangiata Nunaata Sermia, SW Greenland.

James M. Lea

Significant uncertainty surrounds the influence of atmospheric and oceanic forcing on the fluctuations of tidewater glacier outlets of the Greenland ice sheet (GrIS), with the majority of studies focussing on dynamics over the last two decades. Although numerical model based projections exist anticipating the future dynamics of major GrIS outlets, these have been made using temporally limited model calibration periods (<5 years) compared to the centennial timescales that they seek to predict over. The ability of these numerical models to simulate the centennial timescale dynamics of GrIS tidewater glaciers has therefore not been explicitly tested.

This thesis seeks to calibrate a well-established one-dimensional tidewater glacier numerical model against post-Little Ice Age maximum (LIAmax) observations of a major tidewater glacier outlet of GrIS. The study site chosen is Kangiata Nunaata Sermia (KNS); the largest tidewater outlet in SW Greenland south of Jakobshavn Isbræ. This glacier is known to have undergone retreat of >20 km since its LIAmax, though the timing of this retreat and response to climate forcing is currently poorly constrained.

Utilising a range of source material, it is demonstrated that KNS is likely to have achieved its LIAmax by 1761, experiencing either one, or two multi-kilometre retreats by 1859, and retreats of a similar scale between 1921-1968, and 1997-2012. Terminus fluctuations of KNS were in phase with climate anomalies, where data were available for comparison (1871-2012). To allow accurate comparison to numerical model output, the accuracy of different methods of quantifying glacier terminus change was also evaluated. Two new methods were devised so observations could be matched with greater accuracy than existing methods allowed. Glacier sensitivity to climate forcing was evaluated using the numerical model. The results demonstrated that multi-annual to decadal behaviour of KNS could be simulated, with atmospheric forcing likely to be the most significant driver of fluctuations.

Contents

List of Figures

List of Tables

Chapter 1

Introduction

This thesis will seek to investigate the controls on the stability of a large tidewater glacier outlet of the Greenland Ice Sheet (GrIS) over centennial timescales. The study is motivated by the uncertainty surrounding the multi-decadal to centennial timescale controls on tidewater glacier behaviour in Greenland, and the potential for future changes in oceanic and/or atmospheric forcing to increase mass loss from GrIS.

1.1 Tidewater glaciers and the importance of Greenland

Tidewater glaciers allow potentially significant volumes of ice to be rapidly lost from ice masses via their termini calving into a fjord/ocean. Although tidewater glaciers can be found in glaciated regions across the globe, the majority are found in Greenland and Antarctica where calving from marine margins accounts for ~50% and 99% of all ice sheet ablation respectively (Van den Broeke et al., 2009). A characteristic of these glaciers is that they often accelerate significantly towards their termini, due to the reduction in basal drag arising from the density contrast between glacier ice and sea water. This also means that their termini often experience significantly greater amounts of longitudinal strain compared to those of land terminating margins. Tidewater glaciers therefore tend to be densely crevassed, which in itself has significant implications for glacier flow, mass loss via calving, and their overall stability (Benn et al., 2007a).

The stability of tidewater glaciers are strongly controlled by changes in fjord topography (Meier and Post, 1987; Warren, 1992; Gudmundsson et al., 2012; Jamieson et al., 2012; Carr et al., 2013a). These topographic controls also mean that once a terminus destabilises, dynamic feedbacks can decouple glacier dynamics from climatic controls, producing a strongly non-linear relationship with climate. Depending on a particular setting, these non-linearities can drive rapid (<<10 year) multi-kilometre terminus retreats. High retreat rates can then be sustained alongside increases in both flow velocity and ice mass loss until a new stable configuration is achieved (e.g. Schoof, 2007; Joughin et al., 2008; Durand et al., 2009; Colgan et al., 2012; Pattyn et al., 2012; Favier et al., 2014). This allows tidewater glaciers to maintain large ice fluxes under stable terminus conditions (up

to several tens of cubic kilometres per year), though periods of unstable terminus retreat can increase this significantly.

Despite their importance to global ice mass balance, the processes that control the dynamics of tidewater glaciers remain poorly understood (in physical, spatial and temporal terms). This shortfall in understanding is especially significant when set against the context of a warming climate, with future change at the polar regions set to be amongst the greatest globally (Stocker et al., 2013). The GrIS currently holds the equivalent of ~7 m of sea level rise (Bamber et al., 2013), making the understanding and prediction of how its tidewater glaciers will respond to future warming crucial to estimating sea level change over the next century (Meier et al., 2007; Straneo et al., 2013). This currently represents a significant uncertainty for those involved in the planning of policies and infrastructure associated with adaptation to, and mitigation of future global sea level change (Church et al., 2013).

The GrIS also occupies a crucial geographic position within the global ocean-atmosphere climate system, situated adjacent to areas of saline North Atlantic dense water (NADW) formation such as the Greenland, Irminger Labrador Seas (Bamber et al., 2012; Weijer et al., 2012; Straneo et al., 2013). Constraining potential changes in freshwater fluxes from GrIS therefore may prove crucial to establishing how/if GrIS tidewater glaciers will impact oceanic and atmospheric heat transport at local and global scales (Bamber et al., 2012; Weijer et al., 2012). Given the importance of NADW formation for global ocean circulation (e.g. Stommel, 1961; Rahmstorf et al., 1995), the volume and timing of GrIS tidewater glacier calving into the North Atlantic could therefore potentially impact global climate.

A freshening of these waters has already been observed (Bamber et al., 2012), with GrIS tidewater glaciers known to have undergone widespread retreat over the last 20 years (e.g. Moon and Jougin, 2008; Bevan et al., 2012). This retreat has occurred alongside a sustained period of both oceanic and atmospheric warming (Holland et al., 2008; Box et al., 2009; Murray et al., 2010; Rignot et al., 2012), though given their synchronicity, attempts to disentangle their relative effects on GrIS tidewater glacier stability have been problematic (Joughin et al., 2012; Straneo et al., 2013).

Researching these problems is also hampered by logistical, practical and data related issues that are commonly associated with working in the polar regions, and on ice sheets. The investigation of tidewater glaciers is often especially difficult due to the frequently hazardous, inaccessible and logistically difficult nature of the environments of interest. Such problems that are often encountered include (but are not limited to), (1) often

Figure 1.1 Deploying a transmitting GPS in a heavily crevassed area of the tidewater glacier Narssap Sermia, SW Greenland. The transmitting GPS allows glacier velocity to be relayed via remote satellite link for areas that are likely to become inaccessible after deployment of the instrument. (Photo: D. van As)

extensive crevassing making access to areas of fast ice flow difficult, if not impossible, even via helicopter, (2) presence of a dense mélange of calved ice and fjord ice making glacier termini inaccessible by boats without an icebreaking capability, (3) the unpredictability and magnitude of calving events precluding direct access to (and often the measurement of) terminal areas, (4) large calving events generating tsunamis, making boat-based/low lying onshore fieldwork hazardous.

A variety of innovative solutions have been developed in an effort to combat these problems (e.g. Figure 1.1), however tidewater glaciers in general remain data poor environments. Despite these difficulties, a substantial volume of research has been undertaken into the dynamics of Greenlandic tidewater glaciers over the last two decades (see Carr et al., 2013b, for a review). Many of the field based glaciological datasets available are often limited to this period, supplemented by the ~25 years of good coverage provided by the satellite record (e.g. Bevan et al., 2012). The majority of records of tidewater glacier change are therefore inherently short compared to multi-decadal changes in modes of climate that are known to naturally affect Greenland, such as the North Atlantic Oscillation (Hanna and Cappelen, 2003; Hanna et al., 2008). The ability to contextualise terminus response to recent warmth against dynamics during previous warm periods is therefore impossible without extending records beyond the satellite era. Compared to the intensive investigation of the satellite record, there has so far been little study of this, with relatively few existing studies utilising historical observations (e.g. Csatho et al., 2008; Bjørk et al., 2012), proxy records (e.g. Andresen et al., 2012; Lloyd et

al., 2011), or a synthesis of qualitative historical sources and direct observations (e.g. Weidick; 1959; Weidick et al., 2012).

The response of Greenlandic glaciers to changes in climate forcing over multi-decadal to centennial timescales is therefore, at present, largely uncharacterised. Similarly, previous studies aimed at modelling the future evolution of major tidewater glaciers and ice sheets have tended to make use of only short transient calibration periods (if used at all), compared to the multi-decadal to centennial timescales that they seek to predict over (e.g. Gladstone et al,. 2012; Nick et al., 2013). The validity of the models over these longer timescales has therefore not been explicitly tested. Evaluating the performance of these models against multi-decadal to centennial records of observations would therefore help to substantially increase confidence in their predictive ability, and also constrain parameter space uncertainty. Using longer model calibration periods should then also allow any shortfalls or limitations in the model (or model input) to be identified with greater ease, and help to highlight scenarios where it is (or is not) suitable to apply the model.

1.2 Research Objectives

The dynamics of GrIS tidewater glaciers can have potentially far reaching impacts on both global sea level and climate. Evaluating their impact requires determining the controls on their dynamics, and whether current numerical models are capable of accurately simulating their response to warming over multi-decadal to centennial timescales. Therefore, the aim of this thesis is to generate a quantified centennial timescale record of change occurring at a major tidewater outlet of the GrIS, and evaluate whether an established tidewater glacier numerical model (Nick et al., 2010; 2013) is capable of capturing observed behaviour.

Reconstruction of glacier dynamics will be achieved through a synthesis of remote sensing and field based geomorphological mapping, analysis of historical texts, maps, photographs, and satellite imagery. This will then be compared against available climate data to investigate the relative importance of atmospheric versus oceanic climate forcing. Results from numerical modelling analyses will be used to determine the ability of the model to replicate observed behaviour over multi-decadal to centennial timescales, and the modelled sensitivity of the glacier to atmospheric and oceanic forcing.

It is hoped that this will help to establish the validity of applying the Nick et al. (2010; 2013) tidewater glacier model in a predictive capacity over multi-decadal to centennial timescales. In doing so, this will determine the ability of the model to generate

reliable estimates of sea level contributions/ice volume fluxes from tidewater glaciers. By undertaking a centennial timescale reconstruction of a Greenlandic tidewater glacier we aim to provide a longer term perspective on the behaviour of a major outlet glacier of the GrIS. This will also seek to demonstrate how qualitative historical data can be usefully applied to gain quantitative estimates of glacier extent where no geomorphological, or visual media data are available.

Evaluation of the different methods used to track tidewater terminus change is also undertaken with the aim of determining which is most accurate across the widest range of scenarios. New methods are developed with the dual purpose of both improving methodological accuracy, and allowing direct comparison of observations with the output of flowline numerical models. The results are also intended to provide a basis for a series of recommendations for others to follow when generating quantitative records of tidewater glacier terminus change.

In summary, this thesis will seek to address uncertainties surrounding tidewater glacier dynamics relating to (1) how changes in atmospheric and oceanic forcing impact calving and terminus stability, (2) the formulation/parameterisation of calving processes and climate forcing for inclusion in numerical models, and (3) the ability of models to replicate observed tidewater glacier behaviour over the multi-decadal to centennial timescales.

1.3 Thesis structure

This thesis contains 7 chapters, each presented so they can be read as individual pieces of work. The reasoning for this is primarily because the majority of the research presented (Chapters 4-6) has either been published in, or submitted to, peer-review journals.

Following this chapter, Chapter 2 is intended to provide a summary of previous research that is relevant to the subsequently presented work, while Chapter 3 will describe the field site and the methods applied as part of the thesis. At the time of writing, Chapters 4 and 5 were both published in 2014 as individual papers in the *Journal of Glaciology*, Volume 60, (220), while Chapter 6 has been submitted to *The Cryosphere Discussions* and is awaiting peer-review. Offprints of the published article versions of Chapters 4 and 5 are included as appendices. Finally, Chapter 7 aims to summarise the main conclusions of the

thesis, and how it has contributed to our understanding of the dynamics of Greenlandic tidewater glaciers over centennial timescales, and how they can be modelled.

Chapter 2

Background

Although tidewater glaciers share many processes with land terminating margins that influence their flow, their marine based termini mean they exhibit significantly different dynamics (Carr et al., 2013b). This chapter aims to provide a summary of the physical controls on the flow of tidewater termini, in addition to previous work on how climate forcing affects their dynamics.

2.1 Physical controls on tidewater glacier flow

The marine termini of tidewater glaciers result in several modifications to the force balance compared to land terminating margins. These significantly affect flow behaviour. As with land terminating glaciers, the driving stress, τ_d, exerted by a tidewater glacier between two points on a longitudinal flow profile can be expressed as

$$\tau_d = \rho_i g H \sin \alpha \tag{2.1}$$

where ρ_i = the density of glacier ice, g = the gravitational acceleration constant, H = ice thickness and α = the ice surface slope. The driving stress is balanced by resistive stresses, including the basal drag, τ_b, lateral drag, τ_w, and longitudinal drag, τ_l, such that

$$\tau_d = \tau_b + \tau_w + \tau_l \tag{2.2}$$

For the overwhelming majority of land terminating glaciers basal drag will provide the majority of resistance to glacier flow, given that gravity acts in the vertical (*zz*) plane, meaning that the pressure exerted by a given ice thickness can be expressed as

$$\sigma_{zz} = \rho_i g H \tag{2.3}$$

where σ_{zz} = the normal stress acting in the vertical plane. Also, the lateral margins of a glacier will often occupy a smaller area than the bed, meaning that the latter can normally

support a greater fraction of the driving stress. However, at a marine terminating margin the base of the glacier will be below sea level, meaning that normal stress will be reduced according to

$$\sigma_{zz} = \rho_i g(H - \frac{\rho_p}{\rho_i} D) \tag{2.4}$$

where ρ_p = density of the proglacial water body (hereafter: fjord water), and D = depth of the fjord at the terminus. Since the density contrast between glacier ice and the fjord water will reduce the pressure the glacier exerts on its bed, this also reduces the basal drag. Therefore if the force balance (Equation 2.2) is to be maintained and the driving stress has a fixed value, the residual driving stress must be taken up by lateral and/or longitudinal drag.

In reality, lateral and longitudinal drag can only partially accommodate the reduction in basal drag that occurs near to the terminus of a tidewater glacier. Instead, the glacier dynamically adjusts to reduce the driving stress. This is achieved through flow acceleration towards the terminus, resulting in high longitudinal strain rates, ice thinning, and a reduction in surface slope (Equation 2.2). As a consequence, as basal drag approaches zero and the terminus gets nearer to floatation, lateral and longitudinal drag will begin to balance a greater proportion of the remaining driving stress.

The importance of basal and lateral drag means that subglacial topography and fjord width exert a significant control on the overall resistance to flow of a tidewater glacier. The longitudinal drag term in the force balance also impacts flow behaviour over length scales of 4-10 times ice thickness (Cuffey and Paterson, 2010), though regions of low basal and lateral drag can increase this (Gudmundsson, 2003). This effect allows some marine terminating margins to possess large floating tongues several tens of kilometres in length, with that of Petermann Glacier supported almost entirely by longitudinal drag (Nick et al., 2012). However, since the majority of Greenlandic tidewater glaciers (all but seven) do not possess significant floating ice tongues (Moon and Joughin, 2008), this implies that the driving stress of the majority of grounded termini are likely to be supported predominantly by differing proportions of basal and/or lateral drag.

Given the effect of subglacial and lateral topography on the force balance of a tidewater glacier, they will also impact flow velocities along its flow axis. This can be demonstrated if the depth and width averaged velocity of a glacier, $\bar{u}$, at a given point is expressed as

$$\bar{u} = \frac{Q}{HW} \tag{2.5}$$

where Q = volume of ice flux per unit time, and W = glacier width, meaning that a given ice flux will need to flow at greater speeds through a narrower/thinner section of a glacier. This can also be related to the calculation of the longitudinal strain rate, $\partial\bar{u}/\partial x$, meaning that for a steady state (where ice thickness does not change with time) velocity will be affected by changes in ice thickness and width along a glacier profile, such that

$$\frac{\partial\bar{u}}{\partial x} = \frac{\dot{b}}{H} - \frac{\bar{u}}{H}\frac{\partial H}{\partial x} - \frac{\partial\bar{v}}{\partial y} \tag{2.6}$$

where x = distance along a flowline, $\dot{b}$ = the specific mass balance, $\bar{v}$ = depth averaged velocity perpendicular to a flowline, y = distance perpendicular from a flowline, and the transverse strain rate, $\partial\bar{v}/\partial y$, can be estimated according to

$$\frac{\partial\bar{v}}{\partial y} = \frac{\bar{u}}{W}\frac{dW}{dx} \tag{2.7}$$

(Cuffey and Paterson, 2010: their Equations 3.93 and 3.94, p. 346). Accelerations in glacier velocity due to topography can therefore be related to reducing ice thickness as the glacier flows over a bedrock obstacle (Equation 2.6, second term), and/or decreasing the transverse strain rate via a narrowing of the fjord topography (Equation 2.7). Conversely, glacier decelerations can be associated with increasing ice thickness and width, as a glacier enters a deeper area of the fjord or a topographic widening.

Changes in fjord topography can also potentially have implications for whether a tidewater glacier can remain grounded at its terminus. For example, a terminus advancing into deeper water may not be sufficiently thick to remain grounded (Equation 2.4), while fjord widening can cause flow divergence (Equation 2.7), leading to ice thinning. Such thinning could then lead to the terminus achieving floatation. This behaviour has major implications for the calving behaviour of tidewater termini.

2.2 Calving

Calving from tidewater termini occurs once the tensile stresses near the margin are large enough to produce a crack, or a network of cracks, that fully isolate a block of ice from the rest of the glacier. The processes associated with calving are therefore inextricably linked to those of crevassing. In Greenland calving events can occur at scales ranging from blocks of ice <1 m^3 to the calving of full ice thickness icebergs with areas of >250 km^2. Although events of the latter magnitude only tend to occur due to calving of the Petermann Glacier ice tongue (Johannesen et al., 2011), full ice thickness events that include significant fractions of the calving front (>1 km wide, and extending several hundred metres upstream) occur at multiple tidewater outlets in Greenland (e.g. Figure 2.1). However, smaller to intermediate events are far more common (Amundsen et al., 2008; Joughin et al., 2008b).

The processes governing calving behaviour are multivariate and complex, meaning that it is not currently possible to predict the timing and magnitude of individual events (Van der Veen, 2002; O'Neel et al., 2003). Benn et al. (2007a) suggested a hierarchy of processes that control calving; namely, (1) changes in the strain rates associated with velocity gradients along and across ice flow; (2) large stress gradients occurring at ice cliffs; (3) undercutting of the calving face by melting at/below the waterline; and (4) buoyancy arising due to the density contrast between ice and fjord water.

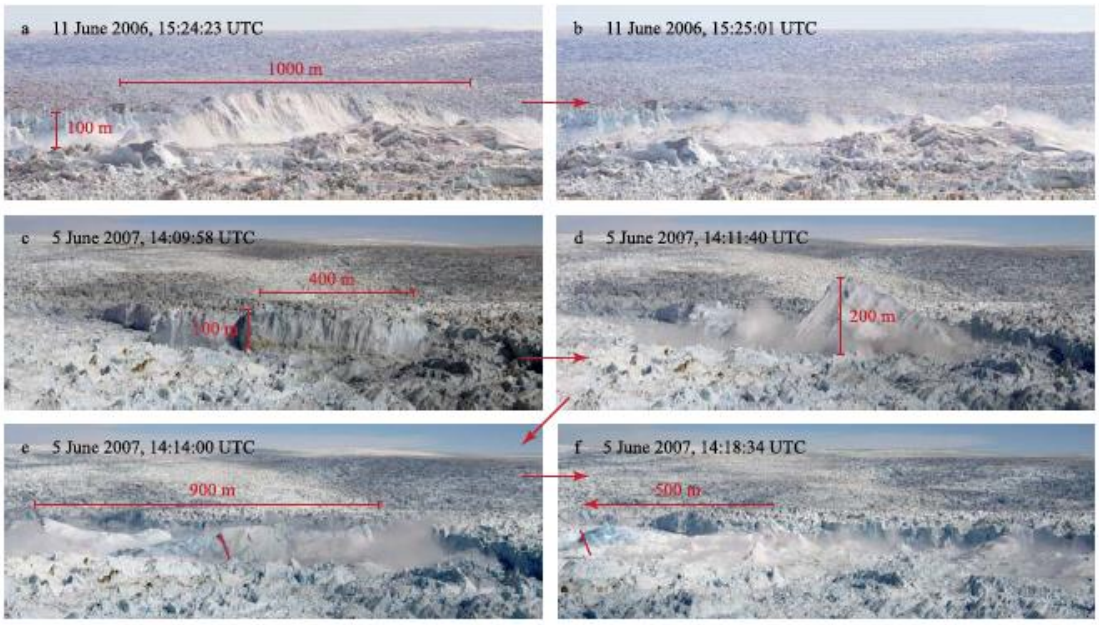

Figure 2.1 Examples of two large full ice thickness calving events from Jakobshavn Isbrae, W Greenland. Lateral extents and freeboard heights are labelled.The first (a,b) observed on 11th June, 2006, and the second (c-f) on 5th June, 2007. Figure from Amundsen et al., 2008.

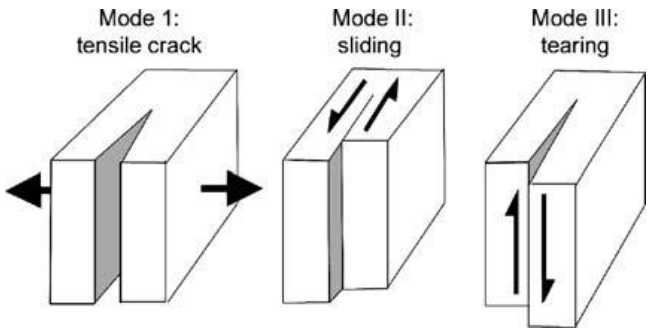

Figure 2.2 Schematic diagram demonstrating the three different modes of crevasse fracturing, namely; Mode 1 – tensile stresses pulling the block apart; Mode 2 – shear stresses acting in parallel but opposing directions; Mode 3 – response to shear in the vertical plane. Figure: Benn et al., 2007a.

2.2.1 Strain rates affecting crevassing and calving

The acceleration of tidewater glaciers towards their termini can result in significant gradients in velocity developing both parallel and perpendicular to the primary flow axis (Section 2.1). These velocity gradients can be sufficient to cause the ice to fracture (i.e. form crevasses) according to three different modes (Figure 2.2). These fractures can then form the basis for pre-existing weaknesses/networks of cracks that can lead to calving.

For tidewater glaciers, the simplifying assumption is often made that crevassing occurs entirely by mode 1 failure. This is because in the majority of cases, crevasses are broadly orientated perpendicular to the primary ice flow direction. This allows convenient and easy estimation of crevasse depth, *d*, from the longitudinal strain rate, $\dot{\varepsilon}_{xx}$, according to

$$d = \frac{2}{\rho_i g}\left(\frac{\dot{\varepsilon}_{xx}}{A}\right)^{\frac{1}{n}} \tag{2.8}$$

where A = multiplier in Glen's flow law, and n = rate factor in Glen's flow law (1955). The depth of the crevasse is therefore expressed by the point at which the extensional stress across the crevasse is balanced by the compressive stress exerted by the weight of the ice itself. This is one of the few empirically validated relations relevant to crevassing (Mottram and Benn, 2009), thus providing a good physical basis for its application within modelling studies (e.g. Nick et al., 2009; 2010; Otero et al., 2010; Cook et al., 2012).

The presence of ponded water within crevasses has also been suggested to significantly affect crevasse depth. Building upon Equation 2.8, this effect can be incorporated within the Nye (1957) formulation according to

$$d = \frac{2}{\rho_i g}\left(\frac{\dot{\varepsilon}_{xx}}{A}\right)^{\frac{1}{n}} + \frac{\rho_w}{\rho_i} d_w \quad (2.9)$$

Where ρ_w = density of glacier meltwater, and d_w = depth of water in the crevasse, with the depth of water in the crevasse allowing it to penetrate deeper (Figure 2.3; Benn et al, 2007a,b). The presence of ponded water provides a mechanism for climate driven changes in surface melt to potentially influence calving behaviour (e.g. Nick et al., 2013; Cook et al, 2012; 2013).

Crevassing processes that occur upstream of the terminus (driven by downstream acceleration of a tidewater glacier, and topographic variability of its channel; Section 2.1), can also have significant implications for calving. As these crevasses are advected towards the glacier terminus, increases in longitudinal and transverse strain rates can lead to the reactivation of these pre-existing weaknesses within the ice (Benn et al., 2007a). It has also been noted that such pre-existing damage can act to soften glacier ice, thus affecting its rheology and susceptibility to further damage (Pralong et al., 2003). Ice dynamics upstream therefore have the potential to directly impact calving behaviour (e.g. Pralong and Funk, 2005; Borstad et al., 2012; Krug et al., 2014).

The acceleration of tidewater glaciers towards their termini, and fjord geometry can therefore impact calving behaviour through (1) increasing strain rates at the terminus through flow acceleration and the topographic configuration of the fjord at the calving margin, and (2) preconditioning ice for calving through the advection of crevassed ice from upstream.

Figure 2.3 Ponded meltwater water in crevasses observed from a helicopter ~6 km from the terminus of Kangiata Nunaata Sermia, SW Greenland, August 2011.

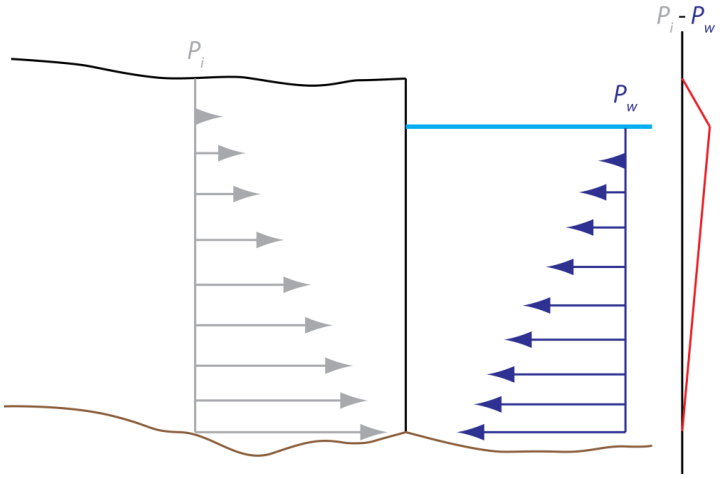

Figure 2.4 Schematic diagram of the stress imbalance at a vertical calving face, showing the pressure exerted by the ice cliff (grey arrows), compared to the backpressure exerted by the water column (blue arrows. The schematic plot on the right (red line) shows the relative pattern and direction of the imbalance between the two. Figure redrawn from Benn and Evans (2010).

2.2.2 Stress gradients at vertical calving faces

The majority of Greenlandic tidewater glaciers have vertical calving faces, meaning that their termini are supported by the back pressure provided by the proglacial water body (Figure 2.4). However, the backpressure acting on the calving face is insufficient to completely balance the outward pressure exerted by the glacier. This imbalance is greatest at the waterline (Figure 2.4). The velocity gradients produced at the terminus therefore encourages deeper propagation of crevasses compared to areas upstream of the calving front. The high strain rates generated by a vertical calving face therefore predispose the terminal areas of tidewater glaciers to extensive mode 1 crevassing, that in turn help to contribute to higher calving rates (Section 2.2.1).

2.2.3 Terminus undercutting

Calving face geometry is modified by conditions within the proglacial water body (Warren et al., 2001; Vieli et al., 2002; Motyka et al., 2003; Enderlin and Howat, 2013; Rignot et al., 2012). The effect of this is to redistribute stresses at the calving face that affect its relative stability and susceptibility to calving. Greenlandic tidewater glaciers are primarily subject to undercutting below the water line (e.g. Enderlin and Howat, 2013; Rignot et al., 2012), rather than at it (e.g. Vieli et al., 2002), leading to considerable difficulty in gaining observations of the morphology and magnitude of the undercut (Straneo et al., 2013).

However, modelling by O'Leary and Christoffersen (2013) demonstrated how different undercut geometries impact where stresses are concentrated, and hence where

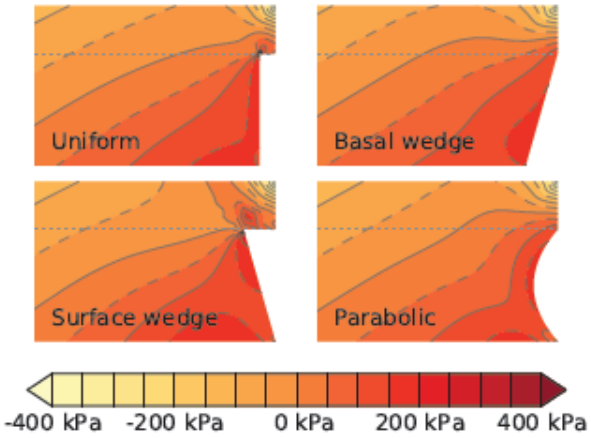

Figure 2.5 Distribution of stress relative to the hydrostatic pressure for different given tidewater glacier terminus geometries. Areas of higher stress are more likely to experience fracture, and hence result in calving. Figure: O'Leary and Christoffersen (2013).

calving is most likely to occur (Figure 2.5). Larger undercuts and sub-aerial fractions of glacier fronts were found to increase the concentration of stress around their respective foci. This has the logical implication that larger undercuts and higher freeboard heights increase the likelihood of calving. Processes that may affect the rate and distribution of undercutting at tidewater termini are discussed below in Section 2.3.3.

2.2.4 Buoyancy

The density contrast between glacier ice and fjord water means that the submarine part of a tidewater glacier is naturally buoyant (Equation 2.4). While this has implications for the force balance and how tidewater glaciers flow (Section 2.1), it can also impact calving behaviour. For example, once a sub-aerial calving event occurs, the overburden pressure exerted by the calved ice on the ice below has been removed. Therefore, the buoyancy of any remaining part of the ice front will increase, given that the height above buoyancy of a given ice thickness, H_{ab}, can be expressed as

$$H_{ab} = H - \frac{\rho_p}{\rho_i} D \tag{2.10}$$

An increase in buoyancy will lead to an increase in tensile stress at the terminus. Coupled with increasing strain rates towards the terminus due to flow acceleration (Sections 2.1 and 2.2.1), this process increases the likelihood of basal crevasses forming. This also enhances the probability of calving occurring. Similar to surface crevasses, basal crevasse heights are a function of longitudinal strain rates, but also the buoyancy of the ice itself. The heights of basal crevasses, d_b, can therefore be estimated according to

$$d_b = \frac{2\rho_i}{\rho_p - \rho_i}\left(\frac{\dot{\varepsilon}_{xx}}{A}\right)^{1/n}\left(\frac{1}{\rho_i g} - H_{ab}\right) \quad (2.11)$$

The effect of basal crevasse growth following a sub-aerial calving event will either be to cause near-instantaneous calving of any remaining sub-aqueous portion of the glacier front (Motyka et al., 2003; Åstrom et al., 2013), or redistribute the stress upglacier. The growth of basal crevasses and their potential linkage with surface crevasses can also help drive full-thickness calving behaviour (e.g. Bassis and Jacobs, 2013).

Buoyancy effects arising from tidal forcing will also inevitably impact every tidewater glacier to some extent, due their marine terminating margins. Although the effects of tides on Antarctic ice shelf and ice stream margins have been extensively observed (e.g. Vaughan, 1995; Bindschalder et al., 2003; Gudmundsson, 2006), their effect on the flow of tidewater glaciers in Greenland (e.g. Dietrich et al., 2007; Podrasky et al., 2012; Walter et al., 2012), and elsewhere (e.g. O'Neel et al., 2003) is comparatively unclear.

Although Walter et al. (2012) observed fluctuations in velocity in phase with tides at Store Glacier, W Greenland, each tidewater glacier will be subject to different tidal forcing due to their individual topographic setting. For example, for an idealised laterally unconfined tidewater glacier where the terminus is just below floatation at mean sea level, low tides will increase basal drag upstream from the terminus, and also increase the height of the sub-aerial ice cliff. Conversely, during high tides, longitudinal strain rates will increase due to a decrease in basal drag, enhancing crevasse depths (Equations 2.8 and 2.11), while change in freeboard height will be minimal since the terminus is at/near floatation at mean sea level.

While the increase in drag and reduction in velocities at low tide would in theory reduce strain rates and crevasse depths, this may be offset by the increase in longitudinal strain rate resulting from the increase in freeboard height (c.f. O'Leary and Christoffersen, 2013). A generalised calving response to low tide conditions is therefore unclear without further work being conducted. By comparison, high tides are likely to produce flow accelerations at the terminus and enhanced calving rates compared to mean sea level conditions. The relative sensitivity of a particular glacier to tidal forcing will therefore depend on (1) the magnitude of the tidal range, (2) how close the terminus is to floatation, and (3) the glacier surface slope and ice thickness upstream of the terminus.

2.3. Climatic factors affecting glacier flow and calving

From the discussion above, it is evident that both atmospheric and oceanic forcing can directly affect the processes that control tidewater glacier flow and calving. However, their relative importance in driving the recently observed changes of Greenlandic tidewater outlets (e.g. Moon and Joughin, 2008; Moon et al., 2012), and the timescales over which they may significantly affect dynamics are still relatively poorly understood (Joughin et al., 2012; Straneo et al., 2013). Below represents a brief summary of current understanding.

2.3.1 Glacier hydrology

Understanding of Greenlandic glacier hydrology and its effect on flow dynamics has significantly benefitted from the study of land terminating margins. Their comparatively simplified flow regime, accessibility afforded by sub-aerial margins, and less crevassed terminal regions have allowed major advances in understanding to be made over the last decade (e.g. Das et al., 2008; Shepherd et al., 2009; Bartholomew et al., 2010; Hoffman et al., 2011; Sundal et al, 2011; Chandler et al., 2013; Cowton et al., 2013; Sole et al., 2013; Tedstone et al., 2013; Doyle et al., 2014). However, the effect of glacier hydrology and meltwater input on flow of the terminal regions of tidewater glaciers is currently less well understood.

The impact of glacier hydrology on the dynamics of tidewater termini is likely to be dependent on the rate and timing of meltwater input, and its distribution across the glacier bed. This will determine the volume of meltwater required to decouple the ice and glacier bed, and hence reduce basal drag (Iken and Bindschalder, 1986; Iverson et al., 1999; Schoof, 2005). At GrIS land terminating margins, the volume and distribution of meltwater supplied to the bed are known to have strong seasonal components, with the subglacial drainage system evolving from a distributed (inefficient) to channelized (efficient) network through the melt season (Cowton et al., 2013). The transition of the hydrological system from an distributed to channelized network from the glacier margin upstream results in ice velocity decreasing, as subglacial water pressure across the majority of the bed decreases (Chandler et al., 2013).

There is some evidence for this also being the case for tidewater glaciers, with Podrasky et al. (2012) observing that between 20-50 km from the terminus Jakobshavn Isbræ, a more intense melt year resulted in behaviour similar to that of a land terminating

margin. Similarly, GPS measurements by Ahlstrøm et al. (2013) for eight different Greenlandic tidewater margins showed evidence for short early-summer accelerations followed by a rapid deceleration. Sole et al., (2011) were also able to demonstrate that such an acceleration/deceleration event at Kangiata Nunaata Sermia (KNS) was accompanied by the rapid discharge of a large turbid plume into its fjord. This occurrence of high proglacial discharge alongside an acceleration of flow velocity has often been associated with the reorganisation of the subglacial drainage system at land terminating margins (e.g. Nienow et al., 1998; Cowton et al., 2013).

Although these changes in subglacial hydrology can have significant impacts on the seasonal dynamics, their net effect on annual glacier velocity at land terminating margins has been demonstrated to be minimal (Sole et al., 2013). This has been shown through observations of summer flow accelerations being offset by lower winter velocities (Sole et al., 2013), meaning that the recent 2012 extreme melt year in Greenland actually had minimal net effect on the annual flow velocity of a land-terminating margin (Tedstone et al., 2013). However, it is less clear whether this is also the case for the annual velocities of marine terminating glaciers. The observations of Sole et al. (2011) at KNS showing a ~1% net effect of summer motion on annual velocity were taken >35 km from its terminus, and upstream of where topographically focussed glacier flow initiates (Joughin et al., 2010a). Consequently, it is not known whether such an observation would be applicable closer to the terminus. Furthermore, the potential effect of fjord mélange inhibiting winter ice flow (see Section 2.3.3) further complicates the possibility of determining the effect of annual meltwater input on annual velocities.

It has also been suggested that meltwater input along lateral shear margins (at both ice-ice and ice-rock interfaces) could also reduce lateral drag, in turn affecting glacier flow (Pfeffer, 2007; Howat et al., 2010; McFadden et al., 2011; Nick et al., 2012). However, to the knowledge of the author the occurrence and significance of this is at present hypothetical, and has not been demonstrated empirically.

2.3.2 Atmospheric effects on crevassing and calving

The ponding of meltwater in crevasses has previously been suggested to allow them to penetrate deeper than under longitudinal strain alone, with implications for enhancing calving rates at tidewater margins (Equation 2.9; Benn et al., 2007a; 2007b; Nick et al, 2009). Higher volumes of surface melt produced by higher air temperatures will therefore result in deeper meltwater ponds at the base of crevasses, and/or allow them to fill more

rapidly. Higher rates of surface melt are therefore likely to encourage deeper, and spatially more extensive top-down hydrofracturing across the terminus region of a tidewater glacier.

The effects of such changes have been incorporated into numerical models via a crevasse water depth calving criterion (Benn et al., 2007a; Nick et al., 2009; 2010; Otero et al., 2010; Cook et al., 2012). Results from one of these models applied to Columbia Glacier, Alaska has demonstrated that changes in crevasse water depths on the order of a few meters were sufficient to drive significant changes in calving and glacier dynamic behaviour (Cook et al., 2012). Further work on Greenlandic outlet glaciers have also shown that temperature driven changes in crevasse water depth have the potential to significantly affect their dynamics over the next century (Nick et al., 2013).

However, these models currently fail to account for the cumulative damage experienced by the ice as it is advected towards the terminus (e.g. Borstad et al., 2012). While enhanced crevassing in the presence of meltwater is predicted by Equation 2.9, ice affected by this must first reach the terminus before it can impact calving behaviour. Therefore, depending on the flow velocity of the glacier, ice may have been subject to crevasse damage resulting from several melt seasons before it ultimately calves. The potential importance of previous melt seasons on calving behaviour is also complicated by the annealing of ice and closure of crevasses once pressure from ponded meltwater is removed. Removal of meltwater could occur via drainage to the bed via hydrofracture through the full ice thickness, or refreezing within the crevasse.

Some of the physical aspects of cumulative damage mechanics have been successfully incorporated into a calving criterion by Krug et al. (2014), and have been successfully validated against observations from Helheim Glacier, E Greenland. Similar to the crevasse water depth calving criterion (Benn et al., 2007a), longitudinal strain rates are observed to exert a first order control on calving behaviour for the model setup. As such, this provides physical consistency within the hierarchy of calving processes described by Benn et al. (2007b). However, significant work remains to be undertaken in determining the relative sensitivities of tuning parameters and how they can be realistically related to changes in climate forcing.

Pre-existing crevasses have also been suggested as conduits through which meltwater can warm ice, and hence affect its rheology (Phillips et al., 2010). This has been termed as cryohydrologic warming, and provides a potential mechanism for runoff to affect the thermal structure of ice sheets at depth on timescales of years to decades. This could potentially lead to higher rates of ice deformation through the warming and softening

of the ice. However, for the effect to be extensive would require significant volumes of meltwater entering a densely packed network of englacial conduits, with the meltwater requiring sufficient englacial residence time to conduct its thermal energy. The terminal regions of tidewater glaciers provide the ideal environment for cryohydrologic warming to be significant, given the presence of often extensively crevassed and damaged ice at the margin of the ice sheet where surface melting is also likely to be most intense.

An implication of this is that according to Equations 2.9 and 2.11, where ice is warmer (and hence softer), crevasses will not penetrate as far for a given longitudinal strain rate. Therefore, multiple warm, high surface melt years may help to suppress crevasse extents through modification of the thermal properties of the ice.

Peaks in subglacial water pressure driven by meltwater supplied to the bed also provide the potential for transient enhancement of basal crevasse heights near tidewater glacier termini. For example, at surging glacier margins, full depth basal crevassing in ice of ~200 m is possible once subglacial water pressures exceed 80-90% of floatation (Rea and Evans, 2011). In principle, such conditions could occur at tidewater glacier margins throughout the year, due to either (1) seasonal reorganisation of the subglacial drainage system (e.g. Sole et al., 2011), (2) diurnal fluctuations in surface melt (e.g. Meierbachtol et al., 2013), or (3) sudden drainage of supraglacial or ice marginal lakes (e.g. Hoffmann et al., 2011). Although subglacial water pressures that generate these high basal crevasses will not necessarily be sustained, glacier flow will advect the crevassed ice towards the glacier terminus. This in turn may form the basis for full-depth calving events.

2.3.3 Ocean-atmosphere effects on calving

The following will briefly summarise current understanding of the controls on fjord circulation and how this impacts on melt rates at Greenlandic tidewater termini. Furthermore, while the presence/absence of a floating ice tongue is known to have a significant effect on the rate and pattern of submarine melting (Figure 2.6; e.g. Rignot and Steffen, 2008; Le Brocq et al., 2013), the overwhelming majority of Greenlandic glaciers are known to have near-vertical calving faces (Moon and Joughin, 2008). The discussion is therefore limited to processes that are likely to be applicable to vertical tidewater margins in Greenland.

The morphology of calving fronts are subject to potentially significant modification by fjord conditions both at and below the waterline (e.g. Vieli et al., 2001; Motyka et al., 2003). This can have significant implications for the distribution of stress at the terminus,

and consequently for calving dynamics (Section 2.2.3; O'Leary and Christoffersen, 2013). The rate of calving face melting is primarily controlled by a combination of two factors; (1) fjord water temperature [dictated by fjord hydrography (Mortensen et al, 2011; 2013) and synoptic scale oceanography (Rignot et al., 2012)], and (2) the rate and volume of subglacial discharge at the terminus (Jenkins, 2011; Xu et al., 2012; 2013). Fjord circulation (e.g. Motyka et al., 2003; Rignot et al., 2010; Mortensen et al., 2011; 2013) will also significantly affect how energy is transferred from the fjord water to the calving face, directly impacting the shape of terminus undercut (Xu et al., 2012; 2013; O'Leary and Christoffersen, 2013).

Rates of terminus undercut are likely to directly impact the rate of calving (O'Leary and Christoffersen, 2013). Based on modelling studies, melt rates at tidewater termini exhibit a linear dependence on fjord temperature, and approximately a cube root dependence on subglacial discharge (Jenkins et al., 2011; Xu et al., 2012; 2013). The latter implies an approximate doubling of the melt rate for an order of magnitude increase in the rate of discharge. The non-linear relationship between discharge and melt rate is primarily a result of the density contrast between the freshwater runoff, and comparatively saline fjord water. This means that once subglacial runoff emerges at the base of the glacier it will become buoyant within the water column. This will rise along the face of the terminus as a spatially confined plume (relative to the width of the calving front), entraining ambient fjord water as it does so (Figure 2.6). This helps to establish a density driven convective mode of circulation where ambient fjord water is drawn into the plume, and the less dense mixed fjord/glacial runoff flows away from the terminus at/near the surface (Motyka et al., 2003; Rignot et al., 2010).

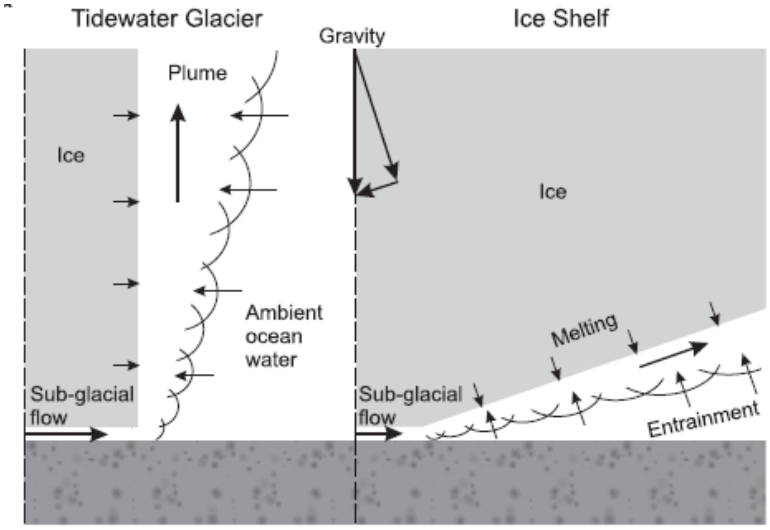

Figure 2.6 Schematic diagram of ambient ocean water being entrained by a buoyant, fresh meltwater plume, occurring at a tidewater glacier and and ice shelf (Figure: adapted from Jenkins, 2011).

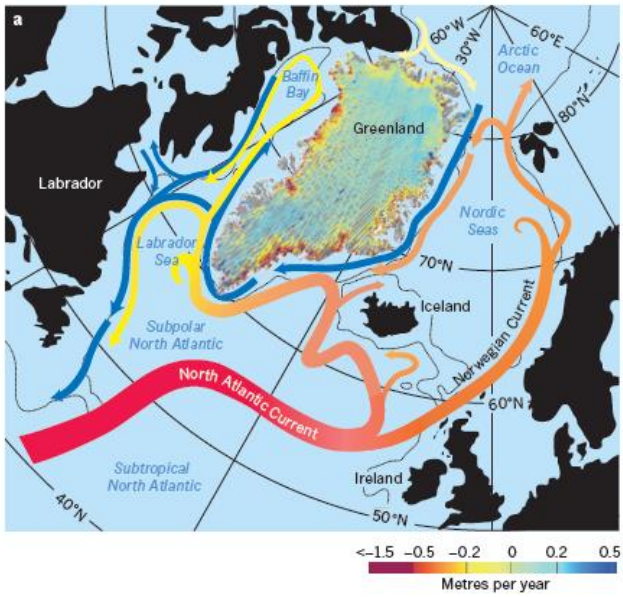

Figure 2.7 Diagram showing the distribution of ocean currents around Greenland, with Atlantic sources coloured red to yellow, and Arctic freshwater sources as blue. Rates of dynamic ice sheet thinning occurring in Greenland are superimposed. Figure: Straneo and Heimbach, 2013.

As the plume is spatially confined, the highest melt rates across the width of a tidewater glacier terminus will be focussed around subglacial runoff portals (Xu et al., 2013). To the knowledge of the author, the effect of this spatial concentration of melt on the distribution of stress across the width of a terminus, and therefore its impact on calving, is yet to be assessed.

The submarine melt rate at a tidewater terminus occurring due to runoff will be a function of (1) the volume of subglacial runoff produced within a glacier catchment, (2) the level of development of the subglacial drainage system (i.e. the efficiency with which it can evacuate meltwater subglacially into the fjord), and (3) the occurrence of supraglacial or ice dammed lake drainage events that cause peaks in subglacial discharge. Submarine melt rates are therefore a function of atmosphere-ice-ocean interactions that vary significantly over sub-seasonal timescales.

The linear dependence of submarine melt with fjord water temperature will be affected by in-fjord circulation and the relative influence of ocean waters within a particular fjord (e.g. Murray et al., 2010; Straneo et al., 2011; Cauché et al., 2013). In-fjord circulation can cause a significant degree of temperature variability in both vertical and horizontal planes (e.g. Mortensen et al., 2011; 2013; Xu et al., 2013), while the connectivity of fjords to deep ocean waters can add a further layer of complexity to fjord hydrography (e.g. Rignot et al., 2010; Straneo et al., 2010; 2012). For example, changes in regional ocean circulation off the coast of Greenland (Figure 2.7), including the warming of currents on both its south-east and west coasts, have previously been suggested to play a

significant role in driving terminus retreat (e.g. Holland et al., 2008; Rignot et al., 2010; Straneo et al., 2010; 2012; Christoffersen et al., 2011; Motyka et al., 2011).

The currents that are suggested to have driven GrIS tidewater glacier retreat are composed of warm, dense, saline waters that flow at depth, and are commonly referred to as Atlantic Waters. The density of these waters means that where shallow fjord sills exist, they can form topographic barriers that relatively insulate the fjords (and the tidewater glaciers therein) from the effects of oceanographic warming (e.g. Mortensen et al., 2011; 2013; Straneo et al., 2012). However, due to a fjord's connection to the open ocean, oceanographic conditions will always have some impact on fjord hydrography.

Where dense Atlantic Waters flow into fjords they will enter at depth, generally capped by cooler, less dense Polar/Arctic Waters. This can lead to potentially strongly stratified water columns (Straneo et al., 2011). Coupled with effects of winds, tides, and local temperature and density gradients within the water column, this can generate highly complex circulation patterns compared to the simple convection driven model described above (Figure 2.6; Motyka et al., 2003; Straneo et al., 2010; 2011). The level of fjord stratification will therefore also be significant when attempting to model or estimate submarine melt rates (Jenkins, 2011; Straneo et al., 2011).

Modelling work by Sole et al. (2012) at Kangerdlugssuaq Fjord has suggested that enhanced subglacial runoff can also result in greater volumes of Atlantic Waters being advected at depth towards the terminus. The modelled increase in heat energy resulting from a doubling of runoff was found to be sufficient to increase summer submarine melt rates by 48%. This demonstrates that high runoff rates can also enhance the relative impact of warmer ocean waters on melt rates where they occur within glaciated fjords.

The impact of the oceans on submarine melt rates at tidewater termini is therefore contingent on (1) the presence/absence of sills that allow ocean waters to enter the fjord, (2) different modes of fjord circulation that modify the water column of the fjord, and hence the distribution of energy available for generating submarine melt, and (3) the volume and rate of subglacial discharge entering the fjord, advecting greater volumes of waters at depth towards the terminus.

A final physical constraint on the calving behaviour of tidewater termini is the occurrence of mélange (i.e. a dense proglacial pack of icebergs and sea ice). As air temperatures fall below zero during winter the mélange freezes and becomes a rigid mass, inhibiting calving by providing backstress to the terminus at the waterline (Figure 2.4; Amundsen et al., 2010). The backpressure provided by the mélange (suggested to be on the

order of 30-60 kPa; Walter et al., 2012) is thought to inhibit calving and ice flow through preventing the overturning of large icebergs that would otherwise calve from the terminus (Amundsen et al., 2010). This has the effect of allowing the terminus to advance during the winter, while also suppressing terminus flow velocities (e.g. Amundsen et al., 2010; Walter et al., 2012). Mélange breakup often precedes air temperatures rising above zero, with ambient fjord water temperature, mélange thickness, glacier thickness and fjord width all suggested to influence its timing (Schild and Hamilton, 2013).

2.4 Evaluating the effects of climate forcing

Atmospheric and oceanic forcing can potentially exert significant controls on tidewater glacier behaviour. However, the above discussion demonstrates that their effect on many processes affecting dynamics remain empirically poorly constrained. A simple, frequently used approach to evaluating their potential impact is to compare observations of glacier dynamics to first order indicators of each type of forcing (e.g. Seale et al., 2011; Bevan et al., 2012; Carr et al., 2013a). For a glacier of interest, it is therefore crucial to establish (1) the pattern of air temperature variability, and (2) a knowledge of how the oceans are likely to impact fjord water temperature near the terminus.

Once suitable records of atmospheric and oceanic change are generated, these can also be used to drive numerical models. Within these models climate forcing variables can be related to the processes described above via parameterisations (e.g. Nick et al., 2013). Although successful model runs (i.e. those that simulate behaviour within an acceptable margin of error) are unlikely to be unique solutions, these can be used to establish (1) whether the model setup and parameterisations are capable of simulating observed behaviour for the given forcings, and (2) the relative sensitivity of the modelled glacier to each type of climate forcing. However, to provide confidence in the model validation procedure, observations must also be accurately comparable to model output. If this is not achieved, the errors introduced could potentially skew validation, and/or lead to the erroneous rejection of successful model simulations. Model success, and the effective interpretation of results, will therefore be contingent on (1) the suitability of climate forcing input, (2) the appropriateness of model parameterisations, (3) the accuracy with which observations are compared to model output, and (4) choice of validation procedure.

Chapter 3

Field site and methods

This thesis aims to elucidate the relative importance of atmospheric and oceanic drivers on the behaviour of a large Greenlandic tidewater glacier since its Little Ice Age maximum (LIAmax), and the ability of a well-established numerical model to replicate this. This is achieved through reconstructing glacier behaviour using a combination of field, remote sensing and documentary data, in addition to numerical modelling.

Given the uncertainty of the relative effects of atmospheric and oceanic forcing on tidewater glacier stability (Joughin et al., 2012; Straneo et al., 2013), these climate forcings need to be well constrained for the study site. The potential to generate a detailed multi-decadal to centennial record of glacier behaviour is also of critical importance. Consequently, this chapter describes the field site, the reasons for its selection, in addition to an overview of the methods and data utilised during the course of the research. This is not intended to be a wholly exhaustive account, with any extra relevant detail being provided where necessary in subsequent chapters.

3.1 Field site

The field site selected for study is Kangiata Nunaata Sermia (KNS), SW Greenland (~64.3° N; Figure 3.1). It is the largest outlet glacier in west Greenland south of Jakobshavn Isbræ, currently flowing at ~6 km a^{-1} at its terminus (Joughin et al., 2010a), attaining calving rates of ~6 km^3 a^{-1} and surface runoff rates ranging from 2-7 km^3 a^{-1} (Van As et al., 2014). This mass loss is discharged into the Kangersuneq branch of Nuup Kangerlua/Godthåbsfjord, choking the fjord with calved ice for much of the year and significantly impacting fjord temperature, salinity and circulation (Mortensen et al., 2011; 2013). The ice dammed lake Isvand is also located ~5 km upstream of the present terminus position on the western margin of KNS. Prior to 2004, this lake drained down a valley into Ameralik, though subsequent to this has undergone periodic subglacial drainage into Kangersuneq (Weidick and Citterio, 2011).

Given the size of its potential annual mass loss, KNS exerts a significant control on the overall mass balance of the south-western sector of the Greenland Ice Sheet (GrIS). It

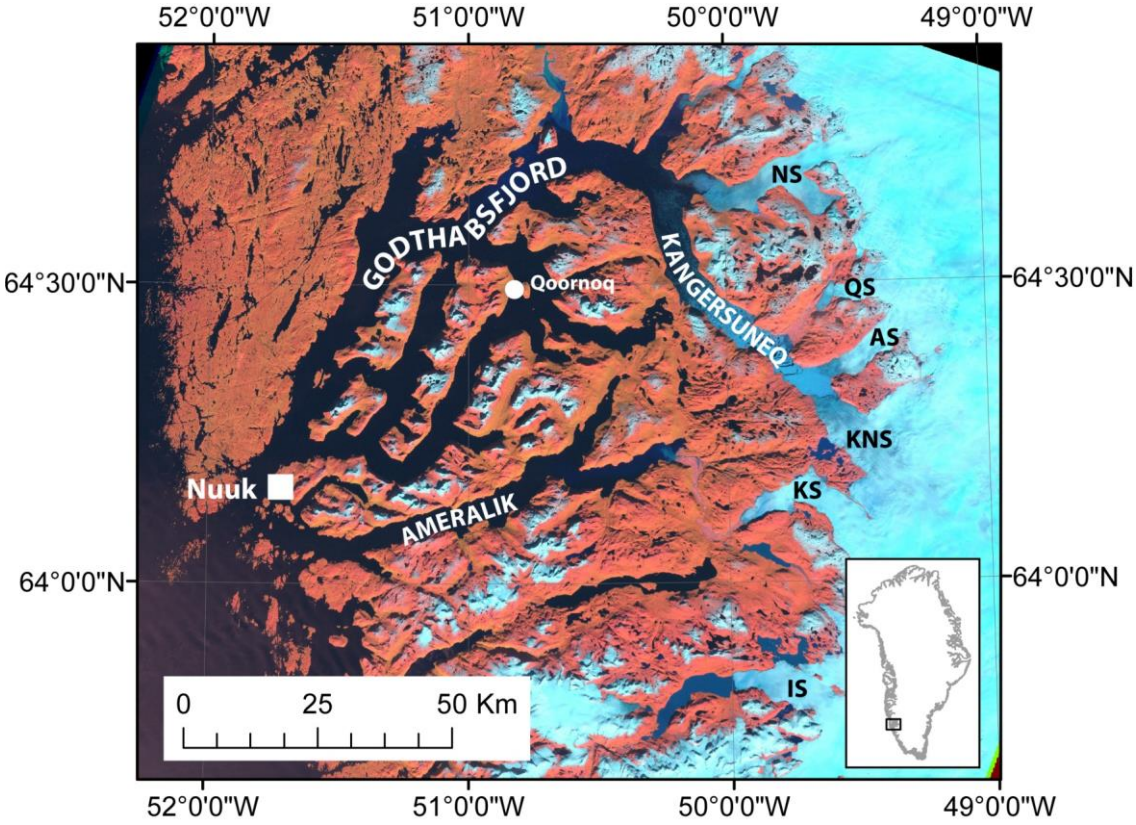

Figure 3.1 Annotated Landsat false colour satellite image (acquired 18/9/2000) showing the location of KNS within Godthåbsfjord, and its location in Greenland (inset). Names of glaciers have been abbreviated as follows: NS – Narssap Sermia; QS – Qamanarssap Sermia; AS – Akullersuup Sermia; KNS – Kangiata Nunaata Sermia; KS – Kangaasarsuup Sermia; IS – Isortuarssup Sermia.

is also known to have retreated significantly (>20 km in total) in more than one phase since its LIAmax, though its precise response to climate forcing over this period has not been explicitly investigated (Weidick, 1959; Weidick et al., 2012). The magnitude of terminus retreat observed since the LIAmax therefore demonstrates the sensitivity of KNS to climate and/or topographically driven terminus change over multi-decadal to centennial timescales. This also makes KNS an ideal test site for evaluating the ability of numerical models to replicate observed glacier dynamics and determine the drivers of these changes.

Several factors also make KNS a suitable location to attempt centennial timescale reconstructions. Firstly, as it retreated from its LIAmax, KNS has left a largely unstudied geomorphological record (Weidick et al., 2012), providing information regarding where the glacier experienced relative stability, and its dynamics during retreat. Secondly, it is positioned ~80 km inland from the first post-Medieval European settlement of Nuuk (colonial Danish: Godthåb), while the Nuup Kangerlua/Godthåbsfjord fjord system is also the location of the abandoned Norse Western Settlement (Vestyrbygd). These factors mean that historical records of the area are more likely to exist following Danish re-colonisation in 1723, while the Norse ruins have continued to attract archaeologists and explorers to the

region since their rediscovery (Egede, 1741). This has generated a wealth of disparate historical source material (some being previously unstudied/unidentified from a glaciological perspective), including written accounts, maps and photographs that span more than two centuries. These observations have significant potential to ascribe precise chronologies to extents reconstructed from geomorphology, and its dynamics during periods where landform evidence is not preserved.

3.1.1 Contemporary dynamics

While the contemporary dynamics of KNS have been studied to some extent (e.g. Sole et al., 2011; Ahlstrøm et al., 2013; Van As et al., 2014), both it, and the south-western sector as a whole have not been subject to the intensity of research experienced at other major Greenlandic outlet glaciers, such as Jakobshavn Isbrae (e.g. Joughin et al., 2004; 2008a; 2014; Csatho et al., 2008; Amundsen et al., 2010; Vieli and Nick, 2011; Podrasky et al., 2012) or Helheim Glacier (e.g. Howat et al., 2005; 2008; Joughin et al., 2008b; Nick et al., 2009; 2013; Murray et al., 2010; Andresen et al., 2012; Cook et al., 2013).

The response of KNS to changes in subglacial hydrology has been observed over sections >35 km upstream of the terminus, and has been described previously in Section 2.3.1 (Sole et al., 2011). While velocity data exist closer to the terminus (~20 km; Ahlstrøm et al., 2013), these have not yet been explicitly analysed from a glacial hydrological perspective. However, they display behaviour broadly in agreement with the findings of Sole et al. (2011), in that a short early summer acceleration is followed by an abrupt deceleration coupled with subsequent short-lived accelerations during the summer. This would imply that the reorganisation of the subglacial drainage system has a significant effect on the flow dynamics of the main trunk of the glacier as well as further upstream (Sole et al., 2011). The overall effect of this on annual motion close to the terminus is however, yet to be established.

During winter, a rigid mélange has been observed to form in the fjord, allowing the terminus to advance by several hundred metres. As this breaks up during the following spring, the terminus returns to approximately its pre-winter terminus configuration (Sole et al., 2011). However, more recent time lapse imagery during the winter of 2010/2011 (*unpublished*) has demonstrated that mélange does not always form at the same time during the winter (Figure 3.2). In this instance, three subglacial outburst floods occurred on 3/12/2010, 24/12/2010, and 1/1/2011 breaking up and clearing mélange from the terminus

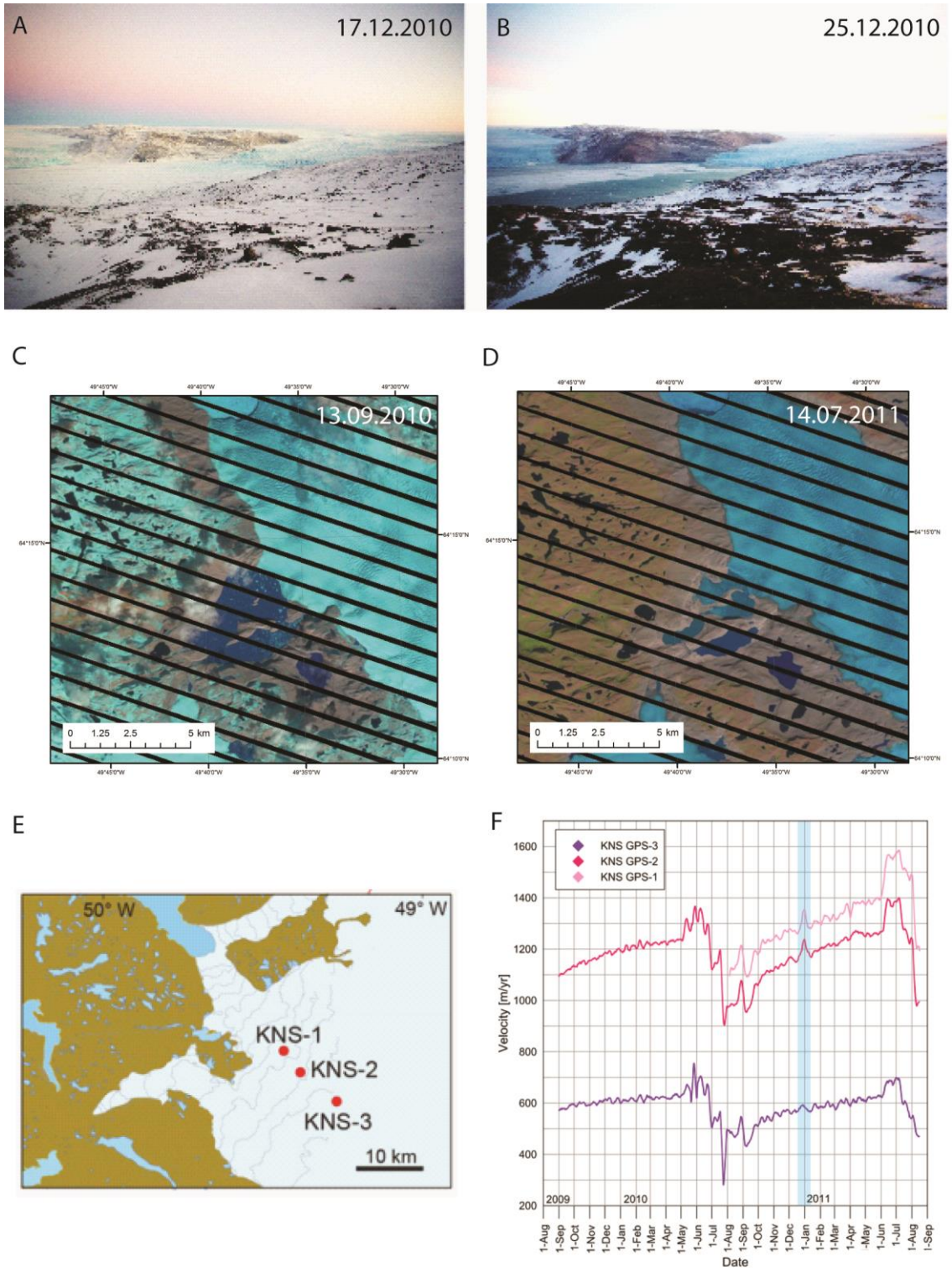

Figure 3.2 Effect of the drainage of the ice dammed lake Isvand on the dynamics of KNS. Time lapse camera images of the terminus of KNS capturing one of the three outburst floods during December 2010/January 2011, showing (A) mélange present in the fjord before the flood, and (B) the mélange having been cleared by the discharge of a turbid plume. Landsat True Colour composite images acquired at (C) the end of the 2010 melt season and (D) near the beginning of the 2011 melt season showing a significant reduction in the extent of Isvand during the winter. (E) The position of each of the GPS stations used to record (D) the velocity of KNS (Figures E and F: Ahlstrøm et al., 2013). The speed-up event caused by the drainage of Isvand is highlighted in blue.

area of the fjord. These outburst flood events prevented early mélange formation (i.e. November/December/January).

When the timings of these events are compared to the GPS measurements of Ahlstrøm et al., (2013), a notable peak in velocity in the lower GPS stations (KNS-1, and KNS-2) is apparent centred on the days around 1/1/2011 (Figures 3.2e, f). This is not evident in the upstream KNS-3 GPS station. This demonstrates that the dynamic event observed was confined to the downstream section of the glacier.

The probable cause of this is a mid-winter drainage event of the ice dammed lake Isvand, increasing subglacial water pressure, reducing drag and enhancing ice flow. This is suggested as a mechanism for the observed acceleration as (1) Landsat imagery from the end of the 2010 melt season and start of 2011 melt season shows Isvand to have lost a significant volume of water (Figures 3.2c, d), and (2) the acceleration coincident with the outburst floods are only observed by the two GPS stations that are closest to Isvand (Figure 3.2e, f). The occurrence of lake drainage during winter is however puzzling, since the reduced subglacial discharge during winter should lead to the re-pressurising of the hydrological system. Potential drainage routes from Isvand to the terminus should therefore be closing, reducing the likelihood of drainage. Although beyond the confines of this thesis, this drainage of Isvand deserves to be the subject of further study, as it could provide a potentially unique insight into the evolution of the subglacial hydrology near a tidewater margin during winter.

Thus far, there has been limited study of KNS' terminus fluctuations over the last 20 years. For time slices where terminus change has been assessed, this has been as part of larger, regional studies of tidewater glacier dynamics (e.g. Rignot and Kanagaratnam, 2006; Moon and Joughin, 2008; Moon et al., 2012). In these studies terminus retreat from 1997 onwards is identified, though this is on the scale of several hundred metres, rather than the multi-kilometre retreats that have occurred at other large outlet glaciers (e.g. Moon and Joughin, 2008).

The surface mass balance (SMB) of KNS is exceptionally well constrained by high-resolution modelling conducted on each of the GrIS outlets in the Nuuk area for the period 1960-2012 (Van As et al., 2014). This utilised regional climate model data resampled to resolutions capable of resolving the comparatively narrow glacier outlets, with results validated against river discharge observations. These show that over the last two decades surface runoff rates from KNS have approximately doubled (Van As et al., 2014).

3.1.2 Post-Little Ice Age dynamics

The post-LIAmax dynamics of KNS have received comparatively more attention than the majority of Greenlandic tidewater glaciers, though again this has been as part of wider regional studies (e.g. Weidick, 1959; Weidick et al., 2012). Previous work has shown that KNS retreated ~20 km from its LIAmax, including 10-13 km before 1860 (Weidick et al., 2012). However, the timing, extent and manner of retreat remain poorly constrained. Similarly, direct knowledge of terminus positions available from photographs during the 20th century have not been explicitly compared to climate data. Therefore very little is known about what has driven the extensive changes at KNS since its LIAmax.

A full discussion of previous work on the post-LIAmax dynamics of KNS is not provided here, since this thesis will seek to add new sources of information, remap, reanalyse and, where necessary, reinterpret the data used to generate previous reconstructions (Weidick, 1959; Weidick et al., 2012). In doing so we will seek to explicitly quantify glacier change at KNS using Geographic Information Systems (GIS) analyses. This will allow a higher degree of accuracy to be attained compared to previous reconstructions where it was not possible to undertake such analyses (see Sections 3.1.2 and 3.1.3, Chapter 4). The results from these analyses will also be directly compared against available climate data. This will be undertaken in both Chapters 5 and 6.

3.1.3 Oceanography

The hydrography of Kangersuneq is exceptionally well constrained compared to other Greenlandic fjords, both at a large spatial scale (Mortensen et al., 2011), and over seasonal timescales (Mortensen et al., 2013). Although the presence of mélange adjacent to KNS means that data are limited close to the terminus, this is a common shortfall in studies of terminal regions of tidewater glaciers (Joughin et al., 2012; Straneo et al., 2013).

At the large scale, Mortensen et al. (2011) identify four different modes of fjord circulation in Godthåbsfjord, namely (1) estuarine circulation (Figure 3.3a), (2) subglacial circulation (Figure 3.3b), (3) dense coastal inflow (Figure 3.3c), and (4) intermediate baroclinic circulation (Figure 3.3d). The intermediate baroclinic circulation is crucial to determining the temperature of intermediate depth fjord waters that are most likely to reach interact with the terminus of KNS. The strength of this mode of circulation increases during warmer years, meaning that air temperatures and sea surface temperatures at the fjord entrance are likely to impact the temperature of fjord water at depth, which in turn affect the terminus. Although occasional inflows of ocean shelf waters do occur, these are

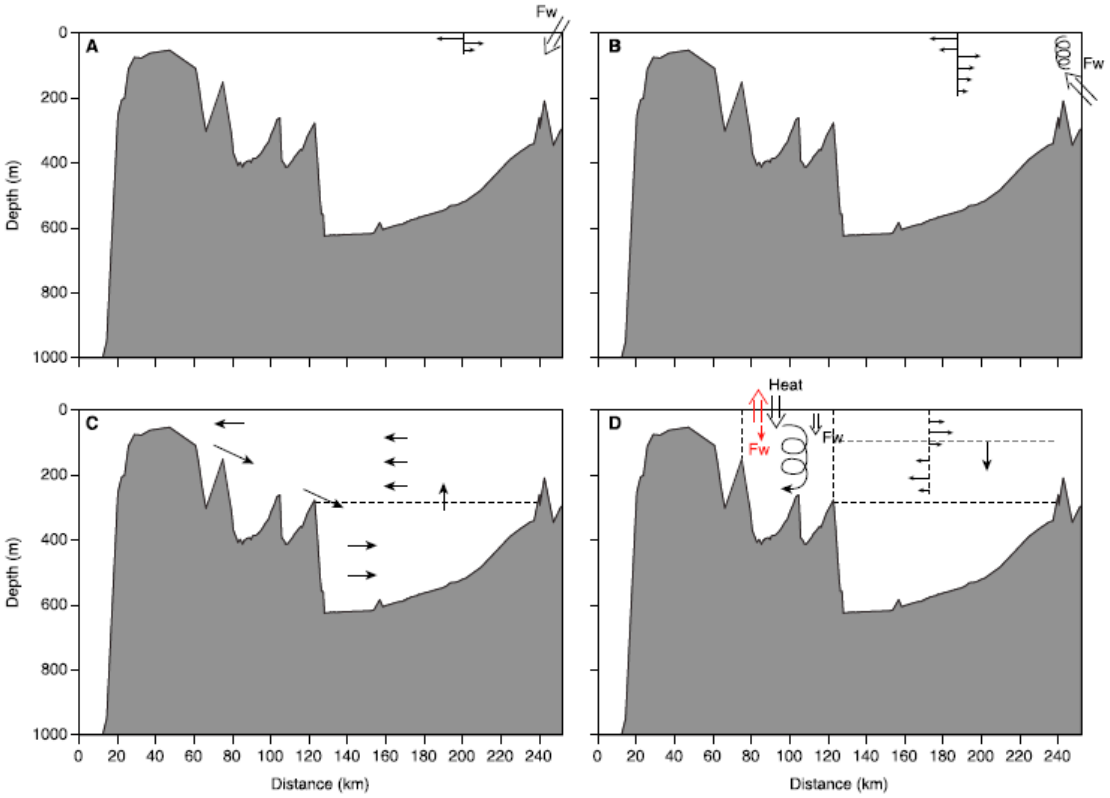

Figure 3.3 Schematic diagrams of the different modes of circulation observed in Godthåbsfjord, including (A) estuarine circulation where surface fresh water (Fw) inputs from glacial and terrestrial runoff encourage outward flow of surface freshwater, and a subsurface compensation current, (B) subglacial convective circulation (described in Section 2.3.3), where buoyant subglacial runoff rises to the surface flowing outward, with a compensation current drawing water towards the glacier from intermediate depth fjord water, (C) dense offshore inflows to the deepest parts of the fjord, displacing overlying waters, and (D) intermediate baroclinic circulation where vigorous tidal mixing in the outer fjord region encourages surface waters to be advected downwards, significantly warming and freshening intermediate depth waters. This generates a horizontal contrast in density between fjord interior and exterior waters, driving an in-fjord current at the surface and an out-fjord current beneath it. Figure: Mortensen et al., 2011.

mainly confined to the outer sections of the ~100 km long fjord system and are separated from the terminus of KNS by a shallow sill in the fjord interior (Figure 3.3c). This means that KNS is largely isolated from changes in ocean shelf temperatures (Mortensen et al., 2011; Straneo et al., 2012).

Fjord circulation in Godthåbsfjord also experiences significant seasonal variation (Mortensen et al., 2013). The largest seasonal contrast occurs adjacent to the tidewater glacier outlets, such as KNS, where changes in subglacial runoff (e.g. Van As et al., 2014) determine the relative strength of density driven convective circulation occurring at their termini (Figure 3.3b). This will have implications for the volume of submarine melt occurring at KNS in summer compared to winter (Section 2.3.3; e.g. Sciascia et al., 2013).

Using conductivity, temperature and depth (CTD) measurements within the inner regions of Godthåbsfjord, near to KNS, Mortensen et al. (2013) have developed a conceptual framework for how fjord circulation changes from summer to winter (Figure

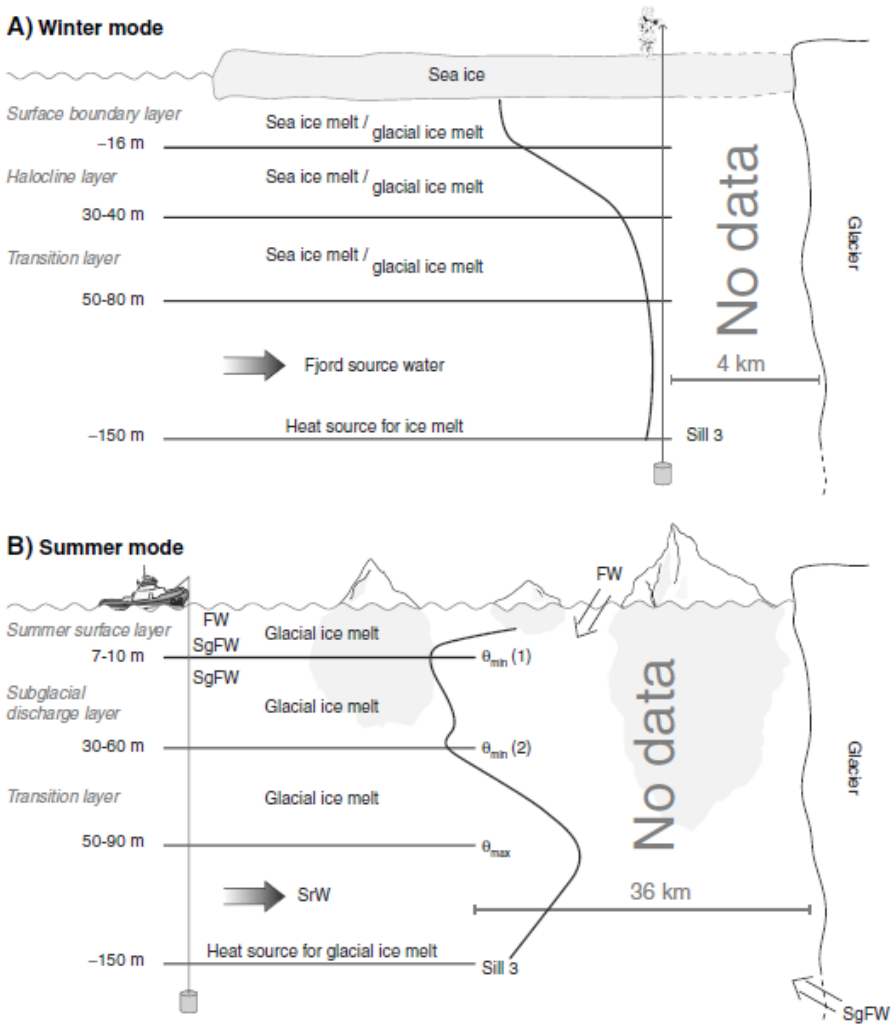

Figure 3.4 Seasonal changes in the circulation regime of Godthåbsfjord close to KNS, showing (A) winter mode where the water column is stratified with minimal freshwater input, and (B) summer mode, where subglacial discharge (SgFW) generates a distinct outward flowing layer of water and temperature profile (θ). This sets up a compensation current towards the bottom of the fjord, drawing in sill region water (SrW) sourced from intermediate depth fjord waters. Figure: Mortensen et al., 2013

3.4). This shows a stratified water column to exist during the winter and a well-developed convective circulation during the summer. Although intermediate depth waters are advected towards KNS in both summer and winter, transport will be significantly stronger in summer where circulation is driven by greater volumes of subglacial runoff.

Significant submarine melt associated with the summer mode of circulation is only likely to begin once the subglacial hydrological system becomes efficient (e.g. Sole et al., 2011). Once this is established, large volumes of subglacial runoff will be able to be rapidly discharged into the fjord. Atmospheric conditions driving runoff will therefore determine when summer submarine melting begins, how long it lasts, and the volumes of intermediate fjord waters that will be advected towards the terminus as a compensation current. Due to intermediate baroclinic circulation, the temperatures of these intermediate waters are in turn likely to have been significantly modified by fjord surface water temperatures and/or SSTs near the fjord entrance (Mortensen et al., 2011).

3.2 Data and methods

3.2.1 Climate data

Both air and ocean temperatures have the potential to be significant drivers of tidewater glacier change, as outlined above. The following outlines the data sources used to determine the relative levels of atmospheric and oceanic forcing affecting KNS.

The closest long record of air temperature to KNS is located ~80 km away at the Nuuk meteorological station. This has the longest record of air temperatures in Greenland, with observations available from 1783, though this is only fragmentary until 1866, after which a continuous monthly average record is available up to the present (Vinther et al., 2006; Cappelen et al., 2012). This record has been subject to rigorous quality control, having been tested for the occurrence of inhomogeneities over the full length of its record (Vinther et al., 2006). It is crucial to undertake such analysis before long observation records such as these are used, since inconsistencies can arise due to changes in instrumentation, station location, operator, and urbanisation. There is therefore an extremely high degree of confidence that this record accurately reflects air temperature change occurring at Nuuk.

Despite the presence of a strong continentality effect, the *pattern* of temperature variability observed at Nuuk is assumed to be comparable to that experienced at KNS (Taurisano et al., 2004). This is assumed given the strong correlation between temperatures observed at Nuuk and Qamanarssup Sermia (QS; Figure 3.1). This has in turn been established on the basis of comparison of the Nuuk record to 10 years of temperature observations at QS (Braithwaite and Olesen, 1993), and 60 years of observations at Qoornoq (Taurisano et al., 2004).

Recent glaciological studies have primarily interpreted deep ocean temperatures to be representative of oceanographic forcing affecting fjord water temperatures (e.g. Murray et al., Rignot et al., 2010; Straneo et al., 2012; Nick et al., 2013). However, given the shallow sill at the entrance to Godthåbsfjord, it is unlikely that deep ocean temperature will have a significant impact on the fjord conditions (Straneo et al., 2012), with little empirical evidence existing to suggest otherwise (Section 3.1.3; Mortensen et al., 2011; 2013). The occurrence of intermediate baroclinic circulation at the entrance to, and within the fjord, mean that sea surface temperatures (SST) and air temperature influenced fjord waters are more likely to affect the temperature of intermediate depth waters within Godthåbsfjord.

For this reason, records of SST are used to represent the oceanographic forcing that KNS is likely to be subject to. This is useful as longer observational records exist for SST compared to deep ocean temperatures (e.g. Woodruff et al., 1987), with modelling and interpolation of disparately spaced historical observations allowing SST to be estimated globally at 1° x 1° resolution back to 1871 (Rayner et al., 2003).

Average SSTs for the region immediately offshore from Nuuk (61° to 65° N 51° to 56° W) were extracted from the HadISST1 dataset (Rayner et al., 2003) for the period 1871-2012. A relatively wide 4° x 5° area was used to allow the general pattern of change of SST in the Labrador Sea to be captured. The area covered is consistent with the scale over which SST anomaly data were pre-processed prior to 1949 (4° x 4° grid; Rayner et al., 2003), therefore we seek to avoid attempting to resolve SST changes at a higher spatial resolution than the data are originally based on. The analyses of Hanna and Cappelen (2003) also provide a high degree of confidence in the HadISST1 dataset for an area nearby to that which has been extracted. In this instance, they validated a HadISST1 derived record from southern Greenland against independent observations of SST for the period 1876-1975 (Smed, 1978; Buch and Hansen, 1988). The HadISST1 data will therefore reflect the pattern of SST change occurring outside of Godthåbsfjord.

3.2.2 Glacier reconstruction

A wide array of source material was explored while undertaking the glacial reconstruction of KNS since its LIAmax. In order to generate a quantitative reconstruction of terminus positions (and their associated uncertainties), only sources that allow absolute and relative estimates of glacier position/geometry are included. Sources that mention the existence of KNS or provide unclear and/or ambiguous information as to its position/geometry are not used or referred to in the main study. Where sources have been previously been presented as providing absolute or relative information of glacier extent, where a reassessment of the source demonstrates that this is not the case, we do however demonstrate why (e.g. Thorhallesen, 1776; Chapter 5).

The greatest source of ambiguity amongst the records used potentially arises from written sources that relate glacier extent. Although their utility has sometimes been viewed as limited in glacier reconstructions, potential exists to gain significant insight into the behaviour of KNS from these sources before the first accurate maps and photographs of KNS become available in the late 19th century. For this location, the magnitude of terminus

change observed since the LIAmax is advantageous, as any description of the terminus is likely to be undertaken in reference to distinct surrounding topographic features.

To obtain an effective assessment of glacier extent, it should be possible to identify both the approximate location that an observation is made from, and the position of the glacier relative to this. This is achieved by comparing observer descriptions to the known geography, place names, and Norse ruin locations, which all provide fixed points of reference. This should allow each written description to be placed within a clearly defined spatial context.

Effective interrogation of written records also necessitates an awareness of the changing of place names in Greenland since recolonisation in 1723, and periods of exploration undertaken prior to this. For example, Godthåbsfjord is the Danish name for the water body also known as Nuup Kangerlua in Greenlandic, while the fjord branch that KNS is located in, Kangersuneq, is also locally known as Isfjorden. At present, all are used interchangeably. The British explorer John Davis also originally named Godthåbsfjord as Gilbert Sound in 1585, before William Baffin renamed it as Ball's River during his voyage of 1612. Subsequently, writers and explorers have also spelled this as Baal's Rivier and Bael's Rivier, leading to further potential confusion (e.g. Cranz, 1820; Giesecke, 1910).

Orthographic changes to the Greenlandic language in the 1850s, and again in the 1970s also mean that each place name will have up to three different spellings. However, these mostly represent superficial changes, with the formal spelling of KNS changing from Kangiata Nunâta Sermia to Kangiata Nunaata Sermia in the 1970s. It is also worth noting that some Danish colonial place names differ entirely from those of the Greenlandic (e.g. Godthåb/Nuuk, and Sandnæs/Kilaarsarfik).

The earliest maps to show KNS also name the glacier as Sermasoak (modern orthography: Sermersuaq) or Isblinken (Møller, 1840), which literally translate as 'The Great Glacier' and 'The Ice Mountain' respectively. However, these names are also interchangeable for the ice sheet at a larger scale so care needs to be taken before taking these names at face value. Although interpretation of place names in written accounts is fraught with difficulties, through careful interrogation they can still provide useful geographic and contextual information.

Once an account has been verified, and an observer position has been reconstructed, digital elevation models (DEMs) of the region (see Section 3.1.3) can be used to constrain the observer's field of view. Viewshed analysis is used to delimit the most plausible extreme extents from an individual observation position. This provides

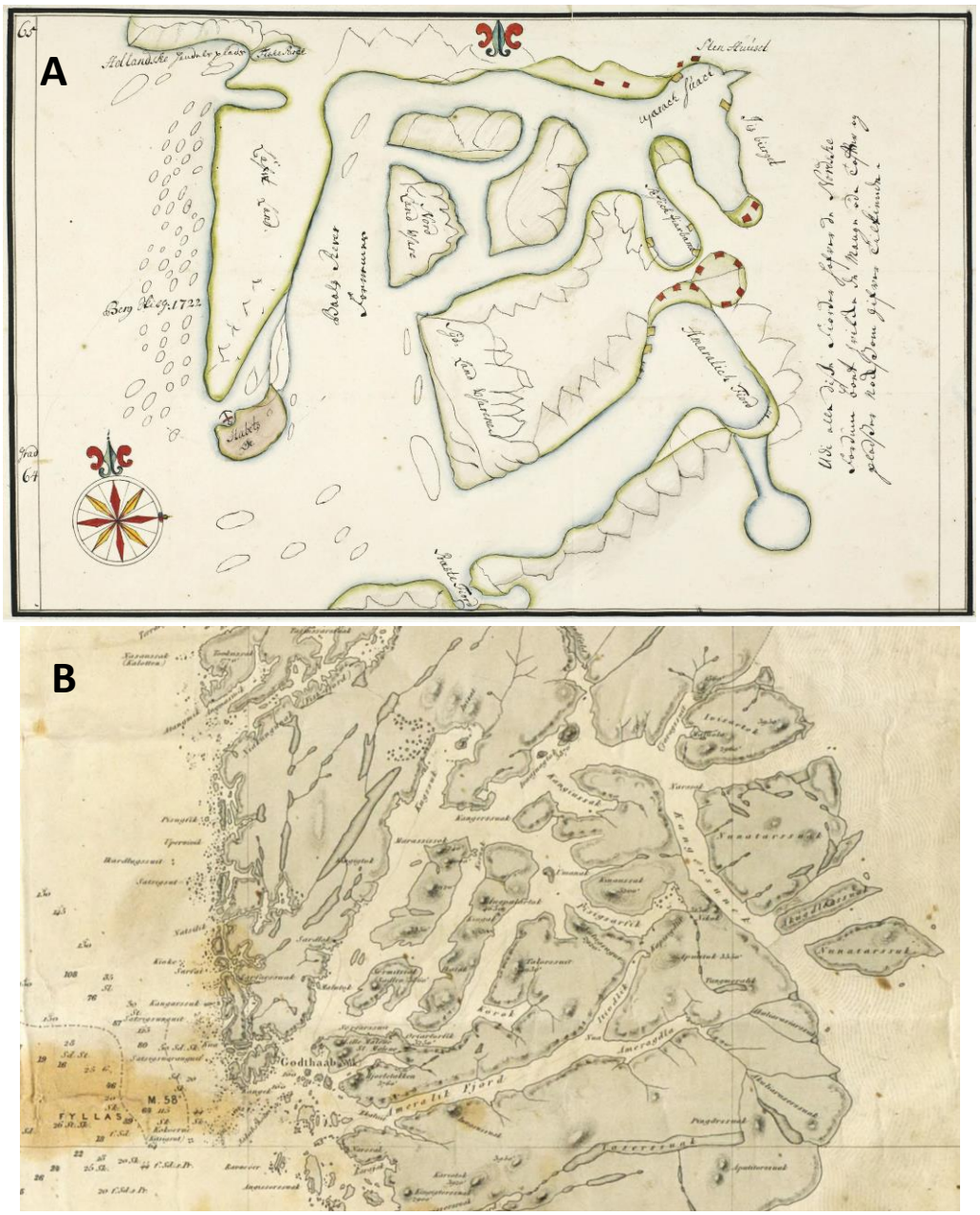

Figure 3.5 Improvement of detail in the maps of Godthåbsfjord, (A) Hans Egede's (1723) map of Godthåbsfjord made just after recolonisation, and (B) 1885 map of Godthåbsfjord (Jensen, 1885).

empirical basis for any error margins that are defined. Where photographs are available, even if the terminus is obscured by foreground topography, this approach allows a quantitative assessment of the glacier extent for a given observer position.

Maps are also used to reconstruct the extent of KNS. Although the earliest maps of Godthåbsfjord do not even show KNS (e.g. Figure 3.5a), there was an incremental increase in the quality of subsequent maps through the 19th century (e.g. Figure 3.5b). Interpretation of the extent of KNS from maps is undertaken with care, since some cartographers were liable to copy details from previous maps where they had little new information. Therefore terminus positions provided by maps were only trusted where details such as coastlines and lakes close to KNS had been refined to better represent reality. This was assessed through comparison to modern maps and satellite imagery. The addition of such detail near to KNS

would demonstrate that the cartographer had visited the region and therefore noted any change in glacier extent. In addition to this, it was decided to take a conservative approach to the interpretation of glacier extent from maps, with each terminus position also possessing an error bar. The magnitude of this error bar was determined by mapping terminus position within a range relative to known topographic features such as valleys or fjord headlands that are included on the map.

Where available, terrestrial photographs of the terminus were also used to delineate terminus position. Vertical aerial photographs were georeferenced using *ArcMap v10.1*, with at least 6 topographic tie points used to rectify each image, using a 2nd order polynomial transformation (Bjørk et al., 2012). Termini were delineated from photographs using topographic reference points to constrain their position from both sides of the fjord. Satellite imagery from the USGS Landsat archive were also imported into *ArcMap* for terminus delineation, where cloud-free images of the terminus region of KNS were available.

Where georeferenced images existed, termini were delimited viewed at a magnification where each pixel was visually resolvable. Landsat imagery were acquired from band 1 Landsat 4-5 Thematic Mapper sensor (1987-1997 in this study) with a pixel size of 30 m, and from band 8 (panchromatic) Landsat 7 Enhanced Thematic Mapper Plus (ETM+) sensor (1999-2012 in this study) with a 15 m pixel size. The failure of the scan line corrector (SLC) on the Landsat 7 ETM+ sensor has led to a ~22% loss of data on each

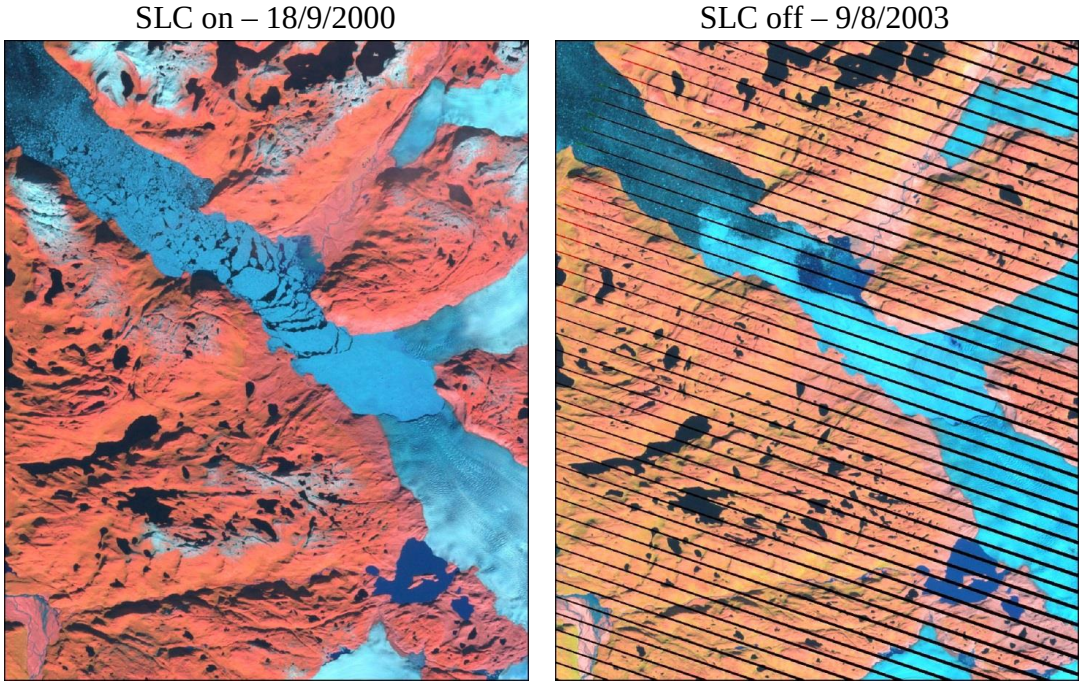

Figure 3.6 Examples of subsets from false colour Landsat ETM+ imagery showing the data loss associated with the failure of the SLC functionality.

scene acquired, distributed as narrow bands towards the edge of the data (e.g. Figure 3.6). Where this occurs, and there is data loss across part of the terminus, a straight line is used to join up the parts of the image where the terminus can be observed. Landsat scenes where the SLC 'no data' stripes obscure large sections of the terminus are discarded and not used in analysis.

3.2.3 Digital Elevation Model

The DEM used for analyses within this thesis is a mosaic of ASTER GDEM v.2 (30 m grid resolution; Tachikawa et al., 2011) and a 1985 aero-photogrammetrical DEM for the region nearby to KNS derived from data collected by the Danish Geodata Agency (25 m grid resolution; K. Kjær, *pers. comm.*) with associated ground control (GR96; Figure 3.7). The vertical errors for each DEM are expected to be ~±12.9 m and ±6 m respectively. For consistency, as part of the mosaicking process, the DEMs were regridded to a horizontal resolution of 30 m, with the aero-photogrammetrical DEM value being preferred where there is overlap. This was done due to the higher grid resolution and vertical accuracy of the latter.

The ASTER GDEM v.2 is generated by the stacking and averaging of all valid ASTER DEM data available for a given area. The DEM data are in turn obtained from stereo pairs of ASTER imagery, which do not require explicit ground control because of

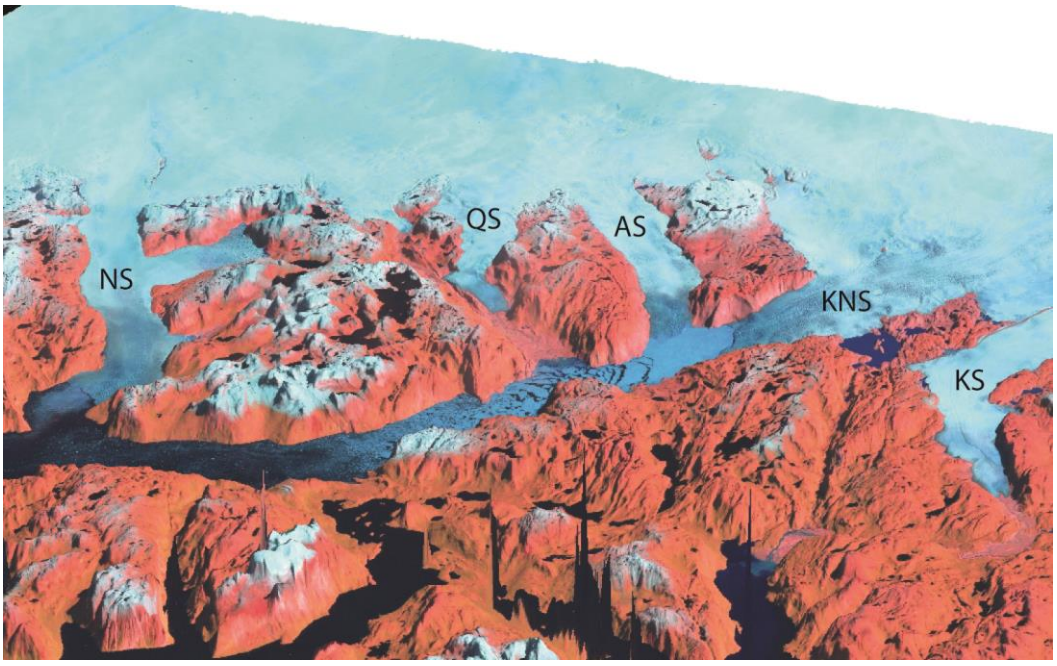

Figure 3.7 3D rendering of the DEM used in this study (3x vertical exaggeration) with a Landsat false colour scene acquired on 18/9/2000 overlaid. Labelled glaciers are: NS – Narssap Sermia, QS – Qamanarssap Sermia, AS – Akullerssup Sermia, KNS – Kangiata Nunaata Sermia, KS – Kangaasarsuup Sermia.

the ASTER satellite's highly accurate on-board location and look angle instrumentation (Fujisada et al., 2012).

The aero-photogrammetrical DEM was derived after scanning a 1985 stereo-pair of photographs at a resolution of 15 μm^2, which corresponds to a ground resolution of ~2 m^2 for each individual image. The derivation of the DEM necessitates some loss of resolution, while a grid sample distance of 25 m^2 was used as it is known to perform well in extracting elevations from areas of low image contrast, such as snow and ice (N. Korsgaard, *pers. comm.*).

3.2.4 Geomorphology

The extent of ice scour, the linear crests of moraines, and areas of fluted moraines were mapped from a composite of high-resolution (2 m^2) GeoEye satellite images freely available on Google Earth, and ground truthed during fieldwork conducted in August 2011.

Where distinct (near-) continuous longitudinal profiles of glacier geometry could be obtained from moraines and ice scour limits, their elevations were extracted from the DEM (Section 3.1.2) at 30 m intervals. This spacing was chose to remain consistent with the horizontal resolution of the DEM. The elevation data extracted from these ice limits were then related to their respective positions on a flowline running down the centre of the fjord (Section 3.2.3), by adapting the newly devised Extrapolated Centreline Method of tracking terminus change (explained in full detail in Chapter 4).

3.3 Numerical model

The numerical model used in this study is a shallow shelf approximation (SSA) based one-dimensional (1D) flowband model, specifically designed to simulate the dynamics of tidewater glaciers (Nick et al., 2010). The model is well-established, and has been applied extensively to large marine margins in Greenland and Antarctica in both contemporary and palaeo- contexts (Nick et al., 2010; 2012; Vieli and Nick, 2011; Jamieson et al., 2012; 2013). Part of these applications has been to generate projections of sea level contribution for the four largest Greenlandic outlet glaciers over the next 100 to 200 years (Nick et al., 2013). However, the model itself remains untested against observations over those timescales, while a lack of multi-decadal to centennial records of observations also means that the calibration period used was necessarily short (5 years). The following briefly describes the model and its boundary conditions.

3.3.1 Force balance

The SSA approximation to the Full Stokes equations is based on the premise that the thickness of the modelled glacier is significantly less than its length (i.e. a low aspect ratio), while vertical shear is not directly incorporated (MacAyeal, 1989). As such, the modelled glacier has uniform velocity with depth. This manner of approximation is most suited to ice masses with a high slip ratio (i.e. where flow from basal sliding significantly exceeds flow occurring via internal deformation). A 1D application of the SSA is therefore suitable for scenarios where fast flow along a single flow axis dominates, such as commonly occurs for tidewater glaciers, ice streams and ice shelves.

The force balance in the model can be described according to

$$\rho_i g H \frac{\partial H}{\partial x} = 2\frac{\partial}{\partial x}\left(H\nu\frac{\partial U}{\partial x}\right) - \mu A_s \left[\left(H - \frac{\rho_p}{\rho_i}D\right)U\right]^{1/m} - \frac{2H}{W}\left(\frac{5U}{\lambda A W}\right)^{1/m} \quad (3.1)$$

where ρ_i = density of ice, ρ_p = density of the proglacial water body, g = gravitational acceleration, x = the along-flow distance, H = ice thickness, D = depth of ice below the surface of the proglacial water body, A_s = bed roughness parameter, A = temperature dependent rate factor, W = glacier width, ν = effective viscosity (dependent on the strain rate), m = friction exponent. Equation 3.1 is a re-written form of Equation 2.2, describing driving stress (left hand side), being balanced by the longitudinal, basal and lateral drag terms (first, second and third terms on the right hand side respectively).

The sliding law is therefore based on an effective pressure dependency (Bindschalder, 1983; Van der Veen and Whillans, 1996), thus allowing the model to replicate the velocity profiles typically observed along the flow axes of tidewater glaciers (e.g. Moon et al., 2012). While parameters have previously been used for varying basal and lateral drag according to runoff (μ and λ respectively; Nick et al., 2013), these are not varied in this study (i.e. both are given values of 1) as there is as yet no empirical basis for their impact on tidewater glacier dynamics over timescales >1 year (Sections 2.3.1 and 3.1.1). Furthermore, where they have been allowed to vary for centennial timescale model runs, their effect on dynamics at timescales >1 year has been found to be negligible (Nick et al., 2013).

3.3.2 Incorporating climate forcing

The model utilises a crevasse water depth based calving criterion (Equation 2.9). This is combined with the calculation of basal crevasse heights (Equation 2.11), so calving will occur once surface and basal crevasses penetrate the full ice thickness. Calving is therefore a function of both the longitudinal strain rate and the surface crevasse water depth, thus providing a direct link between climate forcing and calving rates via surface runoff (Nick et al., 2009; 2010; 2012; 2013; Cook et al., 2012; 2013). The manner of how runoff is scaled to crevasse water depth differs from that described in Nick et al. (2013), and is described in Chapter 6.

Submarine melt is incorporated into the model as a negative mass balance term across each grid cell from the grounding line downstream to the terminus (Nick et al., 2013). Due to the depth-integrated nature of the numerical model, it is not possible to directly simulate the different submarine undercut melt geometries described by O'Leary and Christoffersen (2013). Similarly, the calculation of submarine melt as a function of runoff is not possible without coupling the ice flow model to a melt/runoff model (e.g. Jenkins, 2011; Xu et al., 2012; 2013).

For simplicity, and given the linear dependence of submarine melt rates on fjord temperature (Section 2.3.3), the magnitude of the former is directly scaled to SST. This allows the impact of oceanographic change on terminus stability to be evaluated. The way in which oceanographic change is scaled to submarine melt also differs from that described by (Nick et al., 2013). The new parameterisation, and reasons for implementing it, are fully explained in Chapter 6.

Surface mass balance (SMB) is also directly incorporated across the modelled catchment, with each depth- and width-integrated grid cell having a potentially unique value. The manner of how SMB is varied within the model and the inputs used are described in full in Chapters 5 and 6. The sensitivity of dynamics to changes in SMB is also evaluated.

3.3.3 Catchment boundary, flowline and width definition

Accurate definition of model boundary conditions is crucial to the potential success of a numerical model run. However, significant uncertainties remain for many fjords in Greenland regarding bathymetry and subglacial topography (Straneo et al., 2013). For each boundary condition described below we have endeavoured to minimise uncertainty, with any estimates being derived on a physical basis where possible.

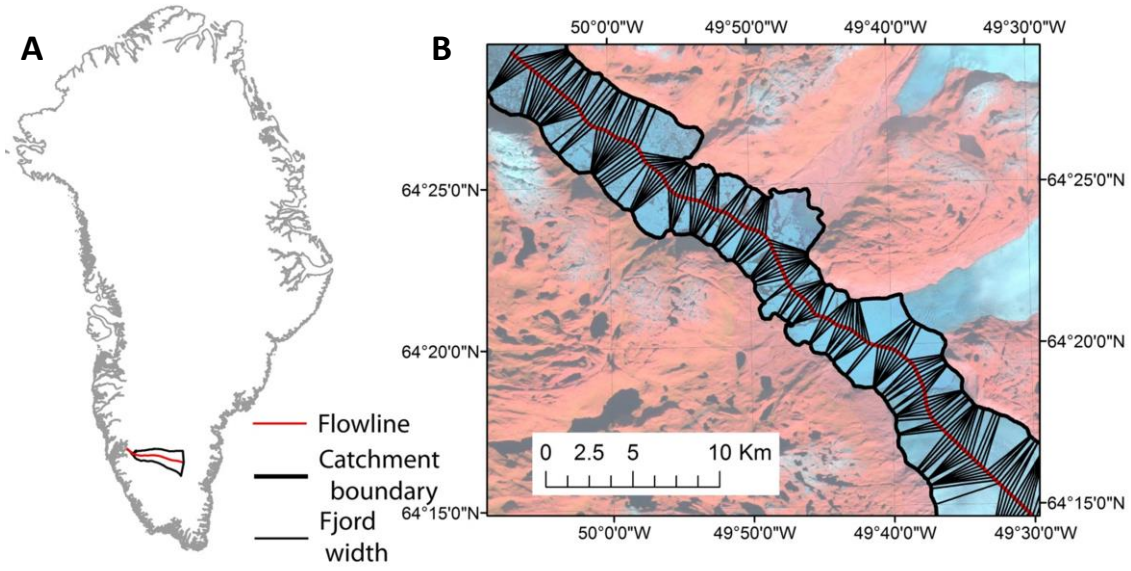

Figure 3.8 Diagrams showing (A) catchment extent and flowline of KNS, and (B) view of the fjord region of KNS (Landsat image acquired 18/9/2000), with flowline, catchment extent, and fjord widths labelled.

The catchment boundaries of KNS are a product of subglacial and surface topography. However, given the absence of detailed direct observations of subglacial topography around KNS (Bamber et al., 2001; 2013), this study uses distributed interferometric synthetic aperture radar (InSAR) data that record the ice flow velocity (Joughin et al., 2010a) to determine catchment extent (Van As et al., 2014). This is based on the premise that the velocity structure of the ice sheet obtained from InSAR can (all things held equal) be used to determine the direction of ice flow. The catchment boundaries used in this study are the same as those derived by Van As et al. (2014) for KNS (Figure 3.8a). These were obtained by applying the *ArcGIS* 'Particle Track' tool to the 2005/2006 InSAR ice flow velocity data (Joughin et al., 2010). Beyond the glacier terminus, the fjord width at sea level was used to define the catchment boundary.

The model flowline was defined to follow the axis of fastest glacier flow according to the same velocity data. This was achieved by inverting the velocity data, and using the *ArcGIS* 'Hydrological Tools' package to determine the most hydrologically efficient flow path for a particle from the ice divide to the glacier terminus. Beyond the current glacier extent, the model flowline was determined by following the positions in the centre of the fjord that maximise the Euclidean (i.e. straight line) distance between the north and south fjord coastlines (Figure 3.8b). This was joined to the InSAR derived glacier catchment flowline to create a flowline from the ice divide to beyond the LIAmax position (Figure

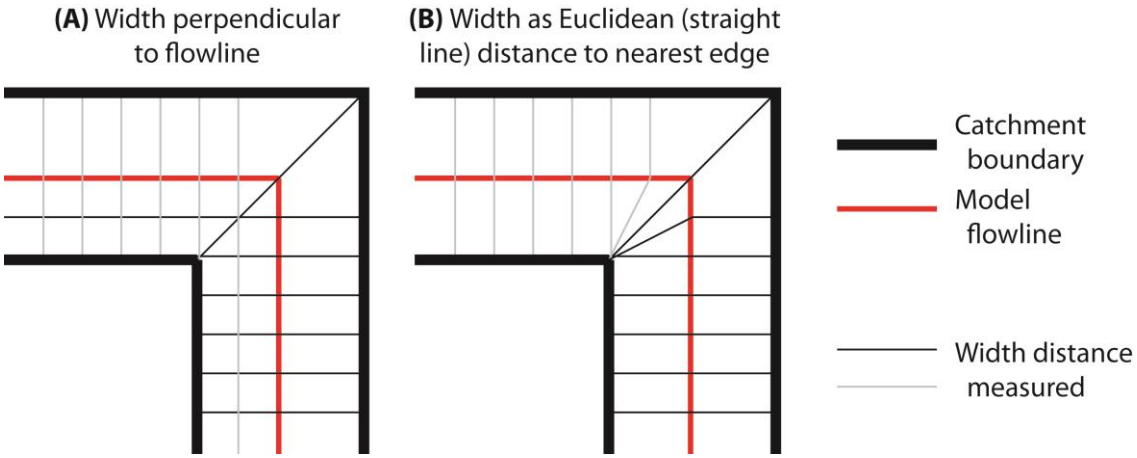

Figure 3.9 Schematic diagram showing the potential effect of a change in fjord orientation on how fjord width is defined for (A) width defined as perpendicular to the flowline, and (B) width defined as the Euclidean distance from the flowline to the edge of the fjord.

3.8). Points positioned 250 m apart were plotted onto the flowline, representing a 250 m along flow grid cell size for the model.

The fjord width for each of these grid cells is calculated by summing the Euclidean distance from each grid point to the respective northern and southern catchment boundaries (Figure 3.8b). This method of fjord width measurement was used rather than the width perpendicular to the flowline due to the fjord (and model flowline) not following a straight track (Figure 3.8b). Therefore where the perpendicular distance is used and a fjord changes orientation, this can result in significant over-estimation of width (Figure 3.9a), compared to the Euclidean distance measure (Figure 3.9b).

3.3.4 Fjord bathymetry and subglacial topography

Basal topography represents a crucial control on glacier flow and terminus stability (Sections 2.1 and 2.2), and has also been demonstrated to exert a control on the stability of modelled flowline glaciers (Enderlin et al., 2013). Its accurate definition within the model is therefore pivotal to its potential success. However, the bathymetry of fjords where major outlet glaciers discharge is often only sparsely known due to the presence of perennial mélange, preventing bathymetry surveys from being easily undertaken (Straneo et al., 2013). Similarly, remote sensing of the subglacial topography of tidewater glacier margins via radar is often hampered by the scattering effects of crevasses and englacial water (Gogineni et al., 2001).

KNS is unfortunately no exception to this. Where point depth measurements are known within the fjord (Figure 3.10; Weidick et al., 2012; Nørgaard-Pedersen, *pers. comm.*), values are translated to the nearest flowline position. Depth values for flowline

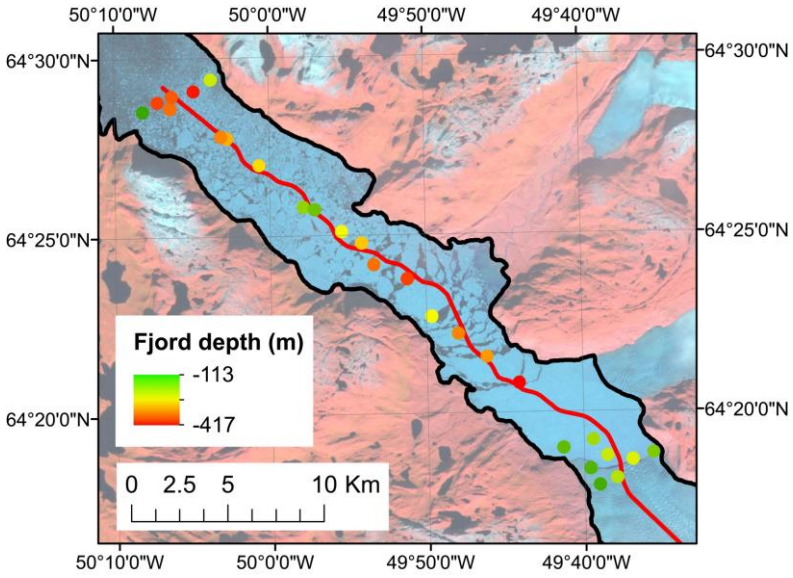

Figure 3.10 Map of the fjord of KNS showing the flowline (red line) and points where bathymetry measurements are available.

positions in between are derived using linear interpolation. Model sensitivity to uncertainty in fjord bathymetry is evaluated as part of Chapter 5.

The subglacial topography of KNS also represents a significant unknown, with little data existing for the lower 40 km of the glacier despite attempts at detailed surveys by OIB/CReSIS in the summers of 2009 and 2011. However, it has been possible to derive a physically based estimate of subglacial topography based on the methodology of Morlighem et al. (2011). In this instance, distributed surface velocity and surface mass balance data are used to determine ice thickness using a mass conservation approach, with existing flightline data used for both parameter tuning and validation (Figure 3.11). Upstream of 40 km, values from a subglacial DEM gridded to 5 km are used (Bamber et al., 2001).

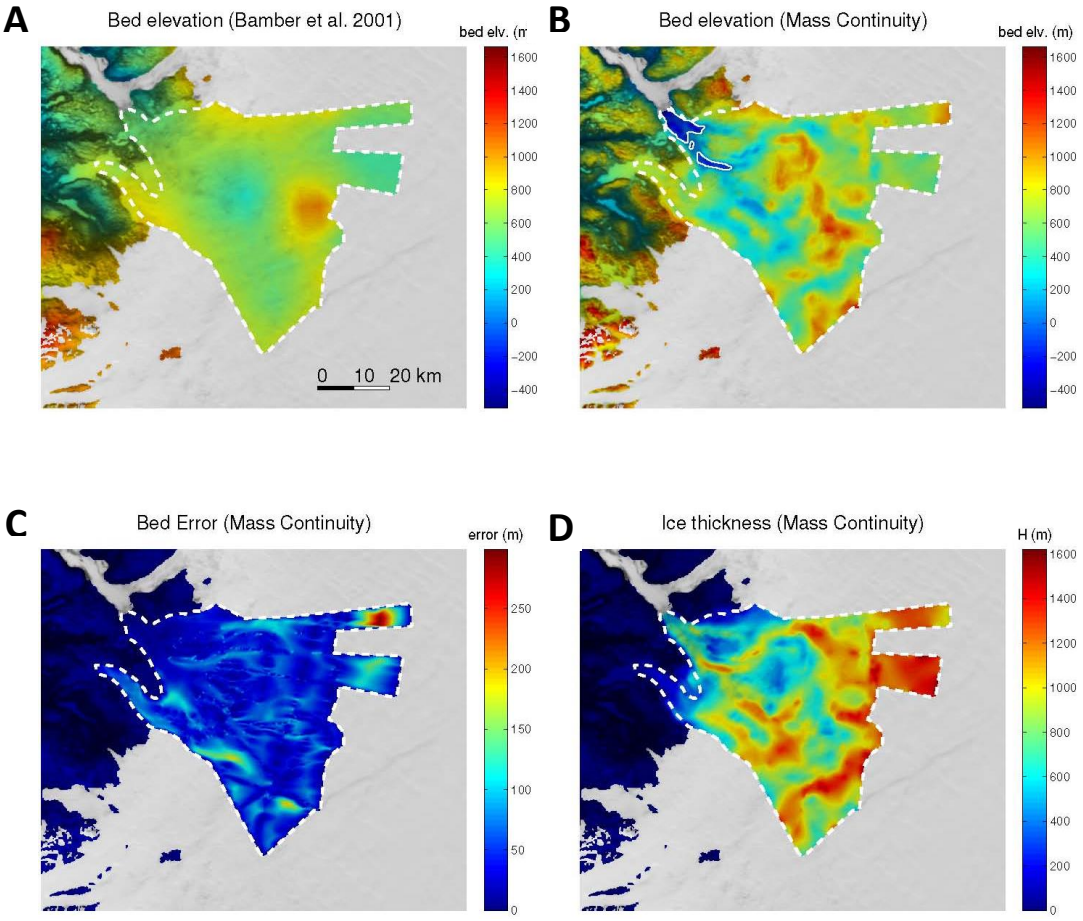

Figure 3.11 Mass continuity approach to subglacial topography reconstruction showing (A) original Bamber et al. (2001) bed topography, (B) the mass continuity bed reconstruction for comparison, with areas below sea level bounded by solid white lines, (C) estimated error for the reconstruction produced, and (D) estimated ice thickness based on the bed topography reconstruction. Data provided by M. Morlighem(U. California, Irvine).

Chapter 4

Evaluation of new and existing methods of tracking glacier terminus change

---

Published in *Journal of Glaciology*. Accepted January, 2014.

Authors: James M. Lea, Douglas W.F. Mair, Brice R. Rea

Affiliation: Department of Geography and the Environment, University of Aberdeen, Elphinstone Road, Aberdeen, AB24 3UF, UK

Citation: Lea, J.M., Mair, D.W.F., Rea, B.R. (2014). Evaluation of new and existing methods of tracking glacier terminus change. *Journal of Glaciology*, 220(60), 323-322. (doi: 10.3189/2014JoG13J061).

Author contributions: JL conducted all analyses and wrote the manuscript. All authors contributed towards the writing process.

Preamble: Effective model validation requires that model output can be accurately compared to observations of glacier terminus change. This is crucial since inaccurate and/or biased observations will have the potential to skew model validation. There are currently a multitude of different methods that have been used to track glacier change (e.g. Moon and Joughin, 2008; Howat and Eddy, 2011; Bevan et al., 2012; Bjørk et al., 2012). A systematic analysis of their relative strengths and weaknesses, potential for systematic bias in certain scenarios, and an evaluation of how this affects the accuracy of each method was therefore required.

To determine which method is most suitable for generating quantitative values of glacier terminus change, each is subject to a range of idealised and real world scenarios. Two new methods were devised to improve accuracy, and allow comparison to a fixed frame of reference such as a fjord centreline/model flowline. The rationale for this was to allow observations of terminus position to be compared directly to model output, thus improving the accuracy of model validation. Results from analyses of idealised and real scenarios are also used to generate a series of recommendations for the relative applicability of individual methods to particular settings/scenarios.

4.1 Abstract

Several different methodologies have previously been employed in the tracking of glacier terminus change, though a systematic comparison of these has not been undertaken. The frequent application of single methods to multiple glaciers over large geographical areas, such as Greenland, raises the question of whether individual methodologies are robust. In this study we evaluate three existing methodologies that have been widely used to track terminus change (the centreline, bow and box methods) against a full range of idealised glaciological scenarios, and six examples of real glaciers. We also evaluate two new methodologies that aim to reduce measurement error compared to the existing methodologies. The first is a modification to the box method that can account for termini retreating through fjords that change orientation (termed the curvilinear box method), while the second determines the average terminus position relative to the glacier centreline using an inverse distance weighting extrapolation (termed the extrapolated centreline method). No single method tested achieved complete accuracy for all scenarios, though the extrapolated centreline method was able to successfully account for variable fjord orientation, width and terminus geometry with the least error.

4.2 Introduction

Quantifying glacier terminus change in a consistent and accurate way is crucial for the accurate monitoring of glacier and ice sheet dynamics over timescales ranging from days to centuries. Multiple methodologies have previously been applied to this problem, each with their own advantages and shortcomings. However, different methods can provide conflicting results when analysing the same glacier termini. As studies are increasingly applying single methods over large geographical areas, trying to quantify terminus change without a knowledge of methodology limitations could result in the unnecessary introduction of errors. This is particularly relevant to studies of Greenland, where retreat of tidewater glacier termini has been both significant and widespread (Box and Decker, 2011; Howat and Eddy, 2011; Jiskoot et al., 2012; Mernild et al., 2012; Moon and Joughin, 2008), especially over decadal to centennial timescales (Bevan et al., 2012; Bjørk et al., 2012). However, the methods discussed below are also of considerable relevance for monitoring tidewater and land terminating terminus change in the other glaciated regions

of the world (e.g. Braun et al., 2011; Cook et al., 2005; Davies et al., 2012; Lopez et al., 2010; VanLooy and Forster, 2008).

In the majority of cases the inconsistencies and inaccuracies between methods will be small. However, where changes in glacier orientation, width or unusual margin geometries occur, significant errors can occur. Under certain circumstances these may render some methods unsuitable for tracking terminus change. Therefore understanding which method is likely to yield the most accurate results in a given scenario is crucial when deciding which methodology to employ. This decision should be based on the aims of the study, level of detail required, and a comprehensive awareness of the advantages and limitations of each methodology. This will allow glacier terminus position to be tracked with greater confidence, and data of greater relevance to the study to be collected. The issues highlighted here are primarily relevant to tidewater calving margins, where terminus geometry can be highly dynamic, and terminus positions can change by several kilometres within a single year. Calving glacier margins account for ~50% of mass loss from Greenland (van den Broeke et al., 2009) and almost all Antarctic mass loss (Rignot et al., 2011), making the accurate tracking of calving margins crucial to improving our understanding of the drivers and controls on dynamics and terminus stability (Murray et al., 2010; Christoffersen et al., 2012; Rignot et al., 2011; 2012).

Existing methodologies that are commonly used to track fluctuations of tidewater calving margins are applied to a range of idealised and real glacier scenarios to evaluate their ability to accurately track terminus retreats of varying complexity. We also present and evaluate two new methods of tracking terminus change including (1) a modification of the ‘box’ method (Moon and Joughin, 2008; Howat and Eddy, 2011) that aims to increase its range of applicability and accuracy, and (2) a method that accounts for the position of the full terminus length relative to the glacier centreline. All of the methods are simple to apply using standard tools available in *ArcGIS v10.1* (ESRI).

4.3 Methods of tracking terminus change

Multiple methods have previously been employed to track changes in calving margin position. The aim of these has been to reduce terminus position to a one-dimensional value representing the distance the glacier has advanced/retreated along its flow axis. The methods that will be analysed in this study are summarised below.

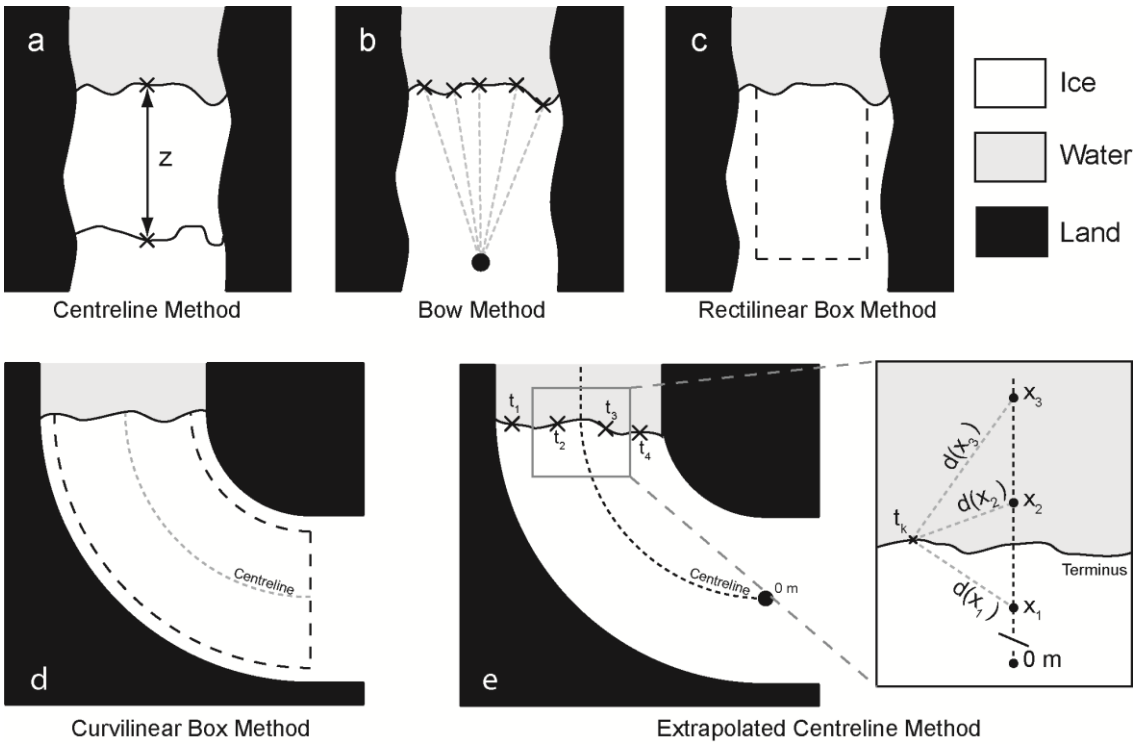

Figure 4.1 Different methods used to ascertain glacier terminus position relative to a fixed point/baseline. (a) Centreline method showing a straight line retreat of the terminus centrepoint by *z*, (b) bow method, showing reference point and the position on the terminus where measurements are taken from (position of reference point relative to the ice front is for illustrative purposes, since it would normally be at least 6 ice widths from the terminus), (c) rectilinear box method, (d) curvilinear box method tracking the glacier centreline, (e) extrapolated centreline method, with inset showing a generalised case of how positions on the glacier centreline, x_n, are related to individual points on the terminus, t_k, with the linear distances between them shown by $d(x_n)$. The inset shows t_k calculated using x_n values taken from a centreline distance range equivalent to the distance between x_1 and x_3.

- *Centreline method* – measures the distance between the centre of successive terminus observations along the glacier flow axis (Figure 4.1a; Bevan et al., 2012; Mernild et al., 2012; Walsh et al., 2012). Definition of the glacier centreline will depend on the aims of a particular study. For example, the centreline can be defined either through manual estimation, as the topographic centreline, or the fastest flow axis of the glacier, while automated methods for determining glacier length have also been employed (e.g. Le Bris and Paul, 2013). In this study, all methods that require a centreline use the topographic centreline, defined as the line representing the mid-point between the lateral ice/fjord margins for the observation where the ice is at its greatest extent. This can be easily and quickly determined by delineating the glacier margins and tracing the line following the maximum Euclidean distance between these down to the glacier terminus. Results of analyses

undertaken will be relevant to centreline dependent methods irrespective of the centreline definition used.

- *Bow method* – determines terminus position relative to a fixed reference point positioned six or more glacier widths upstream from the farthest retreated terminus (Bjørk et al., 2012). At distances ≥6 glacier widths upstream Bjørk et al. (2012) found that terminus change results for a subset of glaciers were convergent. Measurement points are spaced at predetermined distances along the user-delineated terminus, with the average linear distance between these and the reference point giving the overall terminus position (Figure 4.1b). Glacier change can be calculated by simply differencing the relative position values for different termini.
- *Rectilinear box method* – quantifies the change in area between terminus observations of a fixed width rectilinear box drawn over the glacier trunk. This is then converted to a one-dimensional value representing width-averaged terminus change by dividing the area by the width of the box (Figure 4.1c; Howat and Eddy, 2011). This is a variation on the method of Moon and Joughin (2008), who tracked terminus change using boxes that were allowed to have straight, non-parallel sides. The effect of non-parallel sides on results would ideally need correcting for, requiring extra calculations to account for the changing box width for each observation. Further complexities also arise due to the multiple different ways in which box width could be defined, each potentially providing different results for the same termini. For these reasons, and the desire for methodological simplicity, clarity and accuracy, we evaluate only the fixed-width rectilinear box method (hereafter rectilinear box method), since the definition of box width is unambiguous.
- *Curvilinear box method* – as above, however instead of the fixed width box being rectilinear it is curvilinear. This provides a notable advantage over the rectilinear box method in that it allows changes in fjord orientation to be accounted for (Figure 4.1d). This is achieved by generating a box of fixed width tracking the glacier centreline.
- *Extrapolated centreline method* – utilises inverse distance weighting (IDW; Shepard, 1968) to extrapolate positions from the glacier centreline across the complete width of the fjord, allowing the relative position of a terminus to be quantified. The method also allows terminus change to be tracked irrespective of

changing fjord width or orientation. Terminus position is determined by averaging the position of points spaced at regular intervals along a user delineated terminus. The position of each of these points on the terminus, t_k, is an IDW extrapolation calculated from centreline points representing distances of x_n along the centreline (Figure 4.1e). The calculation of t_k first requires determining the weighting value, w, to be allocated for each value of x_n, such that

$$w(x_n) = \frac{1}{d(x_n)^p} \tag{4.1}$$

where $d(x_n)$ = the linear distance between x_n and t_k, and p = the power parameter, which is generally taken to be 2 (Shepard, 1968). Each value of $w(x_n)$ is then normalised so that values of x_n can be extrapolated laterally without tending towards zero with increasing distance from the centreline. This allows each value of t_k to have an equal weighting in the calculation of the overall terminus position, such that

$$w(x_n)_{Norm} = \frac{w(x_n)}{\sum_{n=1}^{m} w(x_n)} \tag{4.2}$$

Before this can be used to calculate t_k according to,

$$t_k = \sum_{n=1}^{m} x_n \, w(x_n)_{Norm} \tag{4.3}$$

where m = the number of centreline positions (i.e. x_n values) used in the calculation. The overall terminus position, T, can then be calculated, such that for q observations of t

$$T = \frac{1}{q} \sum_{k=1}^{q} t_k \tag{4.4}$$

The value of T represents the average distance of the entire terminus from the beginning of the centreline (Figure 4.1e). However, the method in this form without modification is vulnerable to having its results skewed where the centreline is long, and numerous values of x_n occur distal to t_k. To account for this, a search radius for t_k is defined which limits the number of x_n values used in its calculation to a subset. This consists of the x_n values with the lowest associated $d(x_n)$ values within a

defined search radius. The value of m is therefore dependent on the number of x_n values that fall within the search radius. The minimum search radius that should be used for calculation of t_k is determined as part of the experiments conducted below.

This method can be easily applied in *ArcMap v10.1* using the IDW tool to create a raster surface representing the extrapolated centreline, from which T can be calculated for each terminus by extracting their mean z values.

4.4 Glacier configurations tested

Experiments were designed to test the accuracy of each method when subject to different terminus geometries and changes in fjord orientation. By using idealised scenarios rather than comparisons to previously published data, analytical difficulties due to irregular terminus/fjord geometries, differences in user delineation of glacier termini and image resolution are avoided. This allows errors that result solely from the methodologies to be analysed. Finally each method is applied to tracking examples of actual glacier termini, with differences in the results analysed with reference to the idealised scenarios.

4.4.1 Idealised glacier scenarios

Figure 4.2 displays the seven idealised glacier retreat scenarios tested. Each scenario was constructed so a terminus undergoes a width-averaged retreat of R. For simplicity, R is taken to be equal to a single glacier width, W. All results are referred to in terms of glacier retreat, though the inverse of the results from these tests will be relevant for equivalent glacier advances. The experiment scenarios constructed are:

a) Retreat of a linear terminus by R to form a new parallel terminus in a straight fjord (Figure 4.2a)
b) Width averaged retreat of a linear terminus by R to form a new symmetric terminus with a calving bay of $0.25R$ in a straight fjord (Figure 4.2b)
c) Width averaged retreat of a linear terminus by R to form a new asymmetric terminus, with the asymmetry hinged on the centreline (at $0.5W$), and a calving bay of $0.25R$ in a straight fjord (Figure 4.2c)
d) Width averaged retreat of a linear terminus by R to form a new asymmetric terminus, with the asymmetry offset from the centreline by $0.25W$, and a calving bay of $0.5R$ in a straight fjord (Figure 4.2d)

e) Width averaged retreat of a linear terminus by *R* to form a new parallel terminus in a fjord that has changed orientation. The retreated terminus is offset to the right by 0.5*W* (Figure 4.2e)

f) As *e*, but the retreated terminus is positioned perpendicular to the fjord wall (Figure 4.2f).

g) As *e*, but the retreated terminus has a calving bay of 0.25*R* symmetric along the glacier centreline (Figure 4.2g)

In reality, the challenge of tracking glacier terminus change reflects a combination of some or all of the above scenarios.

4.4.2 Real glacier examples

To allow an inter-comparison of results from the different methods, six Greenlandic tidewater glaciers exhibiting a range of retreat behaviour were selected for analysis (Figure 4.3). Together they exemplify a number of potentially problematic scenarios that can arise when tracking change of real termini. The glaciers selected were Narssap Sermia (NS; 64.64° N 49.97° W), Jakobshavn Isbræ (JI; 68.17° N 49.85° W), Petermann Glacier (PG; 80.78° N 60.61° W), Helheim Glacier (HG; 68.61° N 32.93° W), Qalerallit Sermia West 1 (QSW1), and Qalerallit Sermia West 2 (QSW2; 61.04° N 46.72° W). Some of the issues

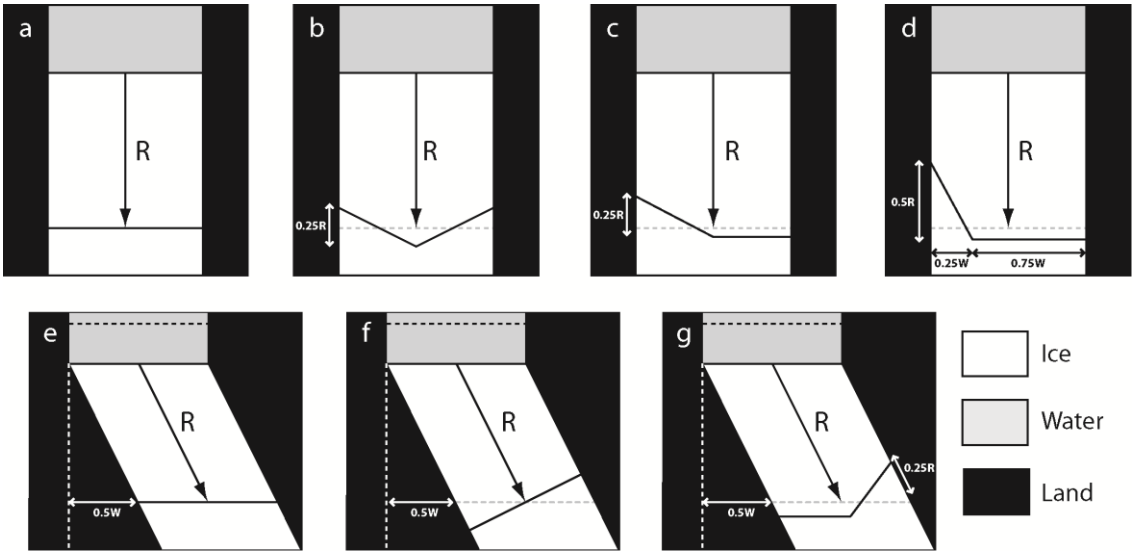

Figure 4.2 Experiments showing the idealised scenarios, where *R* is an identical width averaged retreat for each experiment. The letters of each experiment conform to those indicated in the text. The grey dashed line indicates a width averaged retreat of *R* parallel to the original terminus. Where the rectilinear box method is applied to experiments *e-g*, the box is orientated so that the upstream edge of the box is both parallel to, and centred on the black dashed line indicated. Unless specified in the text, the curvilinear box used for experiments *e-g* is of width *W* and tracks the fjord width.

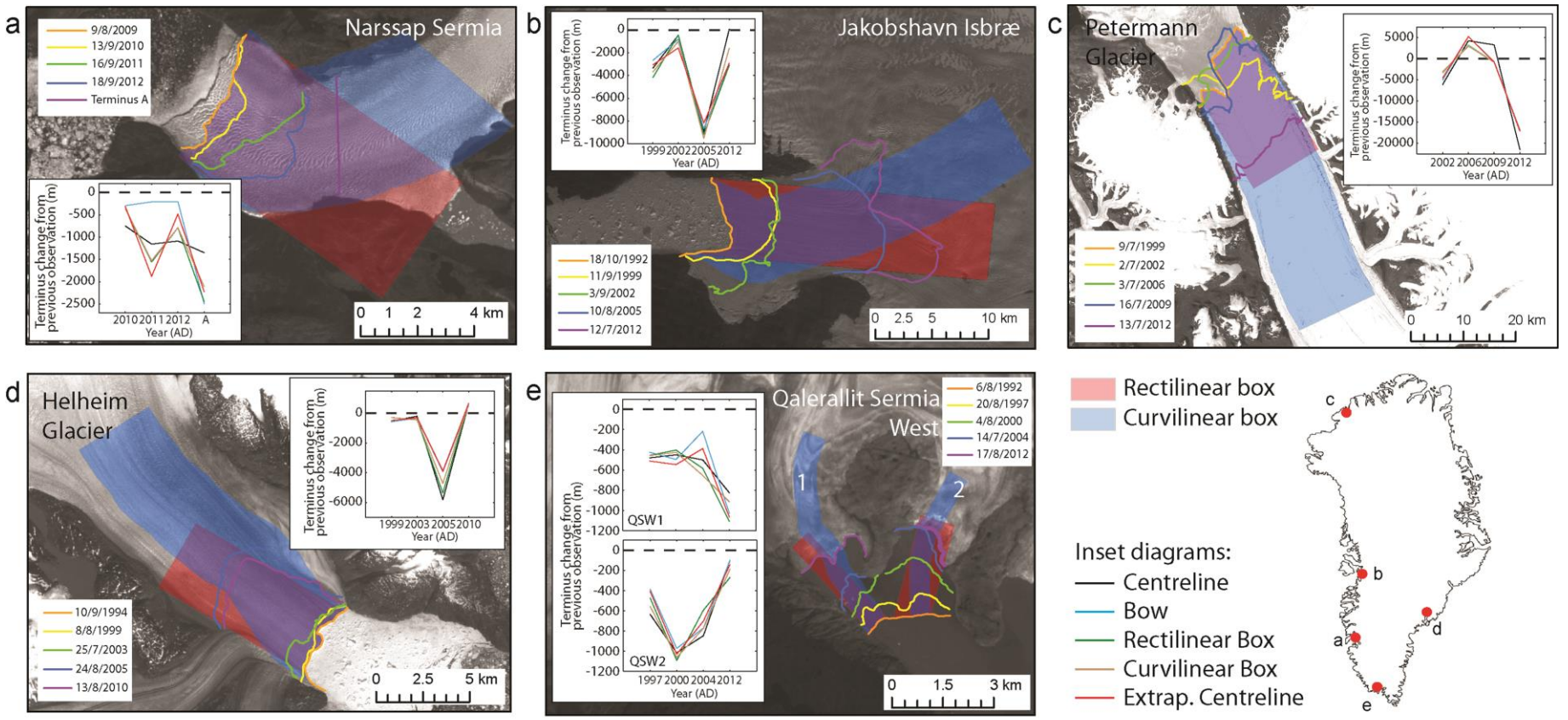

Figure 4.3 Landsat based observations of terminus change at 6 Greenlandic glaciers, and the results given by different methods of tracking terminus change (inset). Glaciers shown are (a) Narssap Sermia (64.64° N 49.97° W), (b) Jakobshavn Isbræ (68.17° N 49.85° W), (c) Petermann Glacier (80.78° N 60.61° W), (d) Helheim Glacier (68.61° N 32.93° W), (e) Qalerallit Sermia West 1, and Qalerallit Sermia West 2 (61.04° N 46.72° W). The rectilinear and curvilinear boxes used to track terminus change are overlaid on the images. Box width was limited to that of the narrowest terminus observation.

associated with the retreat of these glaciers include; the termini of NS changing orientation within the fjord, and demonstrating asymmetry and increasing complexity across the time series analysed; the width of JI changing significantly during its retreat, while embayments with relatively stagnant ice also exist; the terminus of PG is an ice shelf meaning that periodically large calving events of tabular icebergs occur, and identification of the terminus itself can be problematic; HG is a fast flowing glacier retreating through a straight fjord that experiences significant changes in terminus geometry; and QSW retreats from being a single glacier to form two separate termini that are analysed separately (named here as QSW1 and QSW2).

For each glacier, five terminus positions acquired between 1992 and 2012 were delineated from Landsat panchromatic band images, and terminus change quantified using each method. For JI and HG images were preselected for the period after the mélange in their fjord has broken up to allow easier definition of their termini. Termini were delineated at a level of image magnification that allowed individual pixels to be visually resolved. This allowed a consistent level of detail to be maintained when delineating individual termini from different glaciers.

NS was subject to extra experiments (see below) to demonstrate how the bow and box methods deal with issues pertaining to terminus asymmetry, width and fjord orientation when applied to real glaciers. Its terminus retreated significantly between 2009 and 2012 having previously maintained an approximately stable terminus position since the end of the Little Ice Age (Figure 4.4; Weidick et al.; 2012). To allow the relative effects of a change in fjord orientation to be fully evaluated, a straight terminus of semi-arbitrary orientation was also positioned upstream of the 2012 terminus (Terminus A; Figure 4.4).

4.5 Experiments

Terminus change was calculated for all the scenarios outlined, according to the methodologies described above. To allow full interrogation of the methods, additional method-specific experiments were also undertaken for the bow, box and extrapolated centreline methods as described below:

Bow method experiment – the distance between the reference and measurement points used for the bow method is known to exert control on the accuracy and consistency of its

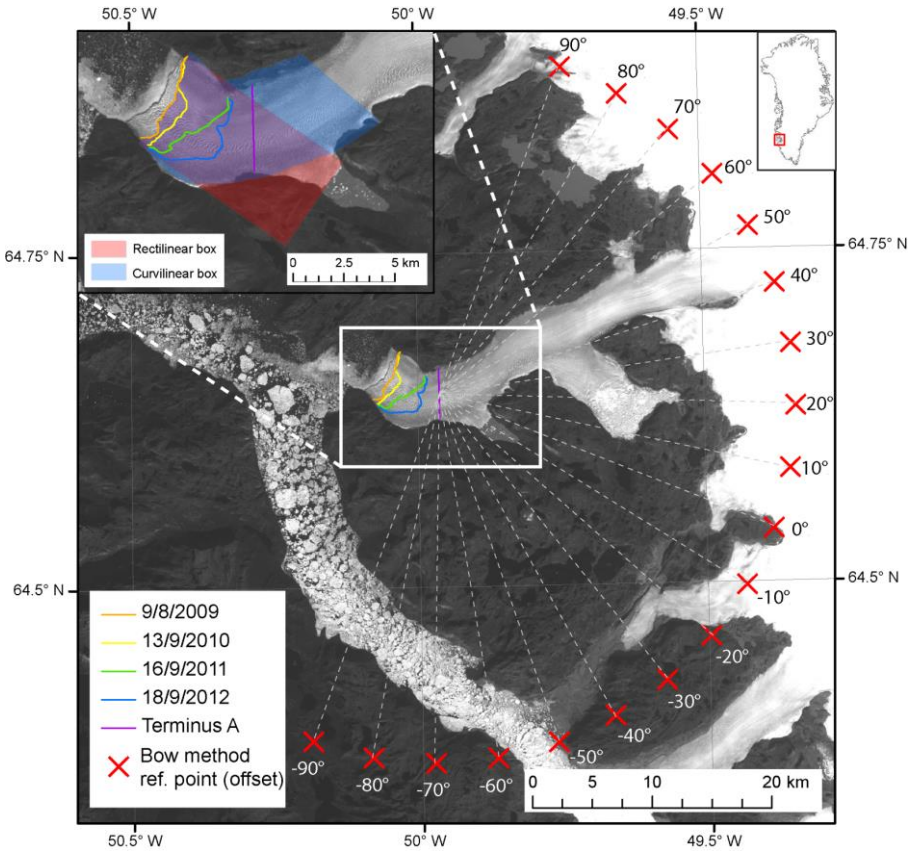

Figure 4.4 Location map of Narssap Sermia showing the reference points used in the bow method indicated by the red crosses, and their associated offsets from a semi-arbitrary 0° position centred on Terminus A. Each reference point is positioned at least 6*W* from Terminus A. The background Landsat image shown was acquired on 15/9/1987.

results (Bjørk et al., 2012). However, the effect of the reference point positions relative to fjord and terminus orientations has not been established. Consequently, the range of effects that could result from changes in fjord orientation upstream of the termini were evaluated by quantifying terminus change for experiments *a*-g using 19 different reference points positioned 6*W* behind the terminus distributed evenly along a 180° arc at 10° intervals. This experiment was also conducted over the same range of reference points for NS to demonstrate how reference point position can affect results for real termini (Figure 4.4). Although the majority of fjord orientations will change by significantly <90° from their original terminus orientation, testing a large range of reference point positions allows the effects of a comprehensive range of potential changes in fjord orientation to be evaluated. The points on the termini used in the calculation of overall position were spaced equidistantly along each terminus at 0.01*W* intervals for scenarios *a-g* and 10 m intervals for NS.

Box method experiment – one of the primary advantages of the box methods are that they are capable of accounting for the natural asymmetry of glacier termini (Moon and

Joughin, 2008). However, since it is necessary to use boxes of fixed width for the method, it is inevitable that parts of the fjord terminus margins will fall either outside or inside the predefined box. To test the relative importance of this, boxes of 0.25-2*W* width (with 0.25*W* increments) were applied to scenarios *a-g*, while boxes of 1-7 km width (with 1 km increments) were applied to NS. This was done for both the rectilinear and curvilinear box methods. Where the terminus end of the box was wider than the delineated glacier terminus, the box was closed by extending the terminus edges with straight lines perpendicular to the upstream edge of the box for the rectilinear box method, and with lines perpendicular to the centreline of the box for the curvilinear box method.

The aim of this experiment is to test the sensitivity of both box methods to the proportion of the glacier terminus that is included in the calculation of terminus change.

Extrapolated centreline experiment – to allow the method to be evaluated in a non-dimensionalised manner for experiments *a-g*, the search radius that defines the number of x_n values used in the calculation of each t_k value needs to be defined in a clear and consistent way. This experiment aims to determine over what scales of search radii the calculated terminus positions begin to converge, so that the value of the search radius can be standardised. Different search radii are tested, from a minimum using individual x_n values in the calculation of t_k, to ranges of x_n values from taken over a centreline distance of 3*W*. These are then applied to the scenarios *e-g* where termini retreat a distance of *R* through a fjord that has changed orientation and exhibit different terminus geometries. Terminus position was calculated from points positioned on the terminus at 0.01*W* intervals, while points representing values of x_n on the centreline were also separated by 0.01*W*.

4.6 Results

4.6.1 Centreline Method

While simple and quick to implement, the centreline method does not account for the full complexity of terminus geometries, and hence cannot provide an accurate value of width-averaged retreat. This is highlighted in experiments *b*, *c*, *d* and *g* where the method overestimates terminus retreat (Table 4.1). Terminus geometry therefore exerts a strong control on the accuracy and applicability of the centreline method.

Experiment	Centreline	Bow	Rectilinear Box	Curvilinear Box	Extrapolated Centreline
a	1	1	1	1	1
b	1.13	1	1	1	1
c	1.06	0.99	1	1	0.99
d	1.06	0.95	1	1	0.95
e	1	0.82	0.87	1	0.98
f	1	0.81	1.05	1	0.93
g	1.13	0.81	0.99	1	0.93

Table 4.1 Summary of results from each method after application to each of the idealised scenarios shown in Figure 2. Results for rectilinear and curvilinear box methods are for box widths of *W* only. All results are given in terms of *R*.

4.6.2 Bow Method

The bow method accurately calculates width-averaged retreat for experiments *a* and *b*, though underestimates terminus retreat in the remaining scenarios (Table 4.1). When compared to Figure 4.5a the underestimates for experiments *e-g* are caused by the position of the reference point relative to the change in fjord orientation. In these cases, the correct retreat value is obtained for reference points offset ~40° from the original (Figure 4.5a). A line from this reference point would be orientated perpendicular to the termini of experiments *e-g*. The error produced by the method can be significant depending on the position of the reference point used to measure terminus retreat, with the -80° and -90° offsets of experiments *e-g* even showing the terminus to have advanced (Figure 4.5a).

The bow method also underestimates retreat for experiment *c*, and more significantly for experiment *d*, where the retreated terminus has a more pronounced asymmetry (Table 4.1). The results curves are also laterally offset to towards the relative

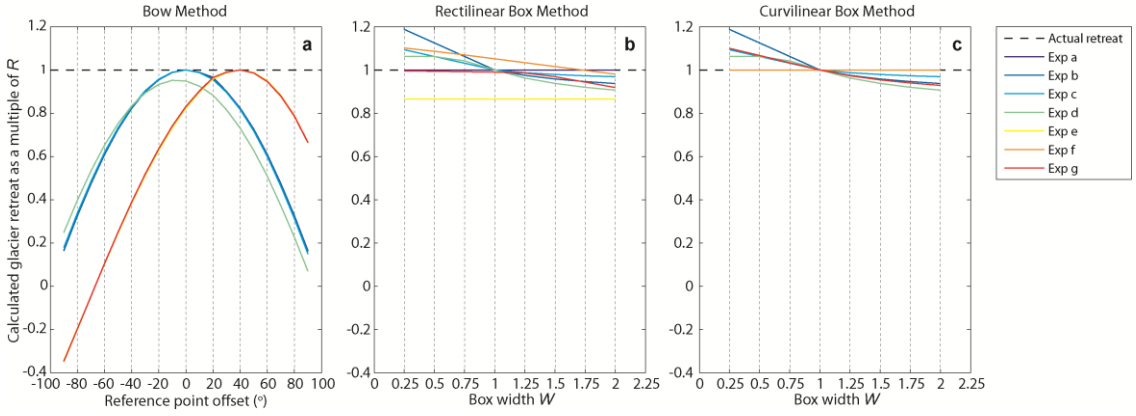

Figure 4.5 Results of experiments testing sensitivity of: (A) the bow method to changes in the position of the reference point from which measurements are taken; (B) the sensitivity of the rectilinear box method and (C) the curvilinear box method to different box widths. The results are from each method applied to the experiments shown in Figure 4.2.

position of terminus asymmetry, compared to the results of experiments *a*-*b* (Figure 4.5a). This offset is greater for the more asymmetric experiment *d*, indicating that terminus asymmetry also exerts a control on the relative accuracy of the technique. However, the effects of terminus asymmetry are markedly less significant than that of the relative positioning of the reference point.

4.6.3 Rectilinear and Curvilinear Box Methods

Where box width equals terminus width, the curvilinear box method successfully measures width-averaged retreat across all scenarios, while the rectilinear box method demonstrates a dependence on fjord orientation (experiment *e*) and terminus geometry (experiment *f*; Table 4.1). The results from the curvilinear box method for experiments *f* and *g* replicated the results from experiments *a* and *b* for the rectilinear method. This demonstrates that the curvilinear method accurately accounts for changing fjord orientation, provided that the box width is identical to that of the terminus (Figure 4.5c; Table 4.1).

Where the boxes were less than the full glacier width, terminus geometry dictated the accuracy of both the rectilinear and curvilinear box methods (Figures 4.5b, 4.5c). For box widths greater than the idealised terminus widths, the curvilinear box method consistently underestimated retreat, with the scale of this underestimation increasing with box width (Figure 4.5c). The overall magnitude of underestimation by the curvilinear box method is dependent on terminus geometry, with only linear termini (experiments *a*, *e* and *f*) being unaffected. By comparison, terminus geometry and changing fjord orientation can result in the rectilinear box method producing both under- and over-estimates where the box is wider than the glacier terminus being measured.

4.6.4 Extrapolated Centreline Method

The initial extrapolated centreline method experiment shows that changing the ranges of x_n values used to calculate values of t_k has minimal effect, with a ±2.5% range of results observed (Figure 4.6). As the search radius increases towards W the method becomes more accurate across all experiment scenarios, with search radii $>W$ producing generally concordant results (Figure 4.6). Consequently, for subsequent analyses, values of t_k were calculated using the nearest x_n values taken from a stretch of the centreline of W length. This was also used for the application of the extrapolated centreline method to NS (where $W \approx 5$ km).

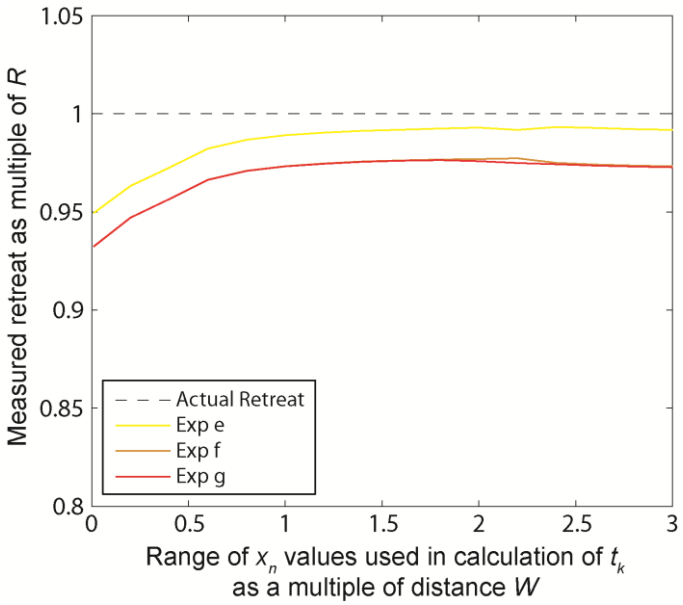

Figure 4.6 Results testing sensitivity of the extrapolated centreline method to the different range of x_n values used in the calculation of t_k and how that affects overall calculated terminus position.

The results of the extrapolated centreline method demonstrate that it succeeds in accurately calculating terminus retreat where termini are symmetrical, however underestimates retreat where termini are asymmetric (Table 4.1). Comparing the results of experiment *c* to experiment *d*, the error increases with asymmetry, though the magnitude of this is still ≤5% (Table 4.1). This demonstrates that the method is capable of accounting for changes in fjord orientation, though is prone to small errors where complex terminus geometries occur.

4.6.5 Narssap Sermia experiments

As observed with scenarios *a-g*, results given by the bow method for NS are also dependent on the positioning of the reference point relative to the termini (Figures 4.4 and 4.7a). For all box sizes tested, the general pattern of retreat calculated by both box methods is comparable (Figures 4.7b, 4.7c). Where the box widths are less than the terminus width of NS (~5 km), the two box methods generate different values since the boxes have different orientations. Therefore even though the boxes may have identical widths, the two methods will be tracking change between different sections of the termini. Nevertheless, both the curvilinear and rectilinear box methods produce very similar results for the retreat of NS from 2009-2012 (Figures 4.7b, 4.7c). However, where the fjord changes orientation for 2012-Terminus A, the rectilinear box method disagrees with that of the curvilinear box method, exceeding it by 339 m (Figure 4.3a).

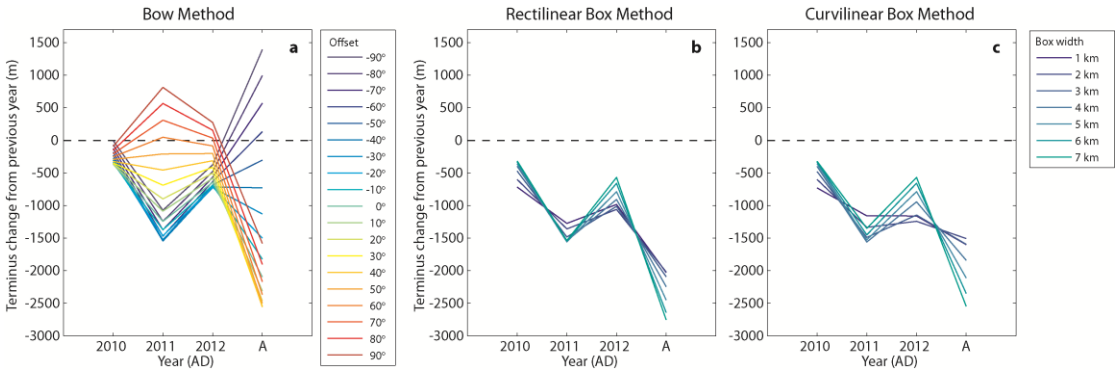

Figure 4.7 Comparison of results tracking the change of Narssap Sermia, showing the sensitivity of: (a) the bow method to changes in the position of the reference point from which measurements are taken; the sensitivity of (b) the rectilinear box method and (c) the curvilinear box method to different box widths.

For the bow method no single reference point from the 180° arc displays comparable results to the box or centreline methods for the entire record from 2009-Terminus A (Figure 4.7). However, a similar pattern and magnitude of change can be extracted from the bow method by using the results of all of the reference points in the 180° arc and taking the single largest retreat value for each year to create a record of terminus change (Figure 4.7).

Different box widths display no systematic behaviour of over or under-estimation between the different NS terminus observations (Figures 4.7b, 4.7c). This is likely a result of differing terminus geometries between observations. A change of fjord orientation can be ruled out as a causal factor of this since for the period between 2009-2012, retreat occurs in a relatively straight section of the fjord (Figure 4.3a). Where the boxes are less than the full terminus width (i.e. <5 km), the magnitude of terminus change values is reduced. Boxes that overlap the fjord edges (i.e. >5 km) tend to display the extreme upper and lower values for terminus change (Figures 4.7b, 4.7c).

4.6.6 Real glacier method intercomparison

Figure 4.3 shows the results of different methods applied to the termini of six Greenlandic tidewater glaciers. Significant variability in the results exists, with no method displaying a consistent bias for under or over-estimation compared to others. In most cases each method produces the same general pattern of terminus change, though the absolute numbers can vary considerably, with examples of discrepancies up to 1.94 km at HG (2003-2005), and 4.76 km at PG (2009-2012; Figures 4.3c and 4.3d). In some cases the methods identify differing patterns of retreat, an example being the bow and extrapolated centreline method results contrasting with those of the other three methods at QSW1 after its terminus becomes diffluent from QSW2 (Figure 4.3e). The bow method also estimates significantly

less retreat compared to the others at NS (a difference of up to 1.67 km), after the termini change orientation by 2011 (Figure 4.3a). Prior to this, terminus observations are positioned directly behind the bow method reference point, with these results being more concordant with other methods compared to subsequent observations. A further notable discrepancy occurs at JI, where the centreline method estimates an advance (84 m between 2005-2012) with other methods estimating a retreat of between 1.58 km to 3.12 km.

4.7 Discussion

Overall, the analyses above allow a distinction to be made between three broad styles of measuring glacier terminus change along a flow axis, namely; one-dimensional terminus change (e.g. centreline method), length averaged change (e.g. bow and extrapolated centreline methods), and area/width averaged change (e.g. rectilinear and curvilinear box methods). When deciding which to apply the choice should primarily be based on an explicit justification of which method is capable of providing the most relevant data to fulfil the aims of a study. Factors that need to be considered with respect to this include (1) whether using a method that quantifies length averaged change or area/width averaged change is relevant to the aims of the study, (2) the level of detail required (3) the importance of accounting for changes in terminus width, (4) any changes in fjord orientation, (5) whether terminus geometries display significant asymmetry or complexity, and (6) whether a specific definition of the centreline or flow axis could significantly affect results. Table 4.2 provides a summary of scenarios where each method is, and is not reliable in providing accurate results. Given the importance of terminus setting variability, the decision as to which method to use should only be made after all termini have been delineated. This will allow comprehensive evaluation of whether certain methods may be comparatively more susceptible to error for particular terminus settings.

An example scenario would be if areas of stagnant/slow flowing ice are not relevant to a study. In such situations including terminus margins, where the occurrence of stagnant ice is most common, may not be necessary and lead to the inclusion of irrelevant information in the data collected. The curvilinear box method may be best suited to such scenarios, given its ability to account for changing orientation along a flow axis. However, if significant width changes occur the extrapolated centreline method could also be usefully applied. This would be relevant if the part of the terminus that is of interest (e.g. ice flowing above a certain velocity) is not of a fixed width.

Method	Capable of accounting for… Fjord orientation	Fjord width	Terminus geometry	Dependent on centreline?
Centreline	Y			Y
Bow		Y	Y*	
Rectilinear box			Y	
Curvilinear box	Y		Y	Y
Extrap. Cen.	Y	Y	Y*	Y

Table 4.2 Summary of situations that each method is capable of accurately accounting for (Y = Yes), and whether results may be dependent on how a centreline is defined. Asterisks highlight that the bow and extrapolated centreline methods do have some dependence on terminus geometry though as explained in the text this is in most cases negligible.

Evaluation of methods

The centreline method has been shown to be the least broadly applicable method over a range of scenarios (Table 4.2). Results from scenarios *a-g* demonstrate that it is incapable of determining width-averaged terminus change, and commonly displays little absolute agreement with any other method (Table 4.1; Figure 4.3). Conversely, the method is possibly the quickest and easiest to implement, and mostly successfully identifies the general pattern of terminus change on the real world glacier examples (Figure 4.3). However, considerable caution should be exercised in the application of this method since it is prone to significant error in both absolute and relative terms. It is vulnerable to substantial under and over estimation of terminus change depending on terminus geometry, recording an advance at JI of 84 m between 2005-2012 when the terminus has clearly retreated substantially (Figure 4.3b). The ability of the method to account for changes in fjord orientation provides an advantage over the rectilinear box and bow methods which are both constrained by fixed frames of reference. The centreline method should therefore be considered useful as a method for gaining cursory insight into the large scale changes occurring at a glacier terminus, though due to its inability to reflect width-averaged change its application to detailed studies of tidewater terminus dynamics should be avoided. It is more suited to tracking changes at land terminating margins where terminus response is likely to be more symmetric (e.g. Lopez et al, 2010; Leclerq and Oerlemans, 2012).

The sensitivity of the bow method to terminus shape, fjord orientation and reference point positioning is demonstrated by the results of both idealised (Table 4.1;

Figure 4.5a) and real glacier analyses (Figures 4.3 and 4.7a). While the general pattern of retreat can be extracted from an arc of reference points, as exemplified by results from NS (Figure 4.7a), this adds complexity to the method requiring extra calculation and user input, compromising the simplicity of the method. Furthermore, since the bow method calculates terminus position using straight line distances from the reference point, this means the method is unable to accurately track terminus change directly along the glacier flow axis when fjord orientation changes. In these situations the method will underestimate the along-glacier distance between the reference point and positions on the terminus. This is likely to be even more significant for smaller non-ice-sheet glaciers where changes in fjord/valley orientation compared to their overall size can be considerable.

Although scenarios *c* and *d* show that effects of terminus asymmetry on the accuracy of the bow method are small, the impact of the relative positioning of the reference point on the end results are significant. The bow method should only be applied on straight glaciers, where the termini to be measured are near-linear and approximately parallel, otherwise the positioning of the reference point may significantly affect results. This is demonstrated by results from NS where termini change orientation and are highly asymmetric (Figure 4.3a).

Both the rectilinear and curvilinear box methods performed well in tracking the terminus change of glaciers of uniform width, though results from the idealised and real scenarios indicate that the latter has wider applicability (Table 4.1; Figures 4.3, 4.5b, 4.5c). When tracking NS terminus change using different box widths, the larger spread of values given by the curvilinear box method compared to the rectilinear method can be accounted for by the two methods measuring different sections of the termini (Figures 4.4, 4.7b, 4.7c). This is because the centre of the rectilinear box will differ from the curvilinear box, as the latter tracks the glacier centreline while the former is indirectly defined by the user when the rectilinear box is drawn. This demonstrates how terminus geometry can significantly affect box method results where the entire width of the glacier is not used to calculate terminus change (Figures 4.5b, 4.5c). This was a significant problem for NS, JI, HG, QSW1 and QSW2 where box widths (limited in size to the narrowest terminus observation) were in some cases unable to cover significant fractions of the delineated termini. This is best exemplified at QSW1 where the pattern of terminus retreat differed significantly from the bow and extrapolated centreline methods that account for full glacier widths (Figure 4.3e).

Conversely, where termini are of roughly uniform width, the curvilinear box method is fully capable of tracking fjord orientation changes and accounting for complex terminus geometries (Tables 1 and 2; Figure 4.3c). Due to its inability to track changes in fjord orientation, the rectilinear box method should only be applied where glaciers retreat through a straight fjord.

It is worth noting that a further variation on the box method could potentially account for changes in glacier width and orientation. This would be achieved through dividing the terminus area into multiple adjoining boxes that are (1) orientated parallel with one another (2) of equal 'b-axis' length (i.e. short axis approximately parallel with flow axis), and (3) of variable 'a-axis' length (i.e. long axis approximately perpendicular to flow axis), allowing changes in fjord width and orientation to be tracked. The accuracy of the method would also improve as the 'b-axis' length is decreased, and the fjord geometry is more accurately captured by the boxes. Application of this method is complex compared to the other methods discussed and hence beyond the confines of this study, however if it could be automated then it would prove a highly accurate method of tracking area/width averaged terminus change.

The extrapolated centreline method performs well where termini are regular, and successfully tracks most asymmetric and complex termini with minimal error (Table 4.1; Figure 4.3). It was anticipated that significant issues with terminus asymmetry and/or complexity may arise when tracking the termini of glaciers such as PG, where the margins are often comparatively fractured. This means that a significant fraction of the total length of their termini can be located near their margins (Figure 4.3c). The effect of this would be to disproportionately weight the terminus position towards the terminus position of the ice margins. However, results for PG proved comparable to other methods (Figure 4.3c). Nevertheless, this is an issue that should be considered before applying the method to termini with significantly fractured margins. Elsewhere the effect of terminus asymmetry will be less significant, with the idealised retreats showing an error of <5% (Table 4.1; Figure 4.6). In most cases, this will lie within the operator delineation error.

Notable advantages of the extrapolated centreline method include its ability to account for the entire terminus length irrespective of changes in glacier width, in addition to changes in fjord orientation. This proved to be especially useful where advance/retreat occurs through a glacier or fjord confluence such as at QSW, or where the terminus area of interest may change between observations.

Finally, the absolute uncertainty surrounding the delineation of each individual terminus position is worth brief consideration. If a given terminus observation is delineated multiple times, and the range of values determined, the absolute error will be different for each method for similar reasons to those outlined above. Nevertheless, where imagery such as Landsat or MODIS is used, the absolute error values in the delineation of individual termini are likely to be negligible compared to the absolute differences given by different terminus change methods (Figure 4.3).

4.8 Conclusions

When selecting a method to track glacier terminus change it is important to consider the aims of the study, and the limitations of each method with regards to changes in glacier width, fjord orientation and terminus geometry. Each method was tested using idealised scenarios designed to highlight potential shortcomings, and hence under which situations each method can be confidently applied. The methods were also applied to real glacier scenarios to highlight where methods can show disagreement, in addition to some of the practical issues that affect terminus tracking. From the results presented, the curvilinear box method accurately measures width averaged retreat, though is unable to fully account for changes in glacier width without incorporating some error. The extrapolated centreline method also performed well in a wide range of scenarios, successfully tracking changes in fjord orientation, width and terminus geometries with minimal associated error. Although potential caveats apply for its application to calving margins similar to PG, results generated were comparable to those of the curvilinear box method for the termini analysed.

These two methodologies represent improvements on existing methods as they fully account for changes in fjord orientation. However, since the extrapolated centreline method is the only method that can directly account for changing fjord orientation, width and terminus geometry, it represents the most accurate method over the widest range of scenarios. The simplicity of the method also means that results can be generated easily and rapidly in only a few steps within GIS software packages such as *ArcMap* for any set of delineated glacier termini. This simplicity and range of applicability is important if attempts are made to track terminus changes across multiple glaciers at regional to continental scale using a single method.

Different methods can still be applied with confidence depending on the level of detail required for a study, the topic of interest, and if individual glacier terminus settings

have been carefully evaluated. However, it is likely that such studies should be looking at either coarse scale changes or be limited in the number of termini they seek to analyse. While results produced may be acceptable, using the extrapolated centreline method will provide a high level of accuracy, is applicable to the majority of settings, and minimises the risk of introducing potentially significant methodological error into results.

Chapter 5

Terminus driven retreat of a major SW Greenland tidewater glacier during the early nineteenth century: insights from glacier reconstructions and numerical modelling

---

Published in *Journal of Glaciology*. Accepted January, 2014.

Authors: James M. Lea[1], Douglas W.F. Mair[1], Faezeh M. Nick[2,3], Brice R. Rea[1], Anker Weidick[4], Kurt H. Kjær[5], Mathieu Morlighem[6], Dirk van As[4], J. Edward Schofield[1]

Affiliations:

[1]Department of Geography and the Environment, University of Aberdeen, Elphinstone Road, Aberdeen, AB24 3UF, UK

[2]The University Centre in Svalbard (UNIS), PO Box 156, NO-9171 Longyearbyen, Norway

[3]Centre for Ice and Climate, Niels Bohr Institute, University of Copenhagen, Copenhagen, 2100, Denmark

[4] Geological Survey of Denmark and Greenland (GEUS), Copenhagen, Denmark

[5]Centre for GeoGenetics, Natural History Museum of Denmark, University of Copenhagen, Øster Voldgade 5-7, 1350 Copenhagen K, Denmark

[6]University of California, Irvine, Department of Earth System Science, Croul Hall, Irvine, CA 92697-3100, USA

Citation: Lea, J.M., Mair, D.W.F., Nick, F.M., Rea, B.R., Weidick, A., Kjær, K.H., Morlighem, M., van As, D., Schofield, J.E. (2014). Terminus driven retreat of a major SW Greenland tidewater glacier during the early nineteenth century: insights from glacier reconstructions and numerical modelling. *Journal of Glaciology*, 220(60). (doi: 10.3189/2014JoG13J163)

Author contributions: JL wrote the manuscript and conducted all numerical modelling, geomorphological mapping and glacial reconstructions. FMN wrote the numerical model used; AW provided historical imagery; KHK provided the digital elevation model used as part of Figures 5.1, and 5.4, with data extracted from it used in Figures 5.2 and 5.9; MM provided a digital elevation model for the lower 40 km of subglacial topography; DvA

provided catchment boundaries used to define width in the model and modelled runoff data. All authors contributed to the writing process.

Preamble: This paper presents a reconstruction of the behaviour of KNS and its modelled sensitivity to climate for the period before climate records are available. The reconstruction is achieved using previously unstudied source material, and a reanalysis of previously identified sources. GIS based analyses are also utilised in a novel manner to gain quantitative estimates of glacier position from qualitative source material. Glacier positions and longitudinal profiles derived from geomorphology are also reconstructed using methods described in Chapter 4, allowing a one-to-one comparison of observations/reconstructions with model data. These analyses result in some significant differences in reconstructed glacier extent compared to previous studies (e.g. Weidick et al., 2012), and the first estimate of when KNS was at its Little Ice Age maximum. Glacier sensitivity to changes in climate forcing is also evaluated through extensive sensitivity tests relating to changes in SMB, crevasse water depth and submarine melt rates. Results from model runs are used to provide information regarding the timescale response of KNS to changes in forcing, and therefore the likely drivers of observed behaviour.

5.1 Abstract

Tidewater glaciers in Greenland experienced widespread retreat during the last century. Information on their behaviour prior to this is often poorly constrained due to a lack of observations, while determining the drivers prior to instrumental records is also problematic. Here we present a record of the dynamics of Kangiata Nunaata Sermia (KNS), SW Greenland, from its Little Ice Age maximum (LIAmax) to 1859 – the period before continuous air temperature observations began at Nuuk in 1866. Using glacial geomorphology, historical accounts, photographs, and GIS analyses, we provide evidence KNS was at its LIAmax by 1761, had retreated by ~5 km by 1808, and a further 7 km by 1859. This predates retreat at Jakobshavn Isbræ by 43-113 years, demonstrating the asynchroneity of tidewater glacier terminus response following the LIA. We also use a one-dimensional flow-band model to determine the relative sensitivity of KNS to atmospheric and oceanic climate forcing. Results demonstrate that terminus forcing rather than surface mass balance drove the retreat. Modelled glacier sensitivity to submarine melt rates is also insufficient to explain the retreat observed. However, moderate increases in

crevasse water depth, driving an increase in calving, are capable of causing terminus retreat of the observed magnitude and timing.

5.2 Introduction

Tidewater glaciers (TWGs) exert a major control on the short and long term mass balance of the Greenland Ice Sheet (Van den Broeke et al., 2009; Alley et al., 2010; Bevan et al., 2012). The availability of satellite data have allowed their dynamics to be documented in detail over the last two decades (Moon and Joughin, 2008; Box and Decker, 2010; Moon et al., 2012). Prior to this, TWG dynamics are poorly constrained by observations, placing limitations on the knowledge of their response to climate change. Multi-decadal records of terminus fluctuations are available for some TWGs back to the 1930s, and limited direct observations exist before this (Bjørk et al., 2012). Therefore, limited potential exists to extend TWG records to their Little Ice Age maxima (LIAmax) due to the sparse and often indirect nature of observations (Weidick, 1959; 1968; Briner et al., 2010; Larsen et al., 2011). Characterisation of TWG behaviour during the 18th and 19th centuries is therefore problematic. However, where this is possible it provides insights into centennial timescale TWG behaviour, and important context for contemporary observations and potential TWG response to future climate forcing.

Predicting the response of the Greenland Ice Sheet (GrIS) to climate change is dependent on understanding how TWG processes and behaviour are affected by climatic forcings (Van den Broeke et al., 2009; Rignot et al., 2011). Although TWG stability is thought to be controlled by a combination of atmospheric and oceanic forcings occurring at the terminus, the precise processes and their relative importance are still poorly understood (Holland et al., 2008; Nick et al., 2009; Murray et al., 2010; Straneo et al., 2010; 2012; Rignot et al., 2010; 2012). Modelling of GrIS is limited further by the short observation periods of dynamics available for calibration and validation, model computational requirements and resolution, and availability of detailed bed topography (Vieli and Nick, 2011). These can be mitigated by employing spatially reduced models to evaluate glacier catchment-scale responses to different forcings (Thomas, 2004; Nick et al., 2009; 2010; 2012; 2013; Colgan et al., 2012; Joughin et al., 2010a). Application of these models where TWG records can be extended to their LIAmax allows the potential drivers of post-LIAmax GrIS retreat to be investigated.

The earliest post-LIAmax TWG retreats in Greenland are known to have occurred prior to the first continuous air temperature record at Nuuk in 1866 (Vinther et al., 2006; Weidick, 1959; 1968; Weidick et al., 2012). This can preclude direct comparison of post-LIAmax TWG response to climate; including the first observed retreat of Jakobshavn Isbrae between 1851 and 1875 (Weidick and Bennike, 2007; Csatho et al., 2008). Application of catchment-scale models where climate data are lacking allow the drivers of individual TWG change to be investigated through model sensitivity experiments. These facilitate comparisons of modelled behaviour to observations, and can be used to identify the range of forcings and likely mechanism(s) required to explain the observed retreat.

This study investigates the post-LIAmax dynamics of Kangiata Nunaata Sermia (KNS), SW Greenland, prior to the instrumental air temperature record. We aim to improve the record of the post-LIAmax fluctuations of KNS using previously unstudied geomorphology, newly uncovered historical sources, geospatial analyses, and previously published lines of evidence (Weidick, 1959; Weidick et al., 2012). Secondly, we evaluate whether the post-LIAmax retreat is best explained by changes in surface mass balance (SMB) or forcing perturbations occurring at the terminus. This is achieved using a one-dimensional flow band numerical model (Nick et al., 2010).

5.3 Field site

KNS is located ~100 km from Nuuk at the head of the Kangersuneq branch of Godthåbsfjord, SW Greenland (Figure 5.1). The terminus retreated significantly during the 19th century, though uncertainty exists regarding the timing and scale of this retreat (Weidick, 1959; Weidick et al., 2012). The glacier catchment is ~31400 km^2, and has a contemporary calving flux in excess of 6 km^3 a^{-1}, making it the largest outlet glacier in western Greenland located south of Jakobshavn Isbrae (Van As et al., 2014). At its LIAmax KNS was advanced over 22 km further down-fjord from its current terminus position, occupying a topographic depression on the west side of the fjord, and forming a large ice dammed lake (IDL) in the forefield of Qamanarssup Sermia (QS; Weidick et al., 2012).

Subsurface West Greenland Current (WGC) waters periodically enter Godthåbsfjord over a shallow (80 m) sill at the entrance to the fjord, establishing a link between the ocean and the terminus (Mortensen et al., 2011; 2013). Fjord circulation allows surface heated waters to mix downward to subsurface fjord waters, which can also

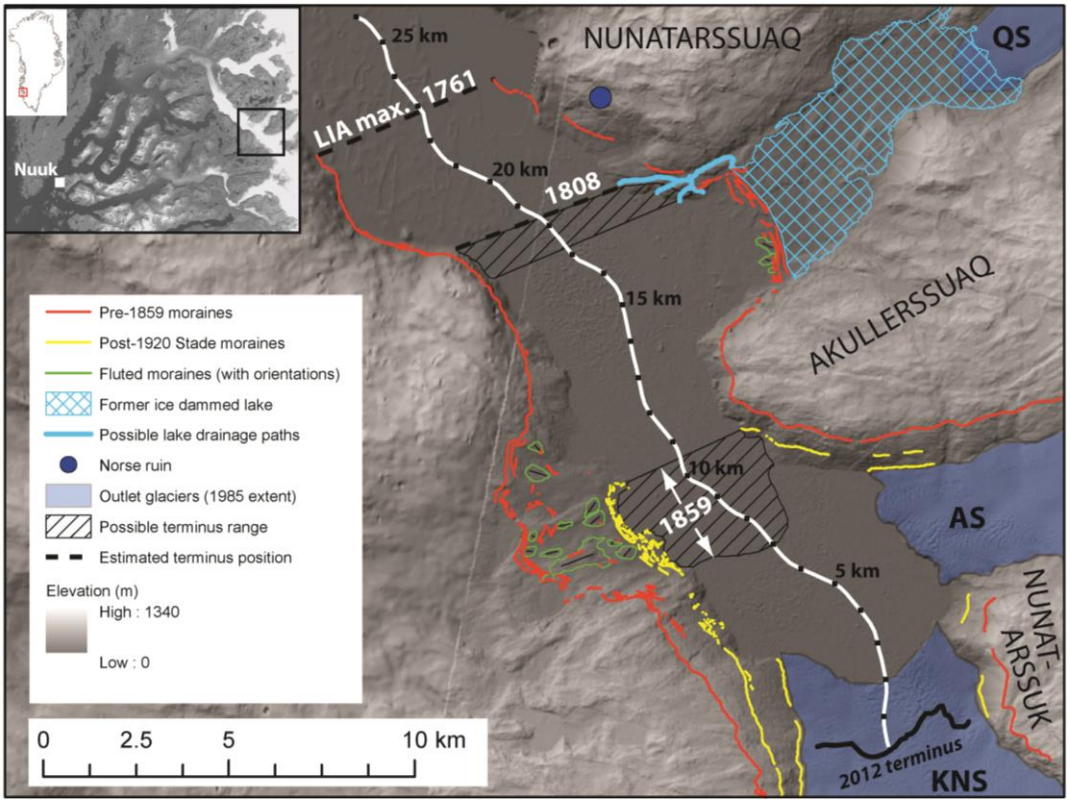

Figure 5.1 Hillshaded digital elevation model (photogrammetric DEM and ASTER GDEM mosaic), showing the post-LIAmax geomorphology, and the possible terminus positions/ranges relative to the 2012 terminus position. The 2012 terminus position was mapped from a Landsat image acquired on 18/9/2012. Minimum extent for 1859 position is taken from 1946 terminus position, observed prior to disintegration of the confluence by 1948 (Weidick and Citterio, 2011). Inset is a panchromatic Landsat image of the Godthåbsfjord region acquired on 19/9/1992.

interact with the terminus (Mortensen et al., 2011). No direct measurements of submarine melt (SM) exist for KNS, although estimates of SM at vertical calving fronts of other West Greenland TWGs range from 0.7±0.2 m d^{-1} to 3.9±0.8 m d^{-1} (Rignot et al., 2012). Within this range, SM for KNS is probably at the lower end due to the sill at the fjord entrance limiting the ability of warm WGC waters to reach the terminus (Straneo et al., 2012).

5.4 Methods for reconstructing and dating glacier terminus positions

The LIAmax extent of KNS is clearly defined by a series of moraines and ice scour limits (Weidick and Citterio, 2011; Weidick et al., 2012). These limits and the geomorphology inside were mapped in detail using high-resolution (2 m^2) GeoEye satellite imagery, and ground truthed during fieldwork conducted in 2011. Reconstructions of glacier geometry were obtained by extracting elevations of mapped moraine limits from a an aero-photogrammetrical derived digital elevation model (DEM) of the KNS terminus area,

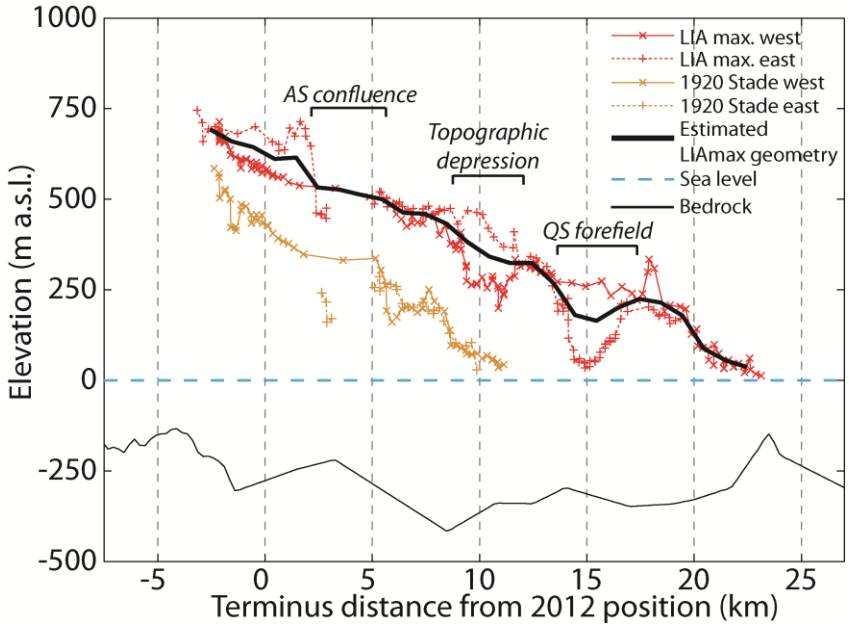

Figure 5.2 LIA and 1920 Stade trimline elevations acquired from the DEM described in the text. Locations of significant changes in topography and the confluence of KNS with AS are labelled. LIAmax geometry is estimated by averaging the western and eastern trimline elevations over 1 km ranges.

based on a 1985 aerial survey conducted by the Danish Geodata Agency with associated ground control (GR96) and error of ±6 m. Where coverage from this DEM was unavailable, ASTER GDEM data (http://asterweb.jpl.nasa.gov/gdem.asp) gridded to 30 m^2 resolution were used (Figure 5.1). Moraine elevations were extracted relative to the glacier/fjord centreline (also used as the model flowline) using the Extrapolated Centreline Method presented in Chapter 4. This allowed moraine elevation profiles to be directly and accurately compared to the modelled glacier elevation profiles (e.g. Figures 5.2 and 5.9).

The date and location of terminus positions were reconstructed using an array of historical sources, which will be discussed in detail below. The physical plausibility of each account was tested where possible, to establish the level of confidence that could be placed in each observation. In some cases, GIS tools could be applied to constrain terminus locations with greater absolute precision than allowed by qualitative analysis alone.

Historical accounts

The earliest terminus position of KNS that can be determined is from the observations of David Cranz in 1761 (published in English in 1820). He describes observing an unnamed glacier in *Baal's Rivier* (a previous name for Godthåbsfjord and Kangersuneq) that "ascends in steps for the space of four leagues [~22 km]", while "[A] low hill […] closed the vista", and "large tracts of ice […] branched off north and south to an unknown distance into the country" (Cranz, 1820, p.34). Cranz's viewpoint has been reconstructed to

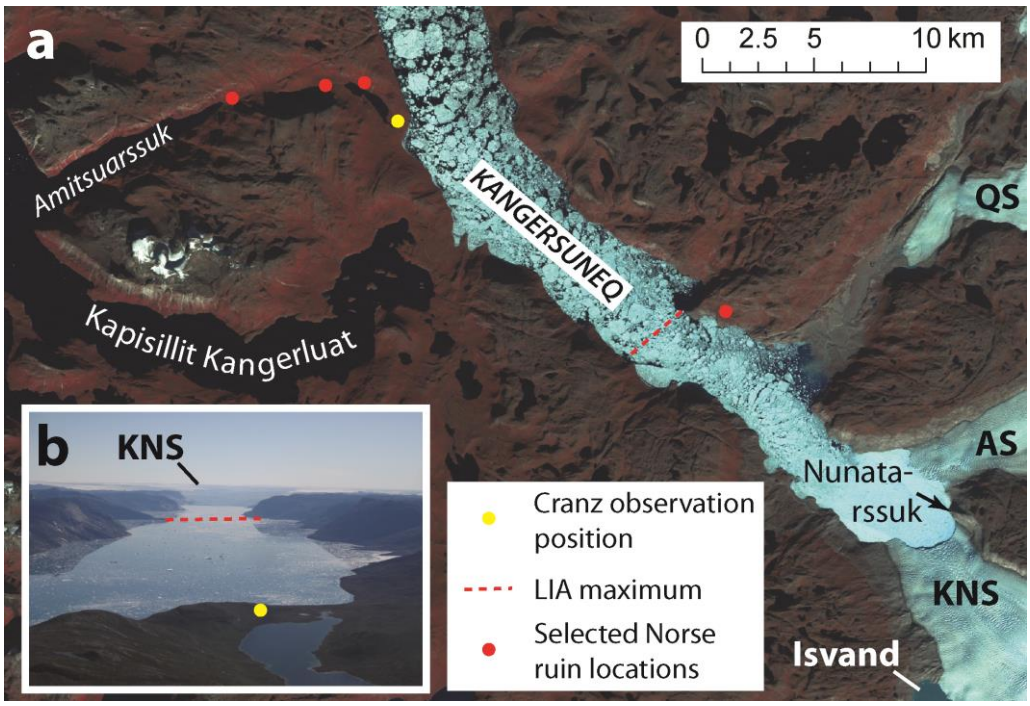

Figure 5.3 Approximate reconstructed location position of Cranz from which he observed KNS in 1761. (A) False colour Landsat image (acquired 15/9/1987) showing location information referred to in the text. (B) Photograph taken from helicopter in August 2011 showing view down Kangersuneq looking towards the south-east, approximating the view of Cranz.

be from the valley separating Kangersuneq and Amitsuarssuk fjord branches (Figure 5.3). This is based on his description of his approach to the observation point, describing hiking along a valley through which flowed a "rivulet, swelling at intervals into pools" and Norse ruins located adjacent to "a great lake of freshwater" (Cranz, 1820, p.33). The valley identified is the only one in the region that fits Cranz's description (Figure 5.3a). KNS is also the only observable TWG from this viewpoint, with Nunatarssuk likely to be the low hill mentioned, located 20 km from LIAmax (Figure 5.3b).

The next reference to KNS is from Egil Thorhallesen who, guided by locals, visited an ice dammed lake (IDL) between 1765-1775 previously identified as Isvand (Figure 5.3; Weidick, 1959; Weidick et al., 2012). The account does not relate a direct observation of the terminus, though is of potential relevance since the ice margin position at Isvand was dynamically linked to the terminus retreat of KNS during the 20th century (Weidick and Citterio, 2011). The wording of Thorhallesen's account is ambiguous in that it reports that "the glacier has laid itself in recent time" over Isvand (Thorhallesen, 1776, p.37). This makes it unclear whether he is referring to a recent advance or retreat of the ice margin from its observed position.

The diaries of Karl Ludwig Giesecke record a visit made to the terminus area of KNS in August 1808 (published in German in 1910). He describes the ice having nearly

overridden the Norse ruins indicated on Figure 5.1 at its maximum extent, though the retreated terminus is still nearby. He makes a comparative assessment of the glacier geometry as being "grösser, steiler, und gefährlicher als der nordöstliche [*larger, steeper and more dangerous than that to the north-east [Qamanarssup Sermia]*; trans. by N. Weitz]" (Giesecke, 1910; p.151), and describes an IDL occupying the QS forefield which "über die Felsenwand hinab am Eisblink ins Meer stürzt [*next to the glacier flows over a rock wall into the ocean*; trans. by N. Weitz]" (Giesecke, 1910; p.151).

Maps and photographic evidence

The first map of Godthåbsfjord from which it is possible to obtain a reliable estimate of the terminus position of KNS was drawn by Samuel Kleischmidt (1859). This shows KNS and AS to be confluent, with the terminus adjoining Akullerssuaq (Figure 5.1). An earlier map by Heinrich Rink (1856) shows KNS to be in a similarly retreated position, though the absence of the valley separating Nunatarssuaq and Akullerssuaq does not allow relative terminus position in the fjord to be identified with confidence. A photograph taken by Rink during the 1850s (in Weidick et al., 2012) shows AS and KNS to be confluent (as evidenced by the presence of a medial moraine), though the terminus itself is partially obscured by foreground topography (Figure 5.4b). This prevents the identification of the exact position of the terminus from this image.

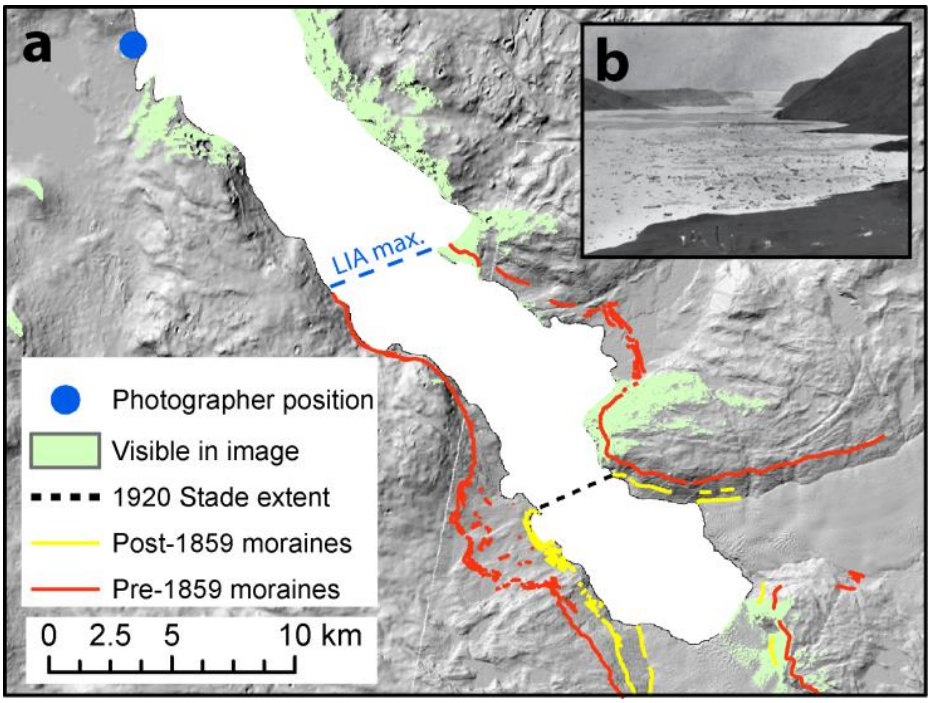

Figure 5.4 Viewshed analysis of image acquired during the 1850's. (A) Hillshaded DEM showing the area visible to an observer standing at the location indicated, and (B) the image of KNS taken in the 1850's by Rink (from Weidick et al., 2012).

5.5 Results

5.5.1 Post-LIAmax geomorphology

Figure 5.1 shows the post-LIAmax geomorphology of KNS. All subsequent mentions of glacier terminus positions are given relative to the 2012 terminus, indicated by the fjord centreline (Figure 5.1). The maximum moraine/ice scour extent extends to 22.6 km, and covers an area 220 km^2 greater than present. Multiple sets of moraines exist on both flanks of the fjord within the LIAmax. These include:

- An upper set of well-developed continuous lateral moraines/ice scour on both sides of the fjord delimiting the LIAmax. On the eastern fjord flank the moraine spans the forefield area of the land terminating glacier Qamanarssup Sermia (QS), while the moraine on the western flank extends inland into the topographic depression opposite Akullerssuaq (Figure 5.1).
- Several other less pronounced moraines lie proximal and sub-parallel to well-developed upper moraines in the QS forefield on the eastern flank, and also within the topographic depression opposite Akullerssuaq on the western flank. Fluted moraines occupy areas within the LIAmax extent of the QS forefield and between the LIAmax and 1920 Stade moraines on the western flank. These are broadly orientated according to the slope of local topography (Figure 5.1).
- A lower set of moraines/ice scour extends to ~10 km along both sides of the fjord. On the eastern flank this wraps around Akullerssuaq, and on the less steep western flank several inset sub-parallel moraines are present. The outer limit of these has previously been related to the culmination of the 1920 Stade (Weidick and Citterio, 2011).

Trimline elevations show that glacier surface elevation from ~20 km to the LIAmax extent did not exceed 100 m above sea level (asl), with an average surface gradient of 1.6° (Figure 5.2). The glacier surface significantly steepens upstream between 20 km and 18 km to 4.2°, before surface elevation appears to decrease where the QS forefield adjoins Kangersuneq between 14 km and 18 km (Figure 5.2). The ice surface steepens to 3.6° as the fjord narrows between 12 km and 14 km, before levelling out between 10 km and 12 km opposite Akullerssuaq as the ice extends into the topographic depression (Figures 5.1 and 5.2). The ice surface rises by ~200 m elevation between 2 km and 10 km (1.4° surface slope), with the gradient doubling to 2.8° between 1 km and 2 km, reaching an elevation of

~600 m asl. This final elevation step change occurs immediately upstream of the confluence with AS (Figure 5.2).

5.5.2 Reconstructing timing of terminus fluctuations: LIAmax-1859

The account of Cranz describing KNS extending from Nunatarssuk for ~20 km corresponds almost exactly with the LIAmax extent of the glacier (Figures 5.2 and 5.3). His description of the glacier profile as "ascending in steps" (1820, p.34) also fits with the reconstructed LIAmax geometry of KNS, with at least three changes in surface gradient identified (Figure 5.2). It is proposed that Cranz observed KNS at, or very near to its LIAmax extent in 1761.

Giesecke's description of an IDL draining directly over land into the fjord provides excellent constraint on the terminus position in 1808. For this drainage to occur, the eastern margin of KNS must be sufficiently retreated from LIAmax to allow the IDL to drain into the fjord over land, rather than subglacially or as an ice marginal channel. To establish the terminus configurations where it is physically possible to maintain an IDL in the QS forefield which also drains into the fjord over land, an analysis of possible lake drainage pathways was conducted using the *ArcHydro* add-on to *ArcMap v.10* software. Using the DEM shown in Figure 5.1, dams were inserted along the LIAmax moraines spanning the QS forefield allowing the IDL and its drainage paths to be reconstructed. Four possible land drainage paths could maintain the IDL, located within a terminus range of ±550 m (Figure 5.1). However, since the majority of this range is within a section of the fjord that begins to widen, from a glaciological perspective the narrower section of the fjord represents a more likely location for the terminus (Mercer, 1961). The 1808 terminus location on the western flank is less certain, though a likely range of terminus configurations is indicated in Figure 5.1.

The smaller, less continuous inset moraines sub-parallel to the LIAmax suggest glacier thinning from the LIAmax. The steep fjord valley side topography that extends between 17-22 km provides low preservation potential for moraines meaning that the style of retreat from 1761-1808 cannot be reconstructed with confidence.

Map evidence places the terminus of KNS as adjoining Akullerssuaq in 1859 (Kleinschmidt, 1859). Viewshed analysis applied to the photograph taken by Rink in the 1850s allows the maximum possible extent of the terminus to be reconstructed (Figure 5.4). From this, the headland that partially obscures the terminus in this photograph

corresponds to the 1920 Stade moraine limit. The terminus was therefore located inside this limit by 1859 (Figure 5.1).

In the topographic depression opposite Akullerssuaq (Figure 5.1), the geomorphology preserves no evidence for stabilisation of the lateral ice margin between the LIAmax/LIAmax-proximal and 1920 Stade lateral moraines. This is despite the shallow slope of this area providing excellent potential to preserve moraines. The presence of fluted moraines in this area suggests that reworking has not been significant, making the destruction of lateral moraines highly unlikely. The ice margin is therefore interpreted to have thinned rapidly, in a single phase, bringing it inside the 1920 Stade moraine extent.

In summary, KNS had achieved its LIAmax by 1761, and subsequently retreated rapidly in either one or two phases. In the single phase scenario, Giesecke observed the terminus partway through the retreat in 1808. Lack of evidence for stabilisation of the lateral ice margin indicates retreat to its 1859 position would have occurred rapidly (i.e. in years rather than decades). The two phase scenario would have KNS retreating and temporarily stabilising at or near to its 1808 extent between 1761-1808, forming the inset lateral moraines adjacent to those of the LIAmax, before retreating rapidly to its 1859 position sometime between 1808-1859.

5.6 Model experiments

The aim of the model experiments is to determine the likely drivers of the reconstructed terminus retreat. Three sets of experiments were run, aiming to test (1) the sensitivity and response timescales of KNS to a range of step changes in SMB, (2) sensitivity to direct forcing of the terminus, including incremental increases in crevasse water depth (CWD), and submarine melt rates (SM), and (3) the response timescales following step changes in terminus forcing. Parameter sensitivity was tested over significant ranges of values to allow full characterisation and evaluation of model behaviour. For each model run, the glacier was tuned to approximate the reconstructed LIAmax geometry (e.g. Figures 5.2 and 5.9), using the process described in the supplementary materials (Section 5.10).

5.6.1 Model description and input

KNS is modelled using a one-dimensional depth-integrated flow-band model (Nick et al., 2010), utilising a crevasse-depth calving criterion, where calving occurs once the combined basal and surface crevasses penetrate the full ice thickness (Benn et al., 2007;

Nick et al., 2010). The crevasse water depth (CWD) variable within this criterion has previously been used to drive models, linking it to air temperature or runoff data (Cook et al., 2012; 2013; Nick et al., 2013), while submarine melting (SM) can be applied as negative mass balance downstream of the grounding line (Nick et al., 2013). Experiments are run using a moving grid, with an along flow grid size of ~250 m. The model has previously been applied successfully to several different TWGs in Greenland (Nick et al., 2009; 2012; 2013; Vieli and Nick, 2011). A description of the force balance equations and calving criterion are provided in Section 5.10, and the parameter values used are presented in Table 5.1.

Basal topography for the lower 40 km of the catchment is derived using a mass continuity approach following the methodology of Morlighem et al. (2011), utilising CReSIS flightlines for validation (Gogineni et al., 2001). For the upper catchment, bed topography is obtained from Bamber et al. (2001). Point measurements of fjord bathymetry were used for bed topography in Kangersuneq, where KNS terminates (Figure 5.2; Weidick et al., 2012). Model sensitivity to bed topography uncertainty is evaluated by experiments outlined in Section 5.10. SMB ablation values are taken from the average 1958-2007 Regional Atmospheric Climate Model (RACMO) output for the catchment of KNS (Ettema et al., 2009). The overall SMB results in contemporary balance calving flux of ~8.2 km^3 a^{-1}; well in excess of the direct contemporary estimates of ~6 km^3 a^{-1} (Van As et al., 2014). SMB values in the accumulation zone are therefore reduced, so as to maintain the contemporary ice sheet elevation over centennial timescale model runs.

This represents a conservative approach to the definition of accumulation SMB values during the LIA, since values have been suggested to be ~10-40% lower over the catchment of KNS during this period (Box et al., 2012). The definition of catchment boundaries in the ice sheet interior, that can affect calving fluxes in the long term, is also

Parameter/Constant	Value
Ice density – ρ_i	900 kg m^{-3}
Meltwater density – ρ_w	1000 kg m^{-3}
Proglacial water body density – ρ_p	1028 kg m^{-3}
Gravitational acceleration - g	9.8 m s^{-2}
Friction exponent - m	3
Friction parameters – μ and λ	1
Glen's flow law exponent - n	3
Glen's flow law coefficient - A	4.5 x 10^{-17} Pa^{-3} a^{-1}
Grid size	~250 m
Time step	0.005 a

Table 5.1 List of parameters and constants used for running the model.

known to represent a potentially significant uncertainty when defining the accumulation zone of an ice sheet glacier (Van As et al., 2012; 2014). However, high resolution SMB modelling of the Nuuk region for 1960-present also indicates that the majority of inter-annual variability in the net balance of KNS' catchment is derived from changes in ablation, where the catchment is likely to be comparatively well defined (Van As et al., 2014). Therefore the majority of SMB driven mass change over the period of interest is likely to have been driven by variability in the ablation zone rather than by changes in accumulation.

Ice contributed by Akullerssup Sermia (AS), the glacier adjacent to KNS, is accounted for in the model as extra SMB across their 5 km confluence (between 3 km and 8 km). The flux is distributed along this confluence proportional to the contemporary across-terminus velocity profile of AS (Joughin et al., 2010b). An approximation of the present-day flux of AS is derived by taking a physically based estimate of the flux of KNS of ~6 km^3 a^{-1} (Van As et al., 2014), and scaling this value using the widths and terminus velocities of both glaciers. This provides a contemporary AS flux estimate of ~1 km^3 a^{-1}. In the model the volume of ice contributed by AS per time step is therefore taken to be a sixth of the modelled flux of KNS immediately upstream of their confluence.

Modelled terminus positions were compared directly to mapped terminus positions using the Curvilinear Box Method (CBM) of tracking terminus change (Chapter 4). This allows direct comparison of mapped results to model results since both the CBM and model track terminus position in relation to the fjord centreline.

5.6.2 Sensitivity to SMB

All SMB experiments were run keeping terminus forcing (CWD and SM) constant. These experiments test terminus sensitivity to step changes in ablation zone SMB, up to 200% of the 1958-2007 RACMO average values. Sensitivity to step changes in accumulation were not investigated, due to the likelihood of accumulation having increased over the glacier catchment following the LIA (Box et al., 2012). Separate model runs were conducted for 10% increments of initial SMB ablation values ranging between 110% to 200%. Sensitivity was evaluated by comparing the model time required for the terminus to retreat, to the known time needed, indicated by the glacier reconstruction.

5.6.3 Sensitivity to forcing at the terminus

Glacier sensitivity to terminus forcing is investigated through application of both incremental and step changes in forcing. The sensitivity of LIAmax KNS to incremental changes in both CWD and SM were evaluated separately to characterise how, or if, they responded differently to small, steady increases in these two forcings. Two sets of model runs with incremental forcing were conducted. The first increased CWD by 1 m every 5th year of the model run while SM was held constant, testing terminus sensitivity to CWD for fixed values of SM. The second increased SM from initial pre-defined values (between 0 km^3 a^{-1} and 1.5 km^3 a^{-1}, at 0.1 km^3 a^{-1} intervals) by 0.025 km^3 a^{-1} every 5th year, while CWD was held constant. By doing this we evaluate terminus sensitivity to small successive increases in SM from given initial SM scenarios at the LIAmax, and constant CWD values.

Glacier sensitivity to different magnitudes of step change in CWD was evaluated by applying these for different constant SM values in each model run. SM values used were determined from the results of the incremental forcing experiments, using only values where modelled retreat behaviour was comparable to the pattern of retreat observed. Experiments were also conducted where different magnitudes of step change in SM are applied. Similar to the SMB experiments, sensitivity was evaluated by comparing the model time required for the terminus to retreat following the step change, to the known timescale of glacier retreat.

5.7 Model results

The modelled evolution of the terminus position is shown with respect to time (Figures 5.5, 5.7 and 5.8) and forcing applied (Figure 5.6). The locations of modelled stable terminus positions driven by SM and CWD forcings are replicated between experiments (Figure 5.6). The majority of model runs also simulate some degree of stabilisation at a topographic narrowing in the fjord at ~12.5 km from the 2012 terminus position, where there is no observational or geomorphological evidence of terminus stabilisation (Figure 5.6). This potential pinning point is thought to be real, rather than an artefact of bed topography uncertainty (see Section 5.10). Each modelled stable terminus position possesses different relative resilience to increasing levels of forcing before retreating to the next stable location. Of the pinning points identified, the 12.5 km position is generally the least resilient to changes in forcing.

5.7.1 SMB forcing

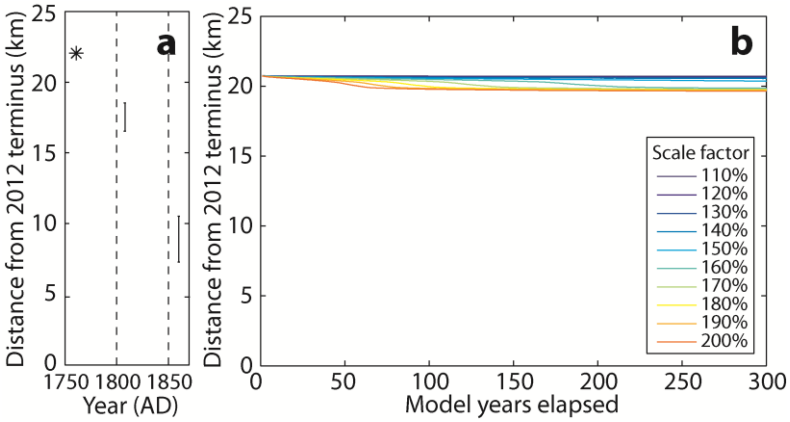

Figure 5.5 Results showing (A) observed terminus retreat, (B) modelled retreat showing impact of multiplying ablation rates by a prescribed scale factor. Model was spun up to be vulnerable to retreat near to its LIA maximum, with CWD = 175 m and no SM applied.

The modelled glacier displays very little sensitivity to changes in ice thickness driven by changes in ablation (Figure 5.5). Even an extreme SMB forcing (ablation = 200% of 1958-2007 RACMO average) produces a retreat <1 km from the LIAmax over 300 model years. It is therefore unlikely that SMB driven changes in ice thickness caused the retreat from LIAmax to the 1808 position.

5.7.2 Incremental terminus forcing

Model results of incremental forcing demonstrate that CWD and SM can potentially initiate rapid terminus retreat over small parameter spaces (Figure 5.6). However, the sensitivity of the modelled glacier to the absolute values of SM or CWD is dependent on the initial conditions of the model run. Model runs with higher SM rates enhance the sensitivity of the modelled glacier to changes in CWD, with the 12.5 km pinning point becoming less well represented as SM increases (Figure 5.6b). Although this pinning point is barely apparent where SM >0.8 km^3 a^{-1} (demonstrating behaviour in agreement with the glacier reconstruction presented), these represent SM rates at the upper

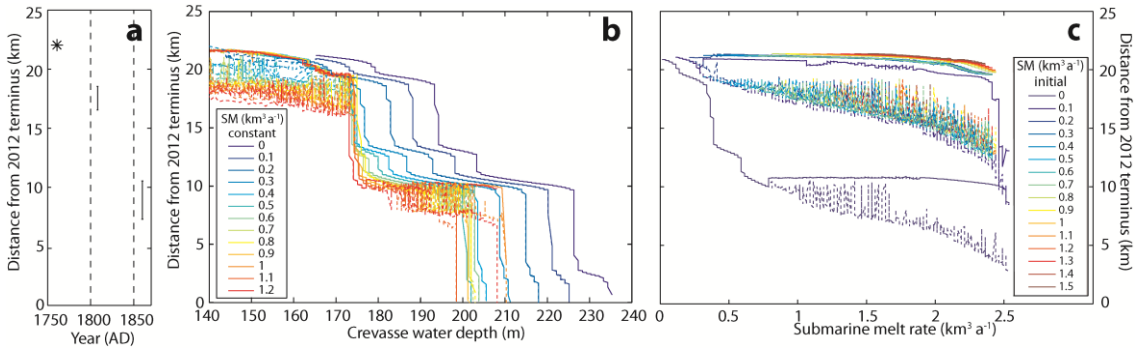

Figure 5.6 Results showing (A) observed terminus retreat, (B) modelled retreat holding SM constant and increasing CWD by 1 m every 5th modelled year, and (C) modelled retreat holding CWD constant, after spinning up to an initial SM at LIAmax, and increasing SM by 0.025 km^3 a^{-1} every 5th modelled year. Narrow dashed curves on panels B and C indicate position of the grounding line.

end, or greater than anything previously observed in Greenland (Rignot et al., 2012; Enderlin and Howat, 2013). These runs also generate instabilities within the model, with the grounding line demonstrating significant oscillatory behaviour (>1 km) over timescales of <1 year (Figure 5.6b).

Only one model run, spun up to the LIAmax with SM = 0 km^3 a^{-1}, retreated significantly in response to increasing SM (Figure 5.6c). Remaining model runs formed floating ice tongues, as high SM rates drove grounding line retreat, while there was sufficient lateral drag for the terminus to remain stable. If increasing SM did drive retreat from LIAmax to the 1920 Stade position, it would have required SM to have dramatically increased, from 0 km^3 a^{-1} to ~0.6 km^3 a^{-1}. However, this run also includes the terminus stabilising at the 12.5 km pinning point, not represented in the glacier reconstruction. Once SM >0.78 km^3 a^{-1} the model run begins to display comparable grounding line variability to that observed in other runs where initial SM rates were >0 km^3 a^{-1} (Figure 5.6c).

5.7.3 Step changes in terminus forcing

Following results from incremental increases in SM (Figure 5.6c), step changes in SM of different magnitudes were applied only where the model was spun up with an initial SM rate of 0 km^3 a^{-1} at the LIAmax (Figure 5.7). The results from these runs demonstrate that an increase in SM to 0.3 km^3 a^{-1} could cause a retreat to the 1859 terminus position, though it would take >200 years to do so. To drive a retreat from the LIAmax to the 1859 position within the timeframe observed (<98 years), requires a step change increase of at least 0.5 km^3 a^{-1}. However, given the lack of geomorphological evidence for a stable margin at 12.5

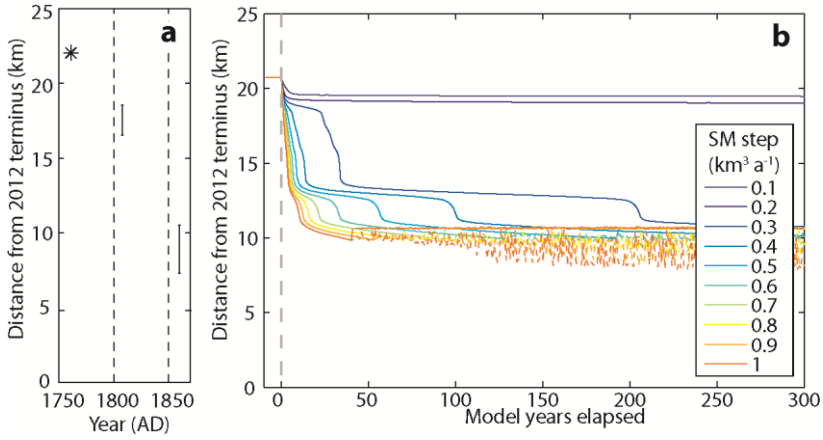

Figure 5.7 Model results showing (A) observed terminus retreat, (B) terminus position following a step change in SM following a 50 year spin up period where SM = 0 km^3 a^{-1}, following the results of the incremental sensitivity tests. CWD is held constant throughout (175 m). Dashed lines indicate position of the grounding line. Application of the step change in each case occurs at 0 years (bold dashed line).

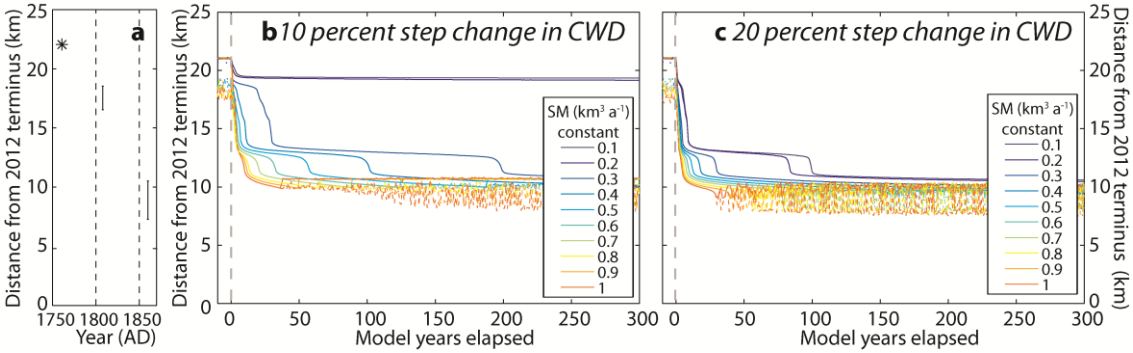

Figure 5.8 Model results showing (A) observed terminus retreat, (B) terminus position following a 10% step change in CWD after a 50 year spin up period, and (C) terminus position following a 20% step change in CWD after a 50 year spin up period. Narrow dashed curves on panels B and C indicate position of the grounding line. Application of the step change in each case occurs at 0 years (bold dashed line).

km, an increase of >0.6 km^3 a^{-1} would probably be required, based on the modelled time needed for the terminus to retreat through the 12.5 km pinning point (Figure 5.7).

Step changes in CWD of 10% (Figure 5.8a) and 20% (Figure 5.8b) were also applied for constant SM ranging from 0.1 to 1 km^3 a^{-1}. As with results from incremental changes in CWD (Figure 5.6b), these show that terminus sensitivity to changes in CWD increases with higher values of SM (Figure 5.8). However, results also demonstrate that moderate step changes in CWD are capable of producing a retreat to the 1859 position for moderate values of SM. For example, where SM >0.3 km^3 a^{-1}, a 20% increase in CWD can drive a retreat from LIAmax to the 1859 position in 31 years.

5.8 Implications of model results

Model results demonstrate that the LIAmax to 1859 retreat of KNS is unlikely to have been driven by changes in SM or SMB. Where changes in SM can produce a retreat pattern comparable to that observed (Figures 5.6c and 5.7), the SM rates required to achieve this are at the upper end, or greater than anything previously observed in Greenland (Rignot et al., 2012; Enderlin and Howat, 2013). The step changes in SM required to reproduce observed retreat that skip the 12.5 km pinning point are also of such a scale (increasing from 0 to ~0.8 km^3 a^{-1}), that they would be equivalent to the SM regime at KNS changing from experiencing one of the lowest, to one of the highest SM rates currently observed in Greenland. For this to occur would necessitate a dramatic change in fjord hydrography. Such a change is thought to be not only unlikely, but also unrealistic, given observations of the contemporary fjord hydrography (Mortensen et al., 2011; 2013), and the likelihood of KNS experiencing low SM rates compared to the rest of Greenland (Straneo et al., 2012).

In comparison, results from experiments with step changes in forcing demonstrate that moderate changes in CWD are capable of replicating the observed pattern of retreat, within a realistic time frame (Figure 5.8). Crucially, these are observed where the model is run with comparatively low SM rates (>0.3 km^3 a^{-1}). These values of SM fall well within the range of SM rates that have been observed for vertical calving fronts elsewhere in Greenland (equivalent to between 0.15±0.05 km^3 a^{-1} and 0.8±0.15 km^3 a^{-1} for KNS; see Section 5.10).

The changes in CWD required to drive this retreat are also consistent with variability from high resolution SMB modelling of KNS for the period 1960-2011 (Van As et al., 2014). For this period significant inter-annual variability in runoff is shown to exist, with values of 3.12±2.40 Gt a^{-1} (2σ, representing inter-annual variability of ±77%). Longer term averages of modelled runoff values also display significant variability. For example, modelled runoff for the period 1991-2010 (3.47 Gt a^{-1}) is 31% higher than the period 1971-1990 (2.65 Gt a^{-1}; Van As et al., 2014). The magnitude of this increase in runoff could feasibly be scaled to changes in CWD even greater than the maximum 20% step change investigated here (Figure 5.8). Given the existence of this scale of multi-decadal variability, it is therefore realistic to suggest that runoff driven changes to CWD was potentially the primary driver of KNS' retreat from its LIAmax to 1859 position.

It has also been established that the 12.5 km pinning point identified in multiple model runs is likely to be real, and not the result of uncertainty in fjord topography (see Section 5.10). The lack of evidence for terminus stabilisation at this location from either observations or geomorphology therefore suggests that the terminus of KNS was able to bypass this pinning point in response to the magnitude of forcing it experienced as it retreated. Unfortunately, at present there is a significant lack of summer temperature observations, or proxy data with sufficiently high temporal resolution/accuracy for the period relating to this study. Therefore it is not possible to attribute the observed terminus retreat to any specific known climate change in Greenland.

5.9 Conclusions

KNS is shown to have retreated by at least 12 km in one or two phases from its LIAmax to 1859. Utilising historical sources we place KNS at its LIAmax in 1761, retreating ~5 km from this position by 1808. This is earlier than any other known post-LIAmax glacier retreat in Greenland. Map and early photographic evidence provide a range of possible

terminus positions for 1859 within the 1920 Stade moraine limit. Geomorphology indicates rapid retreat of at least 7 km to the 1859 terminus from following a retreat from LIAmax to the 1808 terminus position (two phase retreat scenario). However, it is possible KNS retreated in a single phase to the 1859 position, and the terminus was observed in 1808 during this retreat. This provides evidence for at least one, and potentially two significant post-LIAmax retreats of a major Greenlandic TWG occurring in the early 19th, and potentially late 18th centuries. The timing of this predates the post-LIAmax retreat of Jakobshavn Isbræ by at least 43 years, though possibly up to 113 years (Csatho et al., 2008). This highlights the asynchroneity of TWG terminus responses from their LIAmax, and the similarity to asynchronous behaviour of 21st century TWG dynamics (McFadden et al., 2011; Moon et al., 2012). This contrasting behaviour also demonstrates the risk of using dated maximum terminus positions from individual TWGs as indicators of a regional LIA maximum.

Modelling results suggest that terminus stability was largely insensitive to SMB driven ice thickness changes, while SM is likely to have had a minor or modulating effect on the overall terminus retreat over centennial timescales. By contrast, the modelled glacier is very sensitive to changes in CWD, that are capable of driving a retreat of KNS from its LIAmax to 1859 configuration. The changes in CWD required to drive the retreat are also within the range of multi-decadal variability of more recent surface runoff values derived from high resolution SMB modelling (Van As et al., 2014). This highlights runoff driven changes to CWD as a likely potential driver of terminus retreat from LIAmax to 1859.

Given the need to establish the centennial timescale controls on TWG variability (and hence ice sheet response, and likely sea level change), high resolution, high quality, quantitative proxy records of climate forcing are needed to allow adequate evaluation of centennial records of glacier fluctuations, such as the one presented. These include reconstructions of local summer air temperature variability (e.g. D'Andrea et al., 2011), runoff (e.g. Kamenos et al., 2012), and fjord hydrography (e.g. Lloyd et al., 2011). The latter is potentially of significant importance for glaciers such as KNS that drain into fjords with a shallow fjord mouth sill (Mortensen et al., 2011; 2013; Straneo et al., 2012). Such proxy records, alongside instrumental records, and longer term reconstructions of glacier behaviour to their Little Ice Age maxima (and where possible beyond), would therefore allow significant improvements to our understanding of, and context for potential TWG response over the next 100-200 years.

5.10 Supplementary materials

5.10.1 Model description

The model used in this study is designed to simulate the behaviour of tidewater outlet glaciers, and is explained in full detail in Nick et al. (2010). It employs a simple, physically based, non-linear effective pressure sliding law, where the depth integrated driving stress is balanced by longitudinal stress gradients, basal and lateral drag (Van der Veen and Whillans, 1996; Fowler, 2010). These are represented by the first, second and third terms respectively on the right hand side of Equation 5.1, with the driving stress represented by the left hand term:

$$\rho_i g H \frac{\partial H}{\partial x} = 2\frac{\partial}{\partial x}\left(Hv\frac{\partial U}{\partial x}\right) - \mu A_s \left[\left(H - \frac{\rho_p}{\rho_i}D\right)U\right]^{1/m} - \frac{2H}{W}\left(\frac{5U}{\lambda A W}\right)^{1/m} \quad (5.1)$$

where ρ_i = density of ice, ρ_p = density of the proglacial water body, g = gravitational acceleration, x = the along-flow distance, H = ice thickness, D = depth of ice below the surface of the proglacial water body, A_s = bed roughness parameter, A = temperature dependent rate factor [4.5 x 10^{-17} Pa^{-3} a^{-1}, corresponding to ice at -5°C (Cuffey and Paterson, 2010)], W = glacier width, v = effective viscosity (dependent on the strain rate), m = friction exponent. This sliding law allows the modelled glacier to replicate the velocity profiles that are often observed approaching marine termini, and thus provide a good representation of realistic sliding (Nick et al., 2010; 2013; Vieli and Nick, 2011; Jamieson et al., 2012). Constant and parameter values used in the model are outlined in Table 5.1.

Variations in basal and lateral friction due to meltwater supply can also potentially be modelled using the friction parameters μ and λ (Nick et al., 2010; 2012; 2013). However, both are given a constant value of 1 in all model runs shown, since this has primarily been suggested to be most significant over sub-annual, rather than multi-annual to decadal timescales (Howat et al., 2010; Nick et al., 2010; 2012; 2013; Vieli and Nick, 2011).

The model employs a full-depth calving criterion, calculating the penetration depth of both surface and basal crevasses within a field of closely spaced crevasses (Nye, 1957; Benn et al., 2007). Calving occurs when the surface and basal crevasses combined penetrate the full ice thickness (Nick et al., 2010). Where water ponds in crevasses there is the potential for it to force deeper penetration compared to a dry crevasse, according to

$$d_s = \frac{2}{\rho_i g}\left(\frac{\dot{\varepsilon}_{xx}}{A}\right)^{1/n} + \frac{\rho_w}{\rho_i} d_w \tag{5.2}$$

Where d_s = depth of surface crevasse, $\dot{\varepsilon}_{xx}$ = longitudinal stretching rate, n = Glen's flow law exponent, and d_w = crevasse water depth. For a given flow regime, greater values of d_w can therefore instigate higher calving rates that in turn drive retreat.

Basal crevasse heights are also included in calculations of cumulative crevasse penetration, according to

$$d_b = \frac{2\rho_i}{\rho_p - \rho_i}\left(\frac{\dot{\varepsilon}_{xx}}{A}\right)^{1/n}\left(\frac{1}{\rho_i g} - H_{ab}\right) \tag{5.3}$$

where H_{ab} = height above buoyancy of a given ice thickness, calculated as

$$H_{ab} = H - \frac{\rho_p}{\rho_i} D \tag{5.4}$$

This full-depth calving criterion is employed given that instances of full-depth calving behaviour were observed at KNS during fieldwork conducted in August, 2011.

SM is applied uniformly across the entire width of the grounding line. Volumetric rates of SM (e.g. $km^3\ a^{-1}$) are also prescribed within the model rather than linear melt rates per time step (e.g. $m\ d^{-1}$). This is because application of the latter to a 1-dimensional model would result in SM volume being partially dependent on the glacier width. Volumetric rates provide internal consistency between model runs for each time step and location in the modelled fjord. Constant SM values ranged from 0 $km^3\ a^{-1}$ to 1.5 $km^3\ a^{-1}$ (0.1 $km^3\ a^{-1}$ intervals). The latter is equivalent to SM rates of 0 to ~5.25 $m\ d^{-1}$ with increments of ~0.36 $m\ d^{-1}$. This covers the range of values up to 150% of those that have so far been observed for termini in western Greenland (Rignot et al., 2012; Enderlin and Howat, 2013).

To allow direct comparison, previously published daily linear SM rate values ($m\ d^{-1}$) were multiplied by 365.25 to scale them up to units of $m\ a^{-1}$, before being converted to volumetric values. The conversion to volumetric melt rates was achieved by multiplying the annual linear SM values by KNS' contemporary glacier width (~5 km) and fjord depth at the terminus (~225 m). As an approximation, these SM volume values were then halved, to reflect that the majority of SM occurs during summer only, driven by subglacial runoff (Sciascia et al., 2013). These equate to volumetric SM range estimates for KNS of between

0.15±0.05 km^3 a^{-1} and 0.8±0.15 km^3 a^{-1} (Rignot et al., 2012; Enderlin and Howat, 2013). Within this range, the SM value for KNS has been suggested to be low compared to other Greenlandic glaciers, since fjord bathymetry is thought to limit the influence of ocean waters on fjord water temperature (Mortensen et al., 2011; 2013; Straneo et al., 2012).

5.10.2 Model tuning

A variety of basal sliding scenarios are explored during tuning by varying the basal roughness parameter A_s. For simplicity, the catchment is split into two different zones where A_s is set to two different values. These comprise of a rougher upstream and smoother downstream zone. Five different transition positions between these two zones are modelled to establish how this may affect model behaviour (especially potential effects on modelled elevation profiles). The boundary positions investigated between these zones were positioned from 5 km to 55 km from the 2012 terminus position at 10 km intervals. On InSAR velocity maps the latter position marks the approximate location of where rapid ice flow begins (Joughin et al., 2010), providing an intuitive upstream limit to the transition between the higher and lower basal roughness values. 30 different basal sliding scenarios were evaluated, with the feasibility of each evaluated through comparison to glacier elevation profiles reconstructed from the geomorphology (e.g. Figure 5.9).

By applying uniform basal roughness values we aim to avoid circular reasoning that would arise by tuning basal roughness values to predispose KNS to stabilising/retreat at sections where pinning points/retreats have occurred. This allows robust interrogation of model results, making as few assumptions as possible regarding basal roughness. The sensitivity of each modelled glacier to retreat under specific basal roughness scenarios was

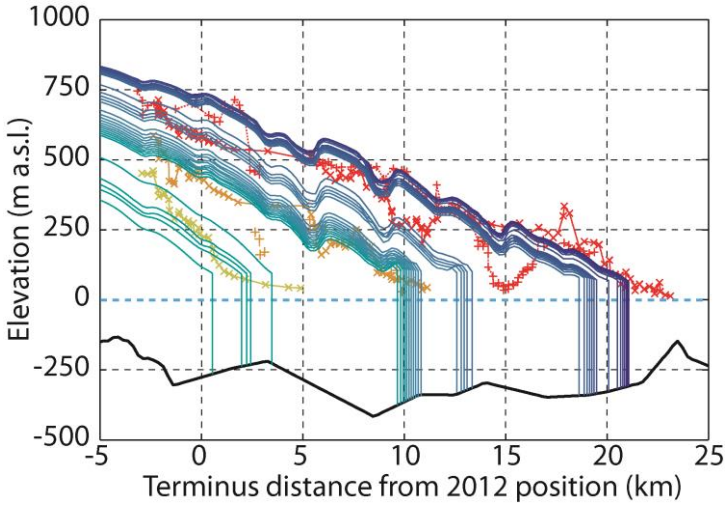

Figure 5.9 Surface elevation profile evolution of the modelled glacier superimposed on the reconstructed elevation profiles for LIAmax (red), 1920 Stade (orange) and 1985 (yellow). Each modelled profile shown represents 1 m increments in CWD every 5th model year.

tested by increasing d_w incrementally. For each scenario the post spin-up value of d_w was increased by 1 m every 5 model years until the terminus retreated beyond the 2012 terminus position, or d_w exceeded 250 m. The latter condition is applied since sections of the fjord are <250 m in depth, meaning that in these regions the terminus is fully grounded, and its position would be defined almost solely as a function of d_w. Where this occurs and the fjord continues to shallow this could potentially force the creation of unrealistic freeboard heights at modelled termini.

Figure 5.9 is an example output of the sensitivity tests, showing the profile evolution of the basal roughness configuration used in this study.

5.10.3 Bed sensitivity

Previously published work has established that model results of tidewater glaciers can be sensitive to uncertainties in fjord bathymetry (Enderlin et al., 2013). To evaluate whether the uncertainty in fjord bathymetry significantly affects modelled terminus behaviour, sensitivity tests were conducted. This involved randomly varying bed elevation where fjord topography is unknown over blocks of 3 grid cells (~750 m), across a vertical range of ±50 m, before then being smoothed over the same distance to avoid step changes in topography. Three sets of experiments were run, (1) varying the bed downstream of the 1920 Stade maximum, holding the downstream section of the fjord constant, (2) varying the bed upstream of the 1920 Stade maximum, holding the upstream section of the fjord constant, and (3) varying the bed downstream of the 2012 terminus position. This evaluates the impact of bed uncertainty, and potentially the section of the fjord where this is important. Each experiment was run for 50 different bed configurations.

Results demonstrate that unknown sections of fjord topography do not have a

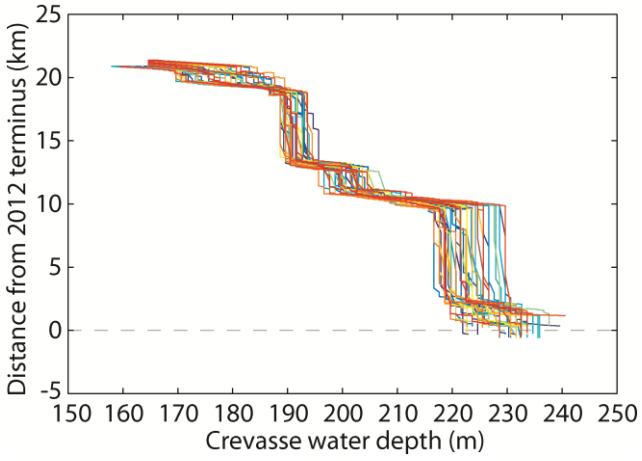

Figure 5.10 Example of terminus sensitivity to random changes in unknown sections of fjord bathymetry along the entire length of the fjord. Results are shown for the retreat pattern of the modelled glacier in response to 1 m increments of CWD every 5th model year, for 50 different bed configurations.

significant effect on the large scale retreat behaviour of KNS (e.g. Figure 5.10). Pinning points identified by the model are therefore suggested to be real, rather than artefacts of fjord topography uncertainty.

Chapter 6

Fluctuations of a Greenlandic tidewater glacier driven by changes in atmospheric forcing: observations and modelling of Kangiata Nunaata Sermia, 1859-present.

Submitted to *The Cryosphere Discussions*, April, 2014.

Authors: James M. Lea[1], Douglas W.F. Mair[1], Faezeh M. Nick[2,3], Brice R. Rea[1], Dirk van As[4], Mathieu Morlighem[5], Peter W. Nienow[6], Anker Weidick[4].

Affiliations:

[1]Department of Geography and the Environment, University of Aberdeen, Elphinstone Road, Aberdeen, AB24 3UF, UK

[2]The University Centre in Svalbard (UNIS), PO Box 156, NO-9171 Longyearbyen, Norway

[3]Centre for Ice and Climate, Niels Bohr Institute, University of Copenhagen, Copenhagen, 2100, Denmark

[4] Geological Survey of Denmark and Greenland (GEUS), Copenhagen, Denmark

[5]University of California, Irvine, Department of Earth System Science, Croul Hall, Irvine, CA 92697-3100, USA

[6]Department of Geography, University of Edinburgh, Drummond Street, Edinburgh, EH8 9XP, UK

Citation: Lea, J.M., Mair, D.W.F., Nick, F.M., Rea, B.R., van As, D., Morlighem, M., Nienow, P.W., & Weidick, A. (2014). Fluctuations of a Greenlandic tidewater glacier driven by changes in atmospheric forcing: observations and modelling of Kangiata Nunaata Sermia, 1859-present. *The Cryosphere Discussions*

Author contributions: JL wrote the manuscript and conducted all geomorphological mapping, glacial reconstructions, GIS analyses, numerical modelling and devised the new climate forcing parameterisations. FMN wrote the numerical model used; DvA provided catchment boundaries used to define width in the model and the modelled runoff data; MM provided a digital elevation model for the lower 40 km of subglacial topography; AW provided historical imagery. All authors contributed to the writing process.

Preamble: This paper follows on from Chapter 5, reconstructing glacier behaviour of KNS for the period where continuous climate forcing data are available. This completes the reconstruction of the dynamics of KNS from its Little Ice Age maximum to 2012. In this paper, the terminus tracking methods outlined in Chapter 4 are used to compare the directly observed terminus positions of KNS to atmospheric and oceanic forcing data. This allows the response of KNS to changes in climate to be evaluated directly. New climate forcing parameterisations within the numerical model, building on those of Nick et al. (2013), are also used to generate an ensemble of model runs that are capable of replicating observed glacier behaviour from a suite of 1500 Monte Carlo simulations. The relative sensitivity of successful runs to atmospheric and oceanic forcing is evaluated by studying the parameter values that scale climate variability to model forcing. These help to identify which climate factors are most likely to drive the behaviour observed at KNS over centennial timescales.

6.1 Abstract

Many tidewater glaciers in Greenland are known to have undergone significant retreat during the last century following their Little Ice Age maxima. Where it is possible to reconstruct glacier change over this period, they provide excellent records for comparison to climate records, and calibration/validation for numerical models. These records therefore allow tests of numerical models that seek to simulate tidewater glacier behaviour over multi-decadal to centennial timescales. Here we present a detailed record of behaviour from Kangiata Nunaata Sermia (KNS), SW Greenland, between 1859-2012 and compare it against available oceanographic and atmospheric temperature variability between 1871-2012. We also use these records to evaluate the ability of a well-established one-dimensional flow-band model to replicate behaviour for the observation period. The record of terminus change demonstrates that KNS has advanced/retreated in phase with atmosphere and ocean climate anomalies averaged over multi-annual to decadal timescales. Results from an ensemble of model runs demonstrate that observed dynamics can be replicated, with changes in atmospheric forcing not needing to be offset by changes in oceanic forcing sensitivity. Furthermore, successful runs always require a significant atmospheric forcing component, while an oceanic forcing component is not always needed. Although the importance of oceanic forcing cannot be discounted, these results

demonstrate that changes in atmospheric forcing are likely to be a primary driver of the terminus fluctuations of KNS from 1859-2012.

6.2 Introduction

Calving from tidewater glaciers (TWGs) accounts for up to 50% of the mass loss from the Greenland Ice Sheet (Van den Broeke et al., 2009). Thus determining controls on tidewater glacier dynamics over decadal to centennial timescales is crucial to understanding their contribution to sea level in a warming climate (Alley et al., 2010; Vieli and Nick, 2011). The ability to achieve this in Greenland has been restricted in part by the relative lack of TWG terminus observations prior to the satellite age, and evidence of terminus locations being spread across a disparate array of sources. However, the synthesis of these sources has previously allowed multi-decadal to centennial records of TWG glacier behaviour to be reconstructed (e.g. Csatho et al., 2008; Bjørk et al., 2012; Weidick et al., 2012).

The generation of such records provide potentially excellent calibration and validation records for numerical modelling efforts (Vieli and Nick, 2011). That is to say that numerical models that are capable of replicating observed terminus behaviour over decadal to centennial timescales will be better placed to predict the future behaviour of a TWG over similar timescales. Despite this, there remain few examples of modelling efforts that have attempted to calibrate their results against multi-decadal observational records (e.g. Colgan et al., 2012). The ability of most numerical models to replicate dynamics over such timescales using realistic inputs therefore remains largely untested.

By undertaking calibration/validation exercises, the sensitivity of terminus position to different climatically forced processes can also be evaluated (e.g. Nick et al., 2013; Cook et al., 2013; Chapter 5). This is achieved by comparing the sensitivity of a modelled glacier to climate forcing against observed behaviour (Nick et al., 2013). With a knowledge of realistic ranges of forcing, this allows evaluation of the relative importance of each in contributing to the observed TWG behaviour.

Changes in oceanic forcing are significant drivers of TWG retreat in Greenland (Murray et al., 2010; Straneo et al., 2010; Rignot et al., 2012), but their relative importance between glaciers appears to be dependent on geographical location, glacier geometry (Nick et al., 2013), and potentially fjord connectivity with the open ocean (Straneo et al., 2012). Model based studies have also helped to demonstrate the sensitivity of some major outlet glaciers to air temperature changes (via enhanced runoff increasing crevasse water depth; Nick et al., 2013; Cook et al., 2013).

Where multi-decadal to centennial timescale climate data exist alongside records of terminus position, these provide the potential for robust evaluation of both numerical models and the importance of different drivers of TWG terminus change. In this study we present a detailed record of terminus fluctuations at Kangiata Nunaata Sermia (KNS), SW Greenland from 1859-present. We then use this to evaluate the ability of a well-established numerical ice-flow model, driven by climate data, to replicate the pattern and timing of change at KNS during this period. Results of this are used to evaluate the sensitivity of KNS to climate forcing data over centennial timescales.

6.3 Field site and climate data

KNS is the largest TWG on the west coast of Greenland, south of Jakobshavn Isbræ (Figure 6.1; Van As et al., 2014). It is known to have undergone significant retreat since its

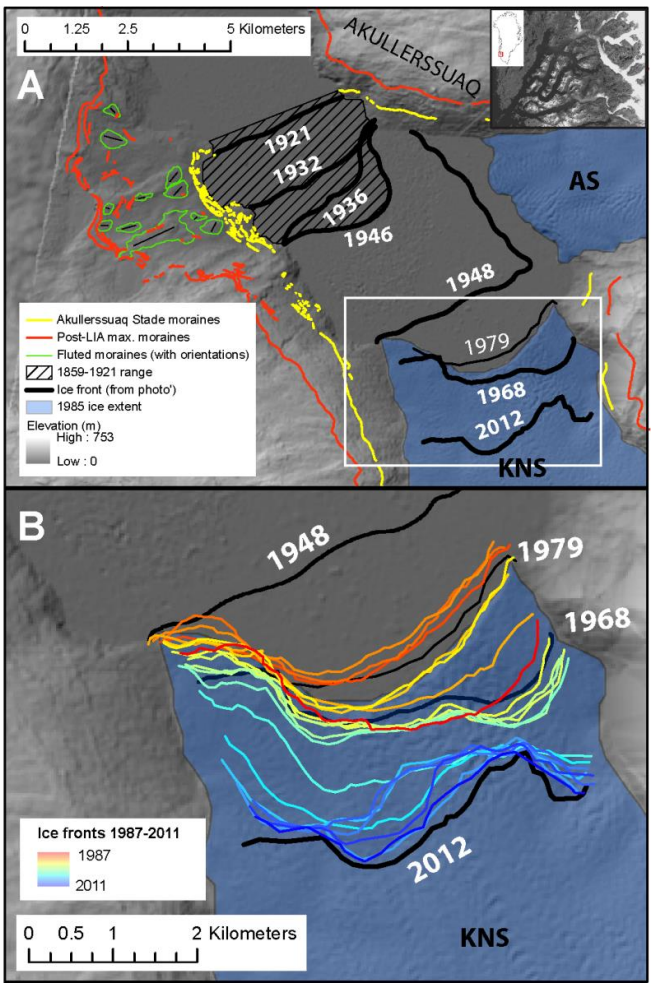

Figure 6.1 Diagrams showing the site location (inset), terminus positions and geomorphology plotted on a hillshaded mosaic of a stereophotogrammetrically derived digital elevation model (DEM) from images acquired in 1985, and ASTER GDEM (Hvidegaard et al., 2012). (A) termini and geomorphology for 1859-2012, with ASM limits delineated in yellow, and (B) a detailed view of termini for the period 1948-2012.

Little Ice Age maximum (Weidick et al., 2012), retreating a total of 22.6 km, with at least 12 km of this retreat occurring prior to 1859 when climate forcing data are unavailable (Chapter 5). It is situated ~80 km inland from Nuuk at the head of Godthåbsfjord, and currently has a calving flux of ~6 km^3 a^{-1} (Van As et al., 2014).

A continuous record of mean monthly air temperature is available at Nuuk from 1866-present (Vinther et al., 2006; Cappelen et al., 2012). Temperatures at Nuuk are known to be strongly correlated to those near to KNS throughout the year (Taurisano et al., 2004), meaning that the Nuuk record can be used as an indicator of the atmospheric forcing at KNS.

As with all TWGs around Greenland, there are no long observational records of fjord water temperatures adjacent to KNS, though detailed hydrographic studies of the fjord have been undertaken recently (Mortensen et al., 2011; 2013). A shallow ~80 m sill at the entrance to the fjord at Nuuk has been suggested to limit the connectivity of the fjord to warm ocean waters at depth. In fjords where shallow sills do not exist, the incursion of these warm ocean waters are thought to have significantly affected the stability of TWGs (Rignot et al, 2012; Straneo et al., 2012). The presence of the shallow sill in Godthåbsfjord also results in significant tidal mixing at the fjord entrance, allowing sea surface waters to be incorporated at depth which are then advected into the fjord (Mortensen et al., 2011). These intermediate level mixed waters have been proposed to significantly influence the energy available for submarine melting at the termini of the TWGs in Godthåbsfjord (Mortensen et al., 2013).

Due to the impact of surface waters near the fjord entrance on the energy balance of the fjord (Mortensen et al., 2011; 2013), and the potentially restricted influence of warm coastal currents at depth (Straneo et al., 2012), we suggest that sea surface temperatures (SSTs) provide a good indicator of the relative oceanographic forcing affecting KNS. Such data have also been used to good effect elsewhere as an indicator of oceanographic forcing where observations at depth are unavailable (e.g. McFadden et al., 2011; Bevan et al., 2012). The HadISST1 1° x 1° dataset provides SST estimates for the period 1871-present (Rayner et al., 2003), with annual averages for the area immediately offshore from Nuuk (62° to 64° N 51° to 53° W) used as an indicator of oceanographic conditions affecting Godthåbsfjord. Although the data used will in part be based on interpolation (especially in the earlier part of the record), the data have been validated for west Greenland against independent records back to 1875 (Hanna et al., 2009). This therefore provides confidence in the results obtained from the HadISST1 dataset.

6.4 Glacier reconstruction data

By 1859 KNS is known to have retreated between 12-15 km from its Little Ice Age (LIA) maximum extent (Chapter 5). The post-LIAmax glacial geomorphology of KNS has been mapped, while previous analysis of a photograph taken in the 1850s, and a map published in 1859 places the terminus position somewhere inside the limit of a significant glacier readvance/stillstand (Chapter 5). We refer to this as the Akullersuaq Stade (after the headland that its maximum extent adjoins), previously named as the '1920 Stade' (Weidick et al., 2012). This is done due to the uncertainty of whether KNS was at its maximum in 1920.

Where the full terminus cannot be observed in photographs, terminus position is determined indirectly using GIS based analyses described below, in conjunction with evidence from maps (e.g. Chapter 5). Subsequent to 1921, intermittent direct observations of the terminus are available enabling mapping of terminus positions from a combination of ground-based, oblique-aerial, vertical-aerial, and satellite imagery (list of sources in Table 6.1).

Landsat panchromatic band imagery was used to map terminus position for 1987-2012. Cloud-free Landsat scenes were selected for analysis, acquired as late in the melt season as possible/just after its end. The start of November was used as the latest date from which images could be selected, since beyond this, mélange in the fjord has been observed to freeze, causing the terminus to advance (Mortensen et al., 2011; Sole et al., 2011). The majority of images were acquired during September or October, though for 1993 and 2003 cloud-free images were only available for dates in August (30/8/1993 and 9/8/2003 respectively). No suitable images were available for the years 1988-1991 and 1998, meaning that annual resolution rates of terminus change were acquired for 1992-1997 and 1999-2012 (Table 6.1).

Where more than 1 year separated terminus observations, annually averaged rates of change were calculated. This provides a continuous record of the trends in behaviour, and inter-annual variability of KNS for the period spanning 1859-2012. This behaviour could then be directly compared to atmospheric and oceanic climate data.

Each terminus position was determined using an adaptation of the box method (Moon and Joughin, 2008; Howat and Eddy, 2011), called the Curvilinear Box Method (CBM; see Chapter 4, for details). This has a marked advantage over the centreline

Acquisition date	Observation type	Source
1850s	Terrestrial photo'	H. Rink (in Weidick et al, 2012)
1859	Map	Kleinschmidt (1859)
1860	Map	Poulsen (1860)
1866	Map	Rink (1866)
1866	Map	Falbe (1866)
1885	Map	Jensen (1885)
1880s?	Sketch (after photo')	Nansen (1890)
1903	Terrestrial photo'	J. Møller in Bruun (1917)
1921	Terrestrial photo'	A. Nissen in Weidick et al (2012)
1932	Terrestrial photo'	A. Roussell in Roussell (1941)
27/08/1936	Oblique photo'	Weidick et al (2012)
10/08/1946	Oblique photo'	Weidick et al (2012)
20/08/1948	Oblique photo'	Weidick et al (2012)
21/06/1965	Terrestrial photo'	Weidick et al (2012)
16/08/1968	Aerial photo'	USGS
15/09/1979	Terrestrial photo'	Weidick et al (2012)
15/09/1987	Satellite	Landsat
19/09/1992	Satellite	Landsat
30/08/1993	Satellite	Landsat
18/09/1994	Satellite	Landsat
14/10/1995	Satellite	Landsat
14/09/1996	Satellite	Landsat
01/09/1997	Satellite	Landsat
15/09/1999	Satellite	Landsat
18/09/2000	Satellite	Landsat
22/10/2001	Satellite	Landsat
23/09/2002	Satellite	Landsat
09/08/2003	Satellite	Landsat
12/09/2004	Satellite	Landsat
24/09/2005	Satellite	Landsat
18/09/2006	Satellite	Landsat
27/09/2007	Satellite	Landsat
23/09/2008	Satellite	Landsat
19/09/2009	Satellite	Landsat
13/09/2010	Satellite	Landsat
16/09/2011	Satellite	Landsat
18/09/2012	Satellite	Landsat

Table 6.1 List of terminus observations and acquisition dates.

tracking or standard box methods as it is capable of accounting for changes in terminus geometry, while also accurately tracking changes in fjord orientation. Furthermore, the box used to calculate terminus change is always centred on the glacier/fjord centreline, which is also the flowline used for the numerical model. Consequently, terminus positions and observed distances of change derived using the CBM can be compared directly to model output.

6.5 The numerical model

The numerical model used is specifically designed to simulate the dynamics of TWGs along a flowband (Nick et al., 2010). It has been successful in replicating the dynamics of

marine terminating outlets in both Greenland (e.g. Vieli and Nick, 2011; Nick et al., 2012; Chapter 5) and Antarctica (Jamieson et al., 2012; 2014), and also been used to make centennial timescale projections of the future contribution of Greenland's major TWG outlets to global sea level (Nick et al., 2013). The model accounts for basal, lateral and longitudinal drag, and includes a robust treatment of grounding line dynamics (Pattyn et al., 2012). Bed topography data for the majority of the catchment are provided by Bamber et al., (2001), though the lower 40 km is generated using a mass continuity based bed reconstruction (Morlighem et al., 2011), validated by OIB/CReSIS flightlines (Gogineni et al., 2001). Where available, fjord bathymetry data are also used where KNS has retreated following its LIAmax (Weidick et al., 2012). Sensitivity analyses conducted in Chapter 5 (Figure 5.10) for this bed configuration demonstrated that the model exhibits broadly comparable patterns of retreat behaviour where bed topography is varied within an uncertainty of ±50 m.

A constant height versus SMB relation is used to calculate SMB for the ablation zone of KNS (Equation 6.1). This is derived from the average RACMO SMB model output for 1958-2007 (Ettema et al., 2009).

$$b(x) = 0.0018 \times h(x) - 2.693 \quad (6.1)$$

Where $b(x)$ = SMB for position x on the model flowline, and $h(x)$ = glacier elevation for position x on the flowline. Due to the tendency for over-estimation of accumulation in RACMO in this region (Van As et al., 2014), positive SMB values in the upstream section of the modelled glacier are prescribed to allow the glacier to maintain its contemporary elevation profile. Irrespective of this, SMB variability has previously been demonstrated to be of minimal importance to results of modelled TWG dynamics over the timescales that are being investigated (Chapter 5). The model is initialised using a glacier geometry approximating that of the Akullersuaq Stade maximum (ASM), derived from geomorphological mapping of associated trimlines (Figure 6.1). Constants and parameter values used are summarised in Table 6.2, while the initial tuning procedure followed for this configuration is the same as that used in Chapter 5. Surface runoff (Van As et al., 2014)/air temperature (JJA average) and SST (annual average) data are used to drive changes in crevasse water depth (d_w) and submarine melting (M) respectively. Seasonal variability in basal and lateral sliding is not included due to its negligible importance over

Parameter/Constant	Value
Ice density – ρ_i	900 kg m^{-3}
Meltwater density – ρ_w	1000 kg m^{-3}
Proglacial water body density – ρ_p	1028 kg m^{-3}
Gravitational acceleration - g	9.8 m s^{-2}
Friction exponent - m	3
Friction parameters – μ and λ	1
Glen's flow law exponent - n	3
Glen's flow law coefficient - A	4.5 x 10^{-17} Pa^{-3} a^{-1}
Grid size	~250 m
Time step	0.005 a

Table 6.2 List of parameters and constants used for running the model

multidecadal timescales (Nick et al., 2013). Parameters which control the model sensitivity to climate forcing are derived using Monte Carlo methods described below.

6.5.1 Relating d_w to air temperature

Changes in the value of d_w have previously been related to runoff variability (e.g. Nick et al., 2010; Cook et al., 2012; 2013), and have been successfully used as a climate linked forcing directly affecting terminus change (Nick et al., 2013). However, the only previously used scaling of surface runoff to d_w requires a baseline d_w value to be prescribed, which it cannot fall below (Nick et al., 2013, their equation S3). We present a new, unrestricted parameterisation that relates seasonal changes in monthly surface runoff to d_w, and allows d_w to freely evolve due to changes in annual runoff (Equation 6.2).

$$d_{wNew} = d_{wPrev} + \alpha_1 (R_{year}\beta_{month} - \frac{R_{base}}{12}) \quad (6.2)$$

Where d_{wNew} = new crevasse water depth for a particular month, d_{wPrev} = crevasse water depth from the previous month, α_1 = coefficient relating crevasse water depth sensitivity to changes in runoff, R_{year} = total runoff for a given year (Gt yr^{-1}), β_{month} = fraction of annual runoff occurring in a particular month, R_{base} = a baseline annual runoff total (Gt yr^{-1}), equivalent to the annual volume of water that is either refrozen within the glacier or drains from the crevasse to the bed. This assumes that the rate of refreezing/drainage of water from crevasses is constant from year to year. Where annual runoff exceeds R_{base}, the average annual d_w will therefore increase, and where runoff falls below R_{base}, the average annual d_w will decrease. Dividing annual runoff into each month's contribution also allows the direct incorporation of d_w's seasonal variability. The value of d_w will therefore reach its

annual minimum prior to the onset of the melt season, and peak in August. The coefficient α_1 allows the sensitivity of d_w to changes in runoff to be adjusted, and is used as a tuning parameter.

6.5.2 Definition of β_{month}

The fraction of annual runoff occurring in each month, β_{month}, is derived from analysis of each month's average runoff from the catchments of both KNS and Akullersuup Sermia (AS) over the period 1960-2012, as given by high resolution surface mass balance (SMB) modelling of the region (Van As et al., 2014). The runoff values for KNS and AS are summed since the glaciers were confluent for much of the time since their LIAmax, including a significant portion of the period of interest of this study (see below; Wedick et al., 2012). Monthly runoff estimates were generated using both Modèle Atmosphérique Régional (MARv3.2; Fettweis et al., 2011), and the Regional Atmospheric Climate Model (RACMO2; Van Angelen et al., 2013). The variability in the monthly fraction of annual runoff is shown for both models in Figure 6.2, with each producing similar patterns and magnitudes of monthly variability. We took the median result from the monthly averages of the two models. This pattern of monthly variability was kept constant from year to year for each model run.

While the model can be forced directly with annual modelled runoff values for the period 1960-2012 (Van As et al., 2014), no such values are available for the century before. Runoff values prior to 1960 are therefore estimated using the relation that exists between average June, July, August (JJA) air temperatures (A_{JJA}) from Nuuk for 1960-2012 (Cappelen et al., 2012) and the modelled runoff values (r = 0.75). A regression

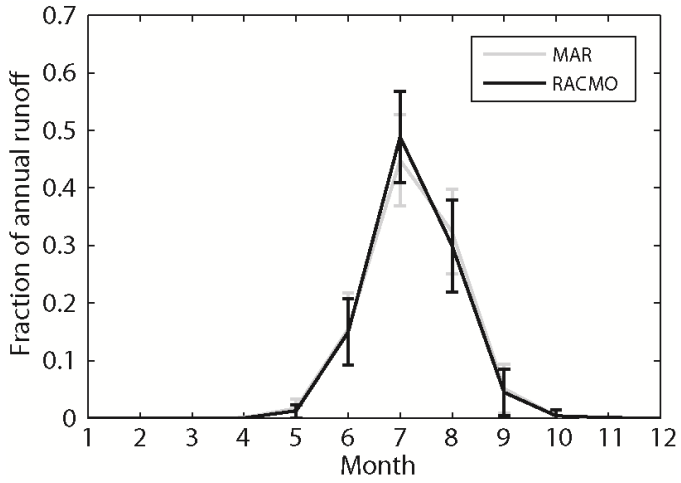

Figure 6.2 Fraction of annual runoff occurring for each month as given by MAR and RACMO2 SMB models for KNS and AS between 1960-2012 (Van As et al., 2014). Error bars are given to 2 standard deviations.

equation is generated from this (Equation 6.3), allowing runoff estimates (Gt a^{-1}) for the period 1866-1959 to be made from the Nuuk air temperature (°C) record (Vinther et al., 2006; Cappelen et al., 2012).

$$R_{year} = 0.91 \times A_{JJA} - 1.53 \quad (6.3)$$

Combined with the 1960-2012 modelled values, this produces a continuous record of estimated annual runoff for 1871-2012. Average monthly variability in runoff is superimposed on this record using the β_{month} term.

6.5.3 Confluence with Akullersuup Sermia

While KNS and AS are confluent in model simulations, variability in d_w at the terminus will be driven by total runoff values from both catchments. The confluence area of the two glaciers is defined on the model flowline as being 5 km, lying between 3 km and 8 km from the 2012 terminus position. However, as KNS retreats through its confluence with AS this will remove the runoff contribution from AS to the terminus, meaning that d_w needs to be scaled to reflect this. Modelled annual runoff totals for each catchment show that KNS and AS respond directly in phase with one another (r = 0.99), with KNS accounting for 70.3% (MARv3.2) or 74.6% (RACMO2) of total runoff (Van As et al., 2014). To allow for this reduction in runoff as KNS retreats through the confluence, the value of d_w is multiplied by a scale factor, γ, that will have a fixed value for each model run of between, α_2 (a confluence scaling factor) and 1, such that

$$d_{wNew} = \gamma \, d_{wPrev} \quad (6.4)$$

Because AS and KNS will at times be partially confluent, the value of γ is also scaled linearly with respect to the relative position of the terminus through the confluence, such that when they are fully confluent $\gamma = 1$, and when fully diffluent $\gamma = \alpha_2$. Values are varied linearly between α_2 and 1 for terminus positions within the confluence according to

$$\gamma = \alpha_2 + (1 - \alpha_2)\left(\frac{x_{conf}}{X_{conf}}\right) \quad (6.5)$$

Where x_{conf} = distance of the terminus through the confluence, and X_{conf} = the total flowline distance over which the confluence occurs. Due to uncertainty regarding the precise

scaling of runoff to d_w as KNS retreats through its confluence with AS, and other confluence effects, α_2 is used as a tuning parameter within the model.

The extra ice flux contribution from AS when confluent with KNS is estimated to be approximately one sixth of that of KNS, based on the contemporary across glacier velocity profiles (Joughin et al., 2010), and terminus widths of AS and KNS. This extra flux is added to the modelled glacier as positive SMB at the confluence of KNS and AS, distributed along the flowline proportionate to the contemporary AS across glacier velocity profile (Chapter 5).

6.5.4 Relating submarine melt rate to sea surface temperature

Submarine melt rate (*M*) has previously been linearly related to deep ocean temperature (DOT) variability using a scaling coefficient (Nick et al., 2013; their equation S2). Using this parameterisation, the highest rates of *M* (expressed in this study in $km^3\ a^{-1}$) would also be associated with the highest inter-annual variability of *M*. This study therefore takes a slightly different approach in that (1) *M* is scaled to sea surface temperature (SST) rather than DOT, for reasons relating to fjord hydrography explained above, and (2) we introduce a constant (minimum) baseline *M* rate, M_{base}, which is added to the linear relation to SST. We therefore calculate *M* ($km^3\ a^{-1}$) according to

$$M = M_{base} + \alpha_3 T_{year} \tag{6.6}$$

Where α_3 = submarine melt rate scaling coefficient, and T_{year} = annual average SST. This allows different minimum background *M* rates to be tested for different model runs, with different sensitivities of *M* to changes in SST superimposed upon this.

6.5.5 Model experiments and evaluation

Tuning parameters α_1, α_2, α_3 and M_{base} were varied randomly within prescribed limits for a total of 1500 Monte Carlo style model runs. The limits for each of the tuning parameters were: (1) α_1, between 0 and 1.5, (2) α_2, between 0.3 to 0.8, (3) M_{base}, between 0 to 0.7 $km^3\ a^{-1}$, and (4) α_3, between 0 to 0.3. These ranges of α_1 and α_2 were chosen to reflect a wide range of potential forcing scenarios, while the values of M_{base} and α_3 were chosen so total *M* could potentially range from 0 $km^3\ a^{-1}$ to values that exceed *M* rates that have been observed for other TWGs in western Greenland (Rignot et al., 2010; Enderlin and Howat, 2013). This allowed the feasibility of different potential drivers of the observed terminus

change to be comprehensively assessed. Runs were conducted for the period 1871-2012, given that this is the period that both atmospheric and oceanic climate records are available for. The model was initialised at approximately the ASM profile and terminus position, as defined by the geomorphology, and given the duration of the spin up period to stabilise for the given forcing scenario. During spin up, d_w was allowed to freely evolve by up to ±3 m a^{-1} to allow the terminus to stabilise at the ASM, with R_{base} and T_{year} held constant. These were defined as the 1871-1920 runoff average (3.107 Gt yr^{-1}) and SST average (2.605 ^{o}C) respectively. These values were used for spin up as it is known the ASM was attained at some point within this window.

Model results were evaluated against their ability to replicate observed terminus dynamics, where absolute terminus positions are known (i.e. 1921 to 2012). The period from 1871-1920 therefore effectively becomes a transient spin up period, where the model is driven using real climate data though terminus position is only known within a range. The ability of each model run to replicate observed dynamics was determined using a weighted regression (R^2) calculation, with the weighting of each terminus observation calculated according to

$$w_n = \frac{D_{n+1} - D_{n-1}}{2(D_k - D_1)} \quad \text{for } n = 1, 2, \ldots, k \tag{7}$$

Where w = weighting in regression calculation, n = terminus observation, k = total number of terminus observations, and D = date of terminus observation. Each terminus observation is therefore temporally weighted according to the median length of time elapsed between the terminus observations that occur before and after observation n. This ensures that the evaluation of model performance is not biased towards the last ~20 years where there is a comparatively high density of observations. Model runs were counted as successful where (1) the difference between the modelled and observed 1921 position was <500 m, (2) the weighted $R^2 > 0.85$, and (3) the gradient of the resulting line of regression was > 0.85.

6.6 Glacier reconstruction results

The geomorphology shows distinct upper and lower sets of lateral moraines on both sides of the fjord, with fluted moraines occupying the intervening space (Figure 6.1a). The upper set are associated with the LIA maximum (Chapter 5), while the lower set were formed

during the Akullersuaq Stade. Fridtjof Nansen's (1890) account of the first traverse of Greenland in 1888, includes a drawing from a photograph showing AS and KNS to be confluent, though the terminus position itself is not visible. Although the original image could not be traced or an exact date of acquisition determined, it is likely to have been taken some time near to the publication date of 1890.

Maps from 1859, 1860, 1866 and 1885 all show the terminus of KNS to be adjoining Akullersuaq and fully confluent with AS (Kleinschmidt, 1859; Poulsen, 1860; Brede, 1866; Rink, 1866; Jensen, 1885). While it is possible that some details on the maps were copied following Kleischmidt (1859), the addition of detail such as lakes on plateaus near to KNS by Jensen (1885) provides confidence that this map faithfully records the contemporary terminus position. There is nothing to suggest that KNS became diffluent from AS at any time from 1859-1885. However, due to a lack of map detail and the Nansen (1890) drawing not including the terminus, these sources cannot be used to provide absolute terminus positions.

The earliest images of KNS are from the 1850s and 1903. Both are taken from approximately the same position, with the terminus partially obscured by foreground topography (Weidick et al., 2012). The presence of medial moraines in each image demonstrates that KNS was confluent with AS. Chapter 5 quantified the terminus position uncertainty for the 1850s photograph using viewshed analysis. Similar analysis has been undertaken for the 1903 image, showing that the uncertainty in terminus position is the same as for the 1850s image (Figure 6.3). The maximum terminus extents for both images are therefore located behind a headland corresponding to the ASM on the eastern side of the fjord (Figures 6.1a, 6.3).

It is not currently possible to say when the ASM was attained from any observational evidence, only that it occurred sometime between 1859-1920. The climate anomalies for the period (compared to 1961-1990 baselines) show that air temperature (AT) and SST anomalies were, on average, antiphased for the period 1871-1903 (Figures 6.4c, 6.4d), though AT and SST anomalies are in phase (negative/near-baseline) for 1903-1920. Conditions are therefore more likely to have been conducive for glacier advance during the latter period.

Terminus position was mapped directly for the remaining images, providing a record of 29 terminus positions spanning the period 1921-2012 (Figures 6.1, 6.4). The first direct terminus observation (1921) shows a slight retreat from the ASM. Subsequent to this, KNS retreated a total of 9.7 km at a non-uniform rate up to 2012, interrupted by short

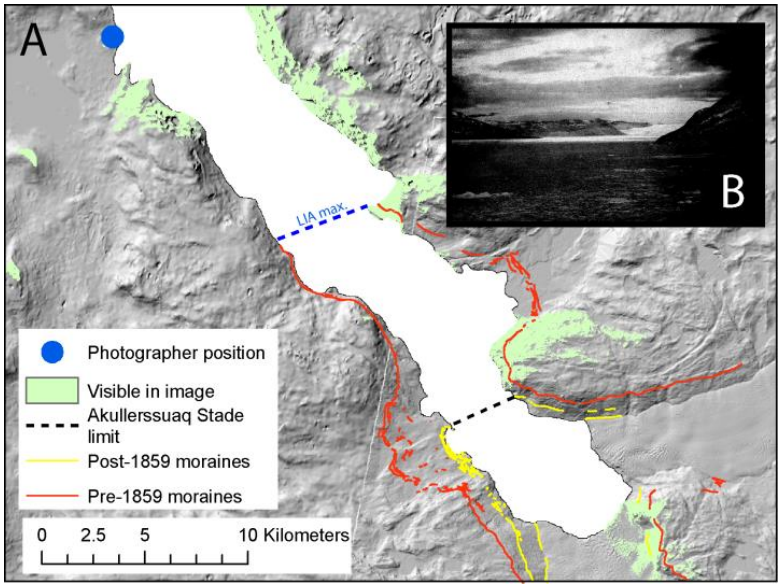

Figure 6.3 Reconstructed photographer position showing (A) the area that would be observable in the photograph shown in (B) that was acquired in 1903.

periods of readvance (Figures 6.4a, 6.4b). Averaged retreat rates of -116 m a^{-1} are observed between 1921-1946, before a rapid retreat of 3.9 km within the 2 year period from 1946-1948 (Figures 6.1a, 6.4). Between 1948-1968 KNS retreated on average by -97 m a^{-1}, before readvancing by +60 m a^{-1} up to 1979 (Figure 6.4b). A terrestrial photograph taken in 1965 with the majority of the terminus obscured shows the termini of KNS and AS to be fully diffluent.

The 1921-1968 period of sustained retreat was accompanied by positive average AT and SST anomalies (Figures 6.4c, 6.4d). The highest AT anomalies occurred during the period 1928-1941, though the largest retreat (between 1946-1948) occurred during a comparatively less extreme period of positive AT and SST (Figure 6.4).

From 1979 to 1987 KNS retreated by -658 m in total (-82 m a^{-1}), before readvancing by +758 m from 1987-1992 (+152 m a^{-1}). Using the near complete 20 year annual record of terminus fluctuations from 1992-2012, KNS advanced for 4 out of 5 years between 1992-1997, followed by retreat in 11 out of 13 years from 1999-2012 at an average rate of -103 m a^{-1}. The latter included 8 annual retreats of >100 m, with the largest retreats occurring in 2004 (-438 m) and 2005 (-316 m). These periods of advance and retreat behaviour occurred during periods of in-phase negative and positive climate anomalies respectively.

Where temporal density of observations was high, terminus behaviour that was antiphased with the prevailing climate anomalies was also observed. Examples of this include a retreat of -626 m observed in 1995 during negative climate anomalies, while two

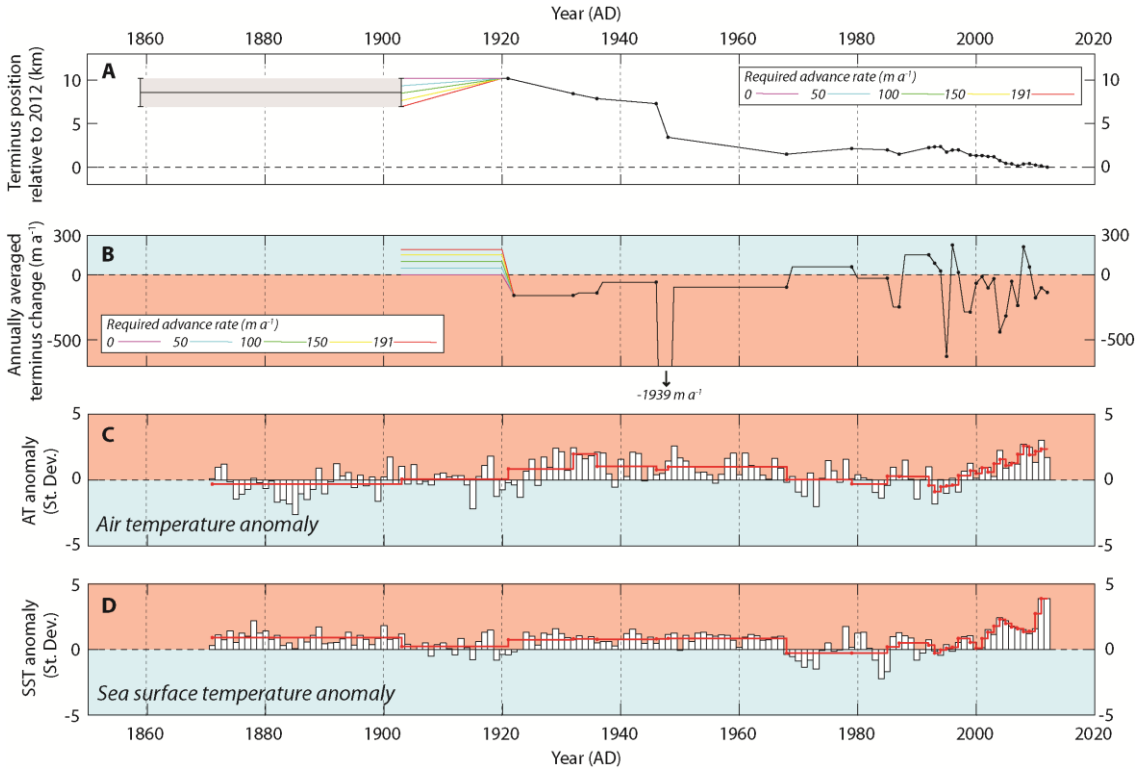

Figure 6.4 (A) Terminus change relative to the 2012 terminus position. Uncertainty in terminus position for 1859-1903 highlighted in grey, with a range of potential advance rates for 1903-1920 indicated. These range from a minimum of no change (0 m a^{-1}) to a maximum possible advance rate of 191 m a^{-1}. (B) Annually averaged rates of terminus change between observations (black dots). Includes terminus advance rates described for 1903-1921 terminus change indicated on *A*. (C) Summer ATA (June, July, August) at annual resolution (white bars), and red line showing the averaged ATA between terminus observations (Cappelen et al, 2012; Vinther et al, 2006). (D) Annual SSTA for the area 61° to 65° N 51° to 56° W at annual resolution (white bars) and red line showing the averaged SSTA between terminus observations (Rayner et al, 2003).

terminus advances occur in 2008 and 2009 despite markedly positive AT and SST anomalies (Figure 6.4). At annual resolution, the magnitude of terminus retreat/advance was also found to be unrelated to the magnitude of either climate anomaly for each particular year.

6.7 Model results

From a total of 1500 model runs conducted, 29 runs (1.9%) successfully replicated the observed dynamics of KNS according to the criteria outlined above (Figure 6.5a). Following the initiation of climate forcing in 1871 (Figures 6.5b, 6.5c), the results of each run are highly comparable up to 1884, with little modelled terminus change observed. Following this, for the period 1884 to ~1910, 6 of the 29 runs (21%) show evidence of

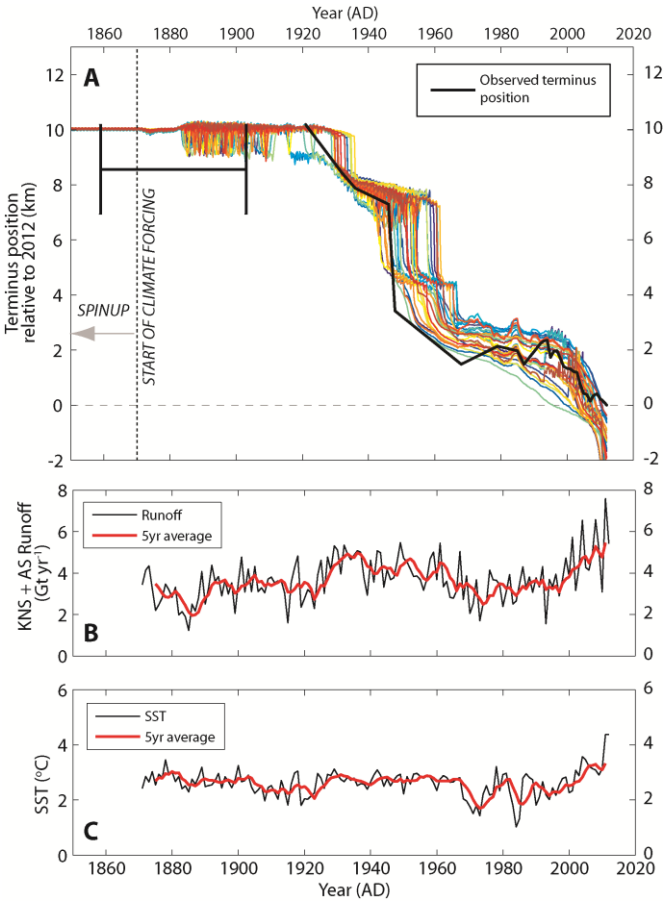

Figure 6.5 (A) Evolution of terminus position for model runs (coloured lines) determined to be successful according to the criteria outlined in the text, with observed terminus position also plotted (bold black line, with positions between observations linearly interpolated). (B) Combined KNS and AS runoff volume estimates for 1871-2012 that are used to drive the model (5 year moving average also plotted in red). (C) Absolute annual SST estimates used to drive the model from Rayner et al. (2003) for the area 61° to 65° N and 51° to 56° W (5 year moving average also plotted in red).

multi-annual terminus retreats and equivalent readvances of >750 m with periodicities of 2-4 years. A further 7 runs (24%) show evidence of at least one short lived (<5 year) oscillation in terminus position of >750 m between 1884 to 1920. None of these model runs significantly exceed the ASM position, and are thus in agreement with the geomorphological evidence presented, and the position of the 1921 terminus observation.

All model runs retreat to the observed 1936 position between modelled years 1929-1936, via a single retreat event of ~1 km. Subsequent to this, modelled retreat to the observed 1946 position is gradual, before the model successfully replicates a large topographically controlled retreat from the 1946 position. There was varying success in modelling the exact timing of this retreat (observed between 1946-1948), with the model ensemble predicting it to occur anywhere between 1943-1962. The position where the modelled terminus restabilises following the retreat through the AS confluence is generally too far advanced by ~1 km compared to the position following the 1946-1948 retreat. All

model runs then go on to over-predict terminus extent for the 1968 observation by between 0.35 to 1.59 km.

Though no model runs exactly match the precise inter-annual terminus fluctuations from 1968-2012, they do capture the general multi-annual to decadal pattern of retreat observed. This is characterised by general terminus stability within a range of ±500 m for the period 1968 to ~1999, before the terminus begins to retreat ~2 km towards the 2012 position. All of the successful model runs identified predict KNS to be in a more retreated position in 2012 than observed by a range of 0.32 to 5.04 km. Where a significant difference between observed and modelled terminus positions has occurred by the end of the model run in 2012, the divergence begins in 2010 at the earliest.

The distributions of tuning parameters for successful runs are shown in Figure 6, with the distribution of all histograms shown to be non-normal. Submarine melting related tuning parameters, α_3, and M_{base}, tended towards the mid to lower ends of the ranges tested (Figures 6.6c, 6.6d). Values of α_3 peak between 0.075 to 0.1, though there is no clearly defined peak in the distribution of M_{base} values.

In contrast, none of the d_w related tuning parameters (α_1 and α_2) approach 0 (Figures 6.6a, 6.6b), with the lowest values being 0.412 and 0.389 respectively. Construction of a correlation matrix comparing all tuning parameter values for all

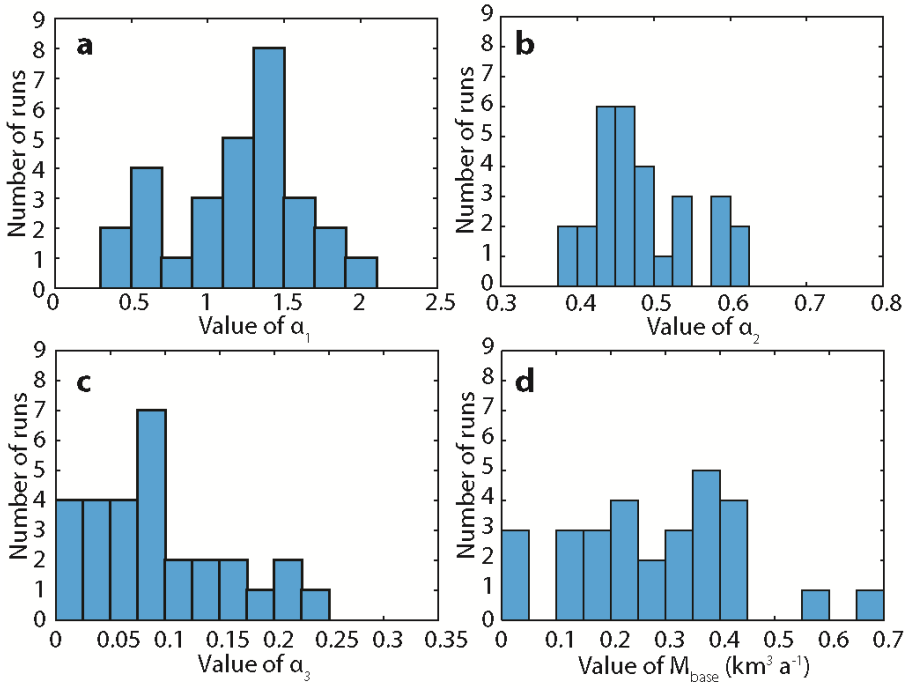

Figure 6.6 The distribution of the tuning parameters (a) α_1 (bin width = 0.2), (b) α_2 (bin width = 0.025), (c) α_3 (bin width = 0.025), and (d) M_{base} (bin width = 0.05 km^3 a^{-1}) for successful runs as defined by the criteria outlined in the text. Minimum and maximum *x*-axis values represent the full range of values tested within the 1500 model runs.

	α_1	α_2	α_3	M_{base}
α_1	-	**-0.92**	0.29	**-0.47**
α_2	**-0.92**	-	**-0.46**	0.29
α_3	0.29	**-0.46**	-	**-0.43**
M_{base}	**-0.47**	0.29	**-0.43**	-

Table 6.3 Pearson correlation coefficient values for tuning parameters of successful model runs (n = 29). Correlation coefficients with p-values <0.05 are highlighted in bold.

successful runs also demonstrates a significant inverse relationship between the value of α_1, and the AS confluence parameter, α_2 (r = -0.92). While other significant correlations are observed (Table 6.3), these are not of sufficient strength to allow confident conclusions to be drawn.

6.8 Discussion

6.8.1 Observed terminus behaviour

From 1903 to 2012 AT and SST anomalies covaried, with the terminus generally undergoing retreat during periods of positive anomalies and advancing/stabilising when near/below baseline climate (Figure 6.4). Exceptions to this in-phase behaviour were only identified for the period 1992-2012, where a higher temporal density of terminus observations exists. However, by averaging annual observations over periods of sustained negative (1987-1997) and positive (1998-2012) climate anomalies, the terminus responds in phase with the climate anomalies. This demonstrates the risks of using short datasets (2-5 years) to determine how a TWG is responding to climate forcing, highlighting the inherent noisiness, potential important of antecedence, and the non-linearity of TWG response to climate.

A notable caveat to this occurs where significant topographically controlled glacier retreats occur, such as the one occurring between 1946-1948. These events could potentially skew annually averaged terminus change rates when attempting to characterise terminus response to climate forcing. The relative importance of this will be entirely dependent on the magnitude of individual events, and most significant where there is potential for multi-kilometre topographically controlled retreat. For example, if the 1946-1948 retreat event was not temporally well constrained, it could have significantly biased the terminus change rate values between 1936-1968 (Figure 6.4b).

Since TWGs exhibit varying degrees of non-linear response to climate forcing, the identification of where and when these rapid multi-kilometre retreat events occur is crucial for interpreting the causes of terminus fluctuations. Where comparatively smaller (i.e. <500 m) climatically anti-phased advance/retreat events occur, their effect on average terminus change rates can be mitigated by averaging change over timescales up to, or greater than a decade. For example, extending the 1992-1997 average (51 m a^{-1} retreat) to cover the period 1987-1997 (91 m a^{-1} advance) provides a more representative impression of multi-annual terminus behaviour, since 5 out of the 6 observations available show terminus advance. Interpreting absolute terminus change rate values should therefore be done with caution, and in most cases will be more representative of the average direction of terminus change rather than the absolute magnitude of annual change.

Taking into account uncertainties due to topographic controls on terminus stability, observations of terminus change over a period of several years are more likely to allow a more accurate evaluation of a TWG's response to climate forcings. However, for this study, deconvolving the relative importance of AT versus SST in driving terminus change is difficult using observations alone, given that both climate drivers vary in phase for 1903-present. It could potentially be argued that AT is the primary driver of change, since the 33 year period of positive anomaly SST from 1871-1903 had relatively little impact on the terminus stability of KNS. However, fjord geometry could also have been a significant factor stabilising the terminus during this time. Arguably this becomes less likely when it is considered that while SST was similar for the period 1921-1948, positive AT allowed KNS to retreat through the same section of fjord and through its confluence with AS within 26 ± 1 years (Figure 6.4). However, given the lack of certainty in terminus position between 1871-1920, it is not possible to robustly verify these arguments.

6.8.2 Implications of modelling

The observed terminus behaviour of KNS from 1921-2012 was successfully replicated by 29 of 1500 model runs using surface runoff and SST records as drivers of terminus change. This demonstrates that the parameterisations used to scale these climate records to d_w and M respectively can successfully be used to simulate the observed pattern of behaviour of a tidewater glacier over centennial timescales. Where the observational record is of sufficient detail to resolve inter-annual terminus fluctuations (1992-2012), the model does not replicate these. This is to be expected given (1) the flowband nature of the model and associated depth and width integrations over each grid cell, meaning that fluctuations of

terminus configurations such as the creation of calving bays cannot be replicated (e.g. Figure 6.1b), (2) the uncertainty in fjord bathymetry and geometry potentially affecting relative terminus stability, and (3) the use of single terminus observations as notionally definitive indicators of annual terminus change, where the complex nature of calving and associated sub-annual terminus fluctuations make any direct one-to-one comparison of modelled results to annual resolution observations inappropriate. Valid comparison of model results to observations should therefore only be attempted over multi-annual timescales where terminus dynamics within calving bays, sub-annual calving events and fine scale uncertainties in fjord topography become comparatively less significant.

For successful model runs, the interrelationships between the parameter values that determine d_w and M sensitivity to the climate records also inform the relative importance of changes in atmospheric and oceanic forcing in driving terminus change. The lack of any significant relationship between α_1 and α_3 demonstrates that a change in model sensitivity to surface runoff is not offset by any change in model sensitivity to SST. Taken alone, this evidence indicates that either atmospheric forcing (via surface runoff) dominates oceanic forcing (via SST), or *vice versa*. However, the occurrence of runs where α_3 does not significantly exceed 0 (i.e. where runs experience negligible M variability) demonstrate that the model can successfully reproduce observed behaviour with nearly no changes in oceanic forcing from year to year. Although some successful model runs did have significant inter-annual M variability (e.g. the maximum range of M values for an entire 141 year model run was 0.76 km^3 a^{-1}), each model run always requires significant atmospheric forcing variability to allow it to replicate observations. The importance of oceanic forcing variability can therefore not be entirely discounted.

The model demonstrates that knowledge of atmospheric forcing variability (via runoff), without needing to vary oceanic forcing, can be sufficient to reproduce realistic patterns of observed glacier behaviour at KNS over the last century. However, the precise physical mechanism by which air temperature could drive observed change requires further investigation. For example, though a combination of modelled and empirically estimated runoff values have been used to drive changes in d_w to force the model, subglacial runoff variability is also known to drive rates of submarine melting at the terminus (Jenkins, 2011; Xu et al., 2012; Sciascia et al., 2013). Therefore we do not rule out that the centennial behaviour observed could also be explained by calving driven by seasonal changes in submarine melt rates, that are in turn a function of subglacial runoff (e.g. Sciascia et al. 2013).

The relative insensitivity to changes in oceanic forcing is not necessarily surprising given the hydrographic setting of KNS – located at the end of a >100 km long fjord system that is thought to be largely insulated from changes in ocean conditions due to the presence of a shallow sill at its entrance (Mortensen et al., 2011; 2013). This has previously been used to suggest that recent changes in ocean conditions (e.g. Straneo and Heimbach, 2013) have not affected the dynamics of KNS significantly (Straneo et al., 2012). The results presented here are therefore compatible with this argument.

The over-estimation of terminus retreat by 2012 of every successful run is thought to result from the poor knowledge of fjord width geometry beyond the contemporary glacier terminus. Upstream of the 2012 terminus, the lateral ice margins are used to define model glacier width, leading to a likely over-estimation of the prescribed fjord width. The divergence between the actual and prescribed fjord width is therefore likely to increase upglacier, increasing the likelihood of model error in this area. This explains why significant divergence from the observational record only occurs once the modelled terminus has retreated ~1.5 km beyond the 2012 terminus. Any attempt at modelling the future fluctuations of KNS will therefore require both improvements to subglacial topography estimates and comprehensive assessments of fjord width uncertainties as part of any predictions.

6.9 Conclusions

Utilising multiple lines of evidence, it has been possible to reconstruct terminus fluctuations of KNS from 1859-2012. This study therefore completes the record of terminus fluctuations of KNS from its LIAmax, in 1761, up to the present (Chapter 5), providing one of the longest, and most detailed records of observed TWG change in Greenland. Results from numerical modelling show that the fluctuations of KNS can be simulated through parameterisations that link surface runoff to a crevasse water depth based calving criterion. Changes in both/either crevasse water depth and/or runoff driven rates of submarine melt are therefore suggested as potential drivers of observed change. Although ocean driven changes in submarine melt rates are not always required for the model to replicate the observed length variations of KNS, results do not allow their importance to be discounted entirely.

Observations of KNS show it to respond in phase with AT and SST anomalies over multi-annual to decadal timescales from at least 1921-2012. However, where inter-annual comparisons to AT and SST are possible (1992-2012), climatically anti-phased terminus

fluctuations are observed. This highlights the inherent noisiness of terminus response over short timescales, the potential importance of antecedence, and the dangers of using similarly short calibration periods for predictive modelling efforts.

Results from numerical modelling successfully capture the terminus dynamics of KNS over multi-annual to decadal timescales, though not precise inter-annual fluctuations. This is due to a combination of uncertainties in fjord topography, and the approximations inherent to the depth and width integrations associated with using a one-dimensional flow-band model.

Nevertheless, this study demonstrates that simple flow-band numerical models of tidewater glaciers can be used to capture TWG dynamics over centennial timescales. This provides validation that these models can be useful tools for both palaeo- and contemporary/prognostic modelling efforts. However, the primary challenge to their use as predictive tools remain the accurate definition of subglacial topography and fjord width, which exert dominant controls on modelled glacier stability. Any future efforts at prognostic modelling of TWGs should therefore seek to account for these uncertainties in addition to those associated with sensitivity to climate forcing.

Chapter 7

Conclusions

The aim of this thesis is to investigate controls on the stability of a large tidewater glacier of the Greenland Ice Sheet (GrIS) over centennial timescales. This was motivated by the uncertainty that surrounds the multi-decadal to centennial timescale controls on tidewater glacier behaviour in Greenland, and the potential for future changes in oceanic and/or atmospheric forcing to increase mass loss from GrIS.

Previous work has established that the current widespread retreat of Greenlandic tidewater glaciers has been driven by instabilities arising at their termini (Nick et al., 2009). There is controversy regarding the relative importance of atmospheric and oceanic changes that have driven extensive retreat observed over the last two decades (e.g. Straneo et al., 2013; Carr et al., 2013b). By reconstructing and modelling of the dynamics of Kangiata Nunaata Sermia (KNS) from its Little Ice Age maximum (LIAmax) to present, this thesis has investigated how KNS responded to changes in atmospheric and oceanic forcing over multi-decadal to centennial timescales. The ability of a well-established one-dimensional flow-band numerical model (Nick et al., 2010; 2013) to simulate observed dynamics was also evaluated. In doing so, its utility as a tool to generate reliable estimates of the behaviour of tidewater glaciers over the next 100-200 years (e.g. Nick et al., 2013) was also tested.

To achieve this, a robust comparison of glacier observations to model results was required. Therefore the first systematic comparison of different methods used to track tidewater glacier terminus change was undertaken to determine their relative accuracies, and how/if the results of each can be related to positions along a model flowline (Chapter 4). This necessitated two new methods of tracking terminus change to be devised. Both of these improve on the accuracy of existing methods, and allow direct comparison of observed terminus positions to a model flowline position.

The LIAmax of KNS was identified to have occurred by 1761, with either one or two multi-kilometre retreats occurring by 1859 (Chapter 5). Comparison of model results to pre-1859 observations showed that reconstructed behaviour could be simulated by modest changes in crevasse water depths within the model (Chapter 5). The increase in crevasse water depths required to drive this retreat was consistent with the magnitude of change in the average modelled surface runoff between the periods 1971-1990 and 1991-

2012. Observed glacier change for this period could not be simulated by driving the model using realistic changes in oceanic forcing only.

Where atmospheric and oceanic forcing data were available for the period 1871-2012, the terminus of KNS was shown to respond in phase with both climate anomalies (Chapter 6). Using the same climate data to drive the model, these dynamics were also successfully simulated. Results showed that significant atmospheric forcing (linked to crevasse water depth via surface runoff) is needed for all model runs to simulate observed behaviour. Variability in oceanic forcing is not necessarily required.

This thesis therefore presents a detailed record of observed glacier dynamics at KNS from its LIAmax to present, which can be accurately related to results of numerical modelling. It also uses model results to determine that atmospheric rather than oceanic forcing is the likely driver of multi-decadal to centennial timescale variability of KNS.

7.1 Quantification of terminus change and glacier reconstruction

Results from Chapter 4 demonstrated that the newly devised curvilinear box method (CBM) and extrapolated centreline method (ECM) related terminus observations to model flowline positions with the minimum error. In contrast to existing methods, these were able to partially or completely account for changes in fjord orientation, width and terminus geometry. The new methods therefore represent improvements on existing ones for both the accurate quantification of terminus change in and of itself, and for allowing accurate comparison of observations to flowline model output.

The ECM also has significant utility as a tool for comparing geomorphology such as lateral moraines to flowline model output. This is demonstrated in Figure 5.9 where the lateral moraines of KNS from the LIAmax and Akullersuaq Stade could be directly compared to the modelled longitudinal glacier profile. This technique enhanced the level of confidence in the model tuning and validation procedures that form parts of Chapters 5 and 6. An implication of this is that the ECM also has significant potential for other scenarios where lateral moraines or DEM evidence is used to constrain flowline glacier profile results. This would be suitable for both steady state (e.g. Rea and Evans, 2007; Benn and Hulton, 2010), or transient modelling setups (e.g. Chapters 5 and 6; Oerlemans et al., 2011; Anderson et al., 2014).

Analysis conducted in Chapters 5 and 6 was also successful in demonstrating that useful, quantitative evidence of terminus positions can be gained from interrogation of

qualitative sources. Using a combination of written accounts, geomorphology, GIS analyses from distal photographs and maps, it was possible to reconstruct glacier behaviour from 1761 to 1903 without the benefit of a single clear photograph of the terminus (the first being available from 1921). Although previous work has been undertaken using similar source material (e.g. Weidick, 1959; Weidick et al., 2012), GIS analyses such as those applied in Chapters 5 and 6 could be applied to other Greenlandic glaciers allowing explicit quantification of observation error bounds.

Utilising such source material is likely to be of greatest use for the periods preceding the photographic record (generally available back to ~1930; e.g. Bjørk et al., 2012). The potential of qualitative data to provide glacier configuration and chronological tie point information demonstrates its utility in augmenting proxy and geomorphological based reconstructions (e.g. Lloyd et al., 2011; Andresen et al., 2012). For example, generating accurate and precise age models for reconstructions is critical when attempting to evaluate behaviour against any independent proxy climate record (e.g. Kobashi et al., 2010; D'Andrea et al., 2011; Kamenos et al., 2012). However, radiometric and other dating technique errors are frequently greater than the potential response timescales of tidewater glaciers to climate. Qualitative observations, made at a known time, can therefore be used within an existing age model to provide precise temporal constraint to a particular glacier configuration.

Photographs of the terminus of KNS obtained by archaeologists working on nearby Norse ruins also provided a useful source of information (e.g. Bruun, 1917; Roussell, 1941). The location of KNS near to a Norse farm ruin is therefore highly advantageous. However, given the proximity of many other glaciers to Norse farm ruins, most notably in the Eastern Settlement (Danish: Østerbygd) ~200 km south of Godthåbsfjord, similar previously unrecognised source material may also exist and be of significant use for reconstructions elsewhere.

Where direct observations of KNS' terminus are available (Chapter 6) there is a high level of confidence in the accuracy of the reconstruction presented. The terminus was shown to respond in phase with climate anomalies averaged over multi-annual timescales for the years 1987-2012 (where observation density is highest), suggesting that the ability to characterise terminus response to climate is not necessarily inhibited by a lack of observations at high (i.e. seasonal/1-2 year) temporal resolution. An exception to this will be relevant where rapid, multi-kilometre topographically driven retreats occur, such as that occurring at KNS between 1946-1948. Fortunately, this retreat of KNS is temporally well

constrained, though if this was not the case, dynamics would need to be reconstructed indirectly using assessments of relative changes in fjord topography and geomorphological evidence. Identification of such behaviour is crucial for establishing whether terminus change in certain sections of fjords are likely to be climatically or dynamically driven. This demonstrates how studying multiple sources of information can provide better constraint for glacier dynamic reconstructions, compared to those utilising only single sources (e.g. only images/geomorphology/qualitative sources).

7.2 Evaluation of applying the Nick et al. model to KNS

The overarching advantage of the 1D model used in this study is its proven ability to emulate the characteristic dynamics of marine terminating glaciers (e.g. Jamieson et al., 2012; 2014; Nick et al., 2010; 2012; 2013; Vieli and Nick, 2011). This thesis has shown that given the correct climate forcing, parameterisations and parameter values, the model is also capable of replicating observed tidewater glacier behaviour over centennial timescales (Chapter 6). This was determined easily due to the model being computationally inexpensive to run. Consequently, this allowed hundreds of model simulations to be conducted, varying tuning parameters according to Monte Carlo methods. In doing so, an ensemble of model runs were produced where the model successfully matched observations, with the nature of the method ensuring that parameter selection was entirely unbiased. Subsequent analysis of the interrelationships between different parameter values could therefore be undertaken confidently, knowing that a broad range of climate forcing scenarios had been fully explored.

Nevertheless, the computational efficiency of the model necessitates the simplification of some boundary conditions and processes that affect glacier flow. These can potentially impact the results and the applicability of the model to certain scenarios, for example:

- *Fjord topography* – the 1D nature of the model requires that ice flow is integrated over both ice depth and width (Section 3.2). This study has been able to simulate realistic behaviour by (1) defining fjord width as the sum of the shortest linear distances to the fjord shorelines, (2) defining bed topography in the fjord from available bathymetry measurements, and linearly interpolating values between them, (3) implicitly assuming a channel with a rectangular cross section. However, the current model set up neglects factors that may impact flow relating to the cross-

sectional shape of the fjord (e.g. Nye, 1965). For KNS, this should have negligible impact on flow given that it is a wide glacier with a large width to ice thickness ratio (>5), meaning that its shape factors will generally approximate $1 - \delta$, where δ = a small number. However, for narrower/thicker glaciers, where the width to thickness ratio is smaller, fjord shape is likely to become a significant factor affecting glacier flow (Nye, 1965). For such situations, Adhikari and Marshall (2012) have determined a range of correction factors for flowline models that parameterise the lateral drag resulting from fjord shape. They state that these are relevant to models of any order of complexity, and therefore offer an alternative parameterisation for lateral drag that is likely to be relevant where the model is applied to narrower/thicker glaciers.

Given previous analyses by Enderlin et al. (2013) using a similar flowline model, the level of uncertainty in bed topography (both contemporary subglacial, and fjord bathymetry) also had the potential to significantly impact model results. However, sensitivity tests undertaken as part of Section 5.10 demonstrated that each model run produced a similar pattern of results. An expanded version of Figure 5.10 showing the results of all sensitivity analyses (Figure 7.1) shows that all runs demonstrate comparable behaviour, with modelled calving fluxes generally converging on the empirically calculated ~6 km^3 a^{-1} values determined by the author as a co-author on Van As et al. (2014). Where notable divergence in results between calving fluxes occur, notably between 2-6 km from the 2012 position, this is a result of (1) changes in modelled terminus position occurring at a higher rate than the model recorded output (every 0.5 year), and (2) this area being the region of the fjord with greatest bathymetric uncertainty (Figure 3.10). The divergence between these model runs also occur primarily over sub-annual timescales as the terminus retreats rapidly through the confluence region of KNS and AS. Therefore despite the apparent wide spread of calving flux values between 2-6 km, the divergence in calving fluxes between model runs is largely transient. This becomes apparent as results display greater agreement for positions between -1-2 km from the 2012 terminus.

- *Climate forcing* – the 1D setup of the model also necessitates that any climate forcing applied to the model is integrated over the width and/or depth of each relevant grid cell. For example, SMB for each grid cell must be defined for an area equivalent to the grid size multiplied by the channel width, which at the ice divide

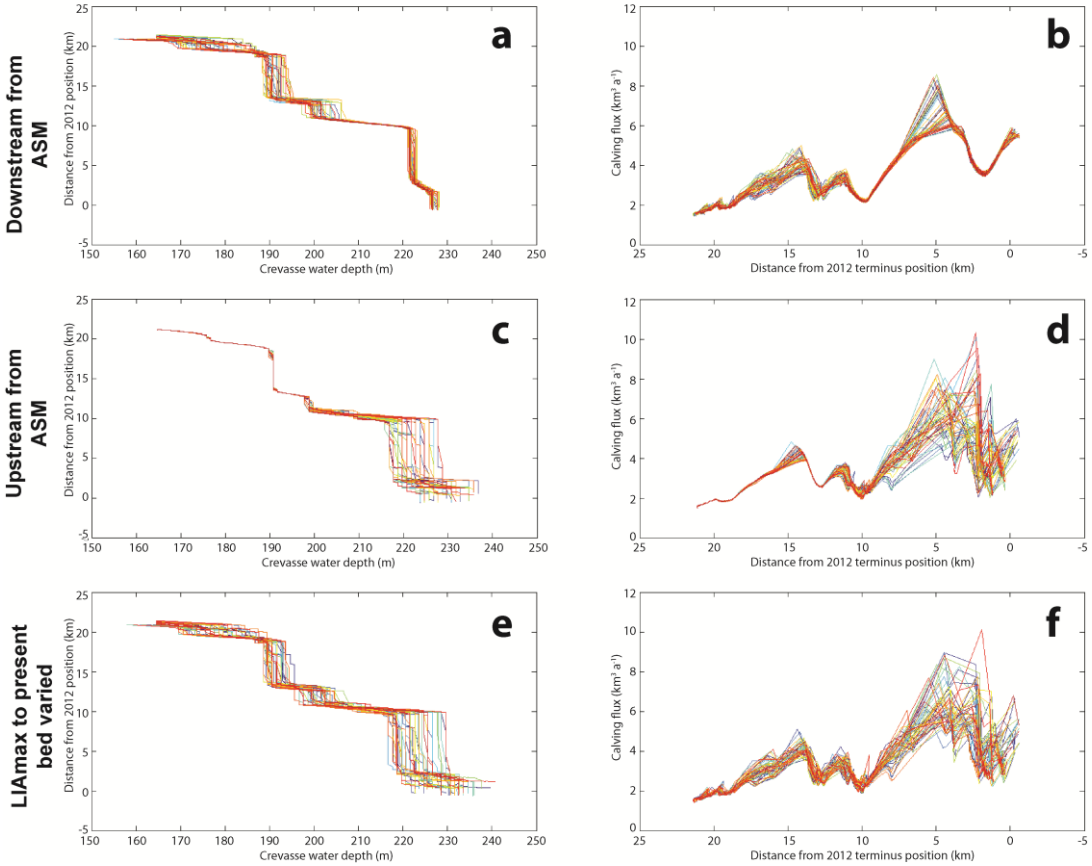

Figure 7.1 Model sensitivity to changes in bed topography as described in Section 5.10 showing terminus position for a given crevasse water depth forcing, and modelled calving fluxes for (A, B) 50 different bed configurations varied randomly downstream of the Akullersuaq Stade maximum (ASM), (B, C) as for A and B but for varying the bed upstream of the ASM, (D, E) as for A and B but for varying all of the bed from the 2012 position to the LIAmax.

of KNS equates to a strip of the ice sheet with dimensions of ~0.25 km by 116.4 km (area of ~29.1 km^2). Representing SMB variability over such an extensive area was accounted for in the model by taking an average SMB value over the relevant region. Similarly, both crevasse water depth and submarine melt rates are integrated over glacier width. Effects such as the concentration of submarine melt around a subglacial drainage portal (Xu et al., 2013) or differing terminus undercut shapes (O'Leary and Christoffersen, 2013) cannot be directly simulated by the model in its current form.

Many processes are also omitted altogether from the model setup used, including glacier hydrology, cumulative damage mechanics (CDM; e.g. Borstad et al., 2012), cryohydrologic warming (CW; e.g. Phillips et al., 2010), and mélange backstress (e.g. Amundsen et al., 2010). Although the model results presented in Chapters 5 and 6 are able to successfully replicate the dynamics of KNS, omitted processes may also affect glacier dynamics. Consequently, for the current model set up either (1) existing parameterisations

and tuning parameter values given by the Monte Carlo simulations are compensating for the absence of omitted processes, or (2) the inclusion of omitted processes in the future model runs will allow it to capture behaviour that is currently not represented in model output.

For example, if they are significant, both CDM and CW are likely to impact flow/calving behaviour over multi-annual to decadal timescales (e.g. Phillips et al., 2010; Borstad et al., 2012). However, the current model setup is capable of capturing the behaviour of KNS over these timescales. It therefore follows that the effects of CDM and CW are either negligible or are indirectly accounted for within the crevasse water depth and submarine melt parameterisations that are already implemented. However, this is not to say that future work does not need to account for these processes. Explicit parameterisation may improve model performance and help to identify their relative importance with respect to glacier flow/calving behaviour.

Conversely, both glacier hydrology and mélange are likely to have significant effects on glacier flow at sub-annual timescales (Amundsen et al., 2010; Walter et al., 2012; Nick et al., 2013). Fluctuations over these timescales are not currently captured by model results (Chapter 6). However, it should be noted that the empirical effect of hydrology on the multi-annual behaviour of tidewater glaciers remains largely unconstrained (e.g. Sole et al., 2013), while the significance of mélange formation at KNS is also uncertain. Adequate simulation of such changes at KNS using the model would also require a calibration dataset including several years of sub-annual resolution velocity and terminus position data (e.g. Nick et al., 2013). At present, such detailed data are not available for KNS.

Where limited velocity data do exist, subglacial drainage system evolution appears to impact seasonal flow velocities near the terminus (e.g. Figure 3.2; Ahlstrøm et al., 2013). Consequently, simple linear relations between runoff and sliding rates are unlikely to accurately represent hydrologically driven dynamic behaviour. The inability to capture sub-annual dynamics arising from hydrology will then also likely impact how mélange forcing will affect modelled behaviour. Adequate simulation of sub-annual timescale dynamics at KNS will therefore require improvement to the hydrological parameterisation within the model setup.

The approximations inherent to a 1D flowline model also mean that their ability to realistically simulate sub-annual or inter-annual timescale fluctuations is questionable. This is because (1) the integration of terminus behaviour over depth and width means that

calving bay dynamics that arise from lateral variability of bed topography cannot be captured by the model, and (2) terminus behaviour over sub-annual to inter-annual timescales often involves the terminus advancing and retreating through such calving bays (Figure 6.1b). Sub-annual/inter-annual calving bay dynamics are therefore only likely to be captured by vertically integrated 2D, or higher order 3D glacier models. The lack of fit between results of the Nick et al. model and inter-annual terminus variability observed from 1992-2012 is therefore not entirely surprising (Chapter 6). Conversely, the model is successful in replicating multi-annual to decadal resolution behaviour of KNS. This provides encouragement that 1D flowline models can capture the pattern and approximate timing of real tidewater glacier behaviour over these timescales.

The success of the model also demonstrates that the relatively low spatial resolution of fjord bathymetry data available for KNS (mostly >1 km spacing; Figure 3.10) was sufficient to allow the model to capture realistic behaviour. When more detailed bathymetric data become available for the fjord, this will allow an evaluation to be made as to whether (1) linearly interpolated bathymetry data coincidentally match reality, or (2) if width variability exerts a relatively greater control on terminus dynamics. It will also allow the model itself to be interrogated in greater detail through a more comprehensive analysis of the effects of changing time steps, grid sizes, and sampling resolution of width and bed topography.

7.3 Predicting the future of KNS

The ability to predict the future evolution of KNS will be primarily constrained by the uncertainty surrounding subglacial topography and fjord width (Chapter 6). Any attempt at conducting forward modelling at KNS, similar to the approach taken by Nick et al. (2013) for other outlets, should therefore seek to account for these uncertainties. For KNS this could be achieved by identifying the range of uncertainties in bed topography and fjord width from the distributed bed reconstruction (Figure 3.11). These could then be varied between model runs according to a Monte Carlo style setup, forcing the model using the climate scaling parameter values identified by successful model runs in Chapter 6.

These forward model runs would therefore be calibrated against 140 years of observational data – currently an unprecedented length for any study aiming to model the future dynamics of a Greenlandic tidewater glacier. They would also account for both boundary condition uncertainty and a range of possible calibrations. Results generated by

the ensemble will therefore provide a median prediction for the future evolution of KNS within a robustly defined envelope of uncertainty. The separate treatment of calibration and boundary condition uncertainties would also allow the relative effect of each on prediction ranges to be evaluated. This would help to identify (1) how effective model calibration is in delivering consistent forward modelling results, and (2) how uncertainties in the definition of boundary conditions may limit the ability of the model to generate a coherent prediction of future tidewater glacier behaviour.

7.4 Outlook

Results from this thesis have demonstrated that the multi-decadal to centennial behaviour of KNS is likely to be driven by atmospheric rather than oceanic forcing. However, each Greenlandic tidewater glacier comes with its own unique climatic and topographic setting, meaning that any attempt to extrapolate findings from one glacier to another should only be done with extreme caution. For example, given that Godthåbsfjord is relatively insulated from changes in deep ocean currents (Mortensen et al., 2011; 2013), findings obtained from KNS are unlikely to be directly applicable to tidewater glaciers with a more open fjord connection to changing ocean currents (e.g. Straneo et al., 2012). Within the context of previous modelling studies of other major Greenlandic tidewater glaciers (e.g. Nick et al., 2013), results presented here help to demonstrate this complexity.

A greater understanding of how sensitivity to forcing varies between glaciers could therefore be gained by undertaking detailed studies of other tidewater glaciers over similar timescales. In order to ascertain a more complete picture of tidewater glacier behaviour in Greenland, this should include studies of glaciers that comprise a full range of catchment sizes and discharges, rather than a pure focus on the intensively studied large outlets (e.g. Jakobshavn Isbræ, Helheim Glacier, Petermann Glacier). This may also help to identify underlying characteristics of tidewater glacier response to climate with respect to velocity, discharge and/or setting, amongst other factors. This is of importance given the non-linearity of tidewater glacier response to climate. Consequently, the 15 outlets that were identified to account for 77% of Greenland ice mass loss since 2000 (Enderlin et al., 2014) may not necessarily be the major contributors to future change.

As longer records of tidewater glacier change are generated, it will also become possible to identify the most dynamic outlets, similar to KNS, and hence which have been most susceptible to past changes in climate forcing. Investigation of these catchments and

their multi-decadal to centennial timescale dynamics will therefore help to establish the range of similarities and differences in the controls on their variability.

Potential also exists for establishing whether a minimum calibration period is required to accurately capture observed behaviour of tidewater outlets. This would be achieved by undertaking model calibration using incremental calibration period lengths, before comparing resulting ensemble outputs to observed behaviour. Although longer records of change will always provide more robust calibration, determining whether a minimum calibration period exists would help to ascertain the absolute need to extend calibration records beyond the 20th century. If a minimum calibration period exists, this could also be used to help rationalise effective use of computational resources through curtailing model calibration and spin up periods.

After demonstrating the applicability of the Nick et al. model over centennial timescales, the potential for millennial timescale simulations of ice stream/outlet glacier dynamics should also be explored in greater detail. The model's computational simplicity allows for potentially hundreds to thousands of forcing scenarios to be tested, with a growing body of literature becoming available for Greenland that would provide suitable model calibration datasets (e.g. Kelley et al., 2013; Lane et al., 2013; Larsen et al., 2013; Roberts et al., 2013). Such simulations would allow identification of forcing scenarios that could potentially instigate rapid glacier response similar to that observed during the last deglaciation. It could also help establish how/if glacier sensitivity to particular forcing changes over centennial to millennial timescales.

For KNS it may be possible to simulate its dynamics through the entire Holocene. This would utilise a combination of the glacier reconstruction results of Larsen et al. (2013) and Chapters 5 and 6 for model calibration. In doing so, the potential dynamism of KNS could be estimated, in addition to its likely extent during the Norse settlement of the region from 985 AD leading up to abandonment in c.1350 AD. This would be of significant interest to archaeologists studying Norse Greenland, given the uncertainty surrounding living conditions in this region, and how inhabitants interacted with the changing climate and ice sheet expansion (e.g. Roussell, 1941; Barlow et al., 1997; Dugmore et al., 2012).

While the behaviour of KNS since the mid-18th century is dominated by retreat, forcing the model over millennial timescales would also allow model performance during advance phases to be evaluated. Significant potential exists at KNS for generating millennial timescale reconstructions of both advance and retreat dynamics, utilising similar

methods to those of Briner et al. (2010). Such reconstructions would therefore provide additional model constraint, and allow model parameterisations to be tested across an even greater range of climate conditions and glacier geometries.

Finally, this thesis provides an example of how disparate data and methods can be integrated to interrogate a particular glaciological problem. Over the course of aiming to investigate the multi-decadal to centennial change at KNS, utilising an array of methodologies has helped to highlight issues and shortfalls that may arise between different areas of glaciological research. For example this approach has led to this thesis applying novel approaches to glacier reconstruction, addressing issues of how to accurately match up terminus observations accurately to model output, and contributed to the continued development and evaluation of a numerical model. Similarly integrative approaches to future studies in glaciology therefore have significant potential to develop novel methodologies that allow more effective uses of available data.

References

Adhikari, S., & Marshall, S.J. (2012). Parameterization of lateral drag in flowline models of glacier dynamics. *Journal of Glaciology, 58*(212), 1119-1132, (doi: 10.3189/2012JoG12J018).

Ahlstrøm, A.P., Andersen, S.B., Andersen, M.L., Machguth, H., Nick, F.M., Joughin, I., Reijmer, C.H., van de Wal, R.S.W., Merryman Boncori, J.P., Box, J.E., Citterio, M., van As, D., Fausto, R.S., & Hubbard, A. (2013). Seasonal velocities of eight major marine-terminating outlet glaciers of the Greenland ice sheet from continuous in situ GPS instruments, *Earth System Science Data*, 6, 27-57, (doi:10.5194/essdd-6-27-2013).

Alley, R.B., Andrews, J.T., Brigham-Grette, J., Clarke, G.K.C., Cuffey, K.M., Fitzpatrick, J.J., Funder, S., Marshall, S.J., Miller, G.H., Mitrovica, J.X., Muhs, D.R., Otto-Bliesner, B.L., Polyak, L., & White, J.W.C (2010). History of the Greenland Ice Sheet: paleoclimatic insights. *Quaternary Science Reviews*, *29* (15), 1728-1756 (doi: 10.1016/j.quascirev.2010.02.007).

Amundson, J.M., Truffer, M., Lüthi, M.P., Fahnestock, M., West, M., & Motyka, R.J. (2008). Glacier, fjord, and seismic response to recent large calving events, Jakobshavn Isbræ, Greenland. *Geophysical Research Letters*,*35*(22), L22501, (doi:10.1029/2008GL035281).

Amundson, J.M., Fahnestock, M., Truffer, M., Brown, J., Lüthi, M.P., & Motyka, R. J. (2010). Ice mélange dynamics and implications for terminus stability, Jakobshavn Isbræ, Greenland. *Journal of Geophysical Research: Earth Surface, 115*(F1), F01005, (doi:10.1029/2009JF001405).

Andresen, C.S., Straneo, F., Ribergaard, M.H., Bjørk, A.A., Andersen, T.J., Kuijpers, A., Norgaard-Pedersen, N., Kjær, K.H., Schjøth, F., Weckstrom, K. & Ahlstrøm, A.P. (2012). Rapid response of Helheim Glacier in Greenland to climate variability over the past century. *Nature Geoscience*, *5*(1), 37-41, (doi:10.1038/ngeo1349).

Anderson, L.S., Roe, G.H., & Anderson, R.S. (2014). The effects of interannual climate variability on the moraine record. *Geology*, *42*(1), 55-58, (doi: 10.1130/G34791.1).

Åström, J.A., Riikilä, T.I., Tallinen, T., Zwinger, T., Benn, D., Moore, J.C., & Timonen, J. (2013). A particle based simulation model for glacier dynamics, *Cryosphere Discussions*, 7, 921-941, (doi:10.5194/tcd-7-921-2013).

Bamber JL, Layberry RL, & Gogineni SP (2001). A new ice thickness and bed data set for the Greenland ice sheet: 1. Measurement, data reduction, and errors. *Journal of Geophysical Research: Atmospheres,106* (D24), 33773-33780 (doi: 10.1029/2001JD900054)

Bamber, J., van den Broeke, M., Ettema, J. Lenaerts, J. & Rignot, E. (2012). Recent large increases in freshwater fluxes from Greenland into the North Atlantic, *Geophysical Research Letters*, 39, L19501, (doi:10.1029/2012GL052552).

Bamber, J.L., Griggs, J.A., Hurkmans, R.T.W.L., Dowdeswell, J.A., Gogineni, S.P., Howat, I., Mouginot, J., Paden, J., Palmer, S., Rignot, E., & Steinhage, D. (2013). A new bed elevation dataset for Greenland, *Cryosphere*, 7, 499-510, (doi:10.5194/tc-7-499-2013).

Barlow, L.K., Sadler, J.P., Ogilvie, A.E., Buckland, P.C., Amorosi, T., Ingimundarson, J.H., Skidmore, P., Dugmore, A.J., & McGovern, T.H. (1997). Interdisciplinary investigations of the end of the Norse Western Settlement in Greenland. *The Holocene, 7*(4), 489-499 (doi: 10.1177/095968369700700411).

Bartholomew, I., Nienow, P., Mair, D., Hubbard, A., King, M.A., & Sole, A. (2010). Seasonal evolution of subglacial drainage and acceleration in a Greenland outlet glacier. *Nature Geoscience, 3*(6), 408-411, (doi:10.1038/ngeo863).

Bassis, J.N., & Jacobs, S. (2013). Diverse calving patterns linked to glacier geometry. *Nature Geoscience*, *6*(10), 833-836 (doi:10.1038/ngeo1887).

Benn, D.I., & Hulton, N.R. (2010). An Excel™ spreadsheet program for reconstructing the surface profile of former mountain glaciers and ice caps. *Computers & Geosciences*, *36*(5), 605-610 (doi: 10.1016/j.cageo.2009.09.016).

Benn, D.I., Hulton, N.R.J. & Mottram, R.H. (2007a). 'Calving laws','sliding laws' and the stability of tidewater glaciers. *Annals of Glaciology*, 46, 123–130 (doi: 10.3189/172756407782871161)

Benn, D.I., Warren, C.R., & Mottram, R.H. (2007b). Calving processes and the dynamics of calving glaciers. *Earth-Science Reviews*, *82*(3), 143-179 (doi: 10.1016/j.earscirev.2007.02.002).

Bevan, S.L., Luckman, A.J., & Murray, T. (2012). Glacier dynamics over the last quarter of a century at Helheim, Kangerdlugssuaq and 14 other major Greenland outlet glaciers. *Cryosphere,* 6, 923-937 (doi:10.5194/tc-6-923-2012)

Bindschadler, R. (1983). The importance of pressurized subglacial water in separation and sliding at the glacier bed. *Journal of Glaciology*, *29*(101), 3-19.

Bindschadler, R.A., King, M.A., Alley, R.B., Anandakrishnan, S., & Padman, L. (2003). Tidally controlled stick-slip discharge of a West Antarctic ice. *Science*, *301*(5636), 1087-1089 (doi: 10.1126/science.1087231)

Bjørk, A.A., Kjær, K.H., Korsgaard, N.J., Khan, S.A., Kjeldsen, K.K., Andresen, C.S. Box, J.E., Larsen, N.K., & Funder, S. (2012). An aerial view of 80 years of climate related glacier fluctuations in southeast Greenland. *Nature Geoscience,* 5 (6), 427–432 (doi: 10.1038/ngeo1481).

Borstad, C.P., Khazendar, A., Larour, E., Morlighem, M., Rignot, E., Schodlok, M.P. & Seroussi H. (2012). A damage mechanics assessment of the Larsen B ice shelf prior to collapse: Toward a physically-based calving law, *Geophysical Research Letters*, 39, L18502, (doi:10.1029/2012GL053317).

Box, J.E. & Decker, D.T. (2011). Greenland marine-terminating glacier area changes: 2000–2010. *Annals of Glaciology*, 52 (59), 91–98 (doi: 10.3189/172756411799096312).

Box, J.E., Yang, L., Bromwich, D.H., & Bai, L.S. (2009). Greenland Ice Sheet Surface Air Temperature Variability: 1840–2007. *Journal of Climate*,22, 4029–4049.(doi: 10.1175/2009JCLI2816.1).

Box, J.E., Cressie, N., Bromwich, D.H., Jung, J.H., Van Den Broeke, M., Van Angelen, J.H., Forster, R.R., Miège, C., Mosley-Thompson, E., Vinther, B., & McConnell, J.R. (2013). Greenland Ice Sheet Mass Balance Reconstruction. Part I: Net Snow Accumulation (1600-2009). *Journal of Climate*, *26*(11). (doi:JCLI-D-12-00373.1).

Braithwaite, R.J., & Olesen, O.B. (1993). Seasonal variation of ice ablation at the margin of the Greenland ice sheet and its sensitivity to climate change, Qamanarssup Sermia, West Greenland. *Journal of Glaciology*, *39*, 267-274.

Brede, N., (1866). *Skizze Kaart over Vestkysten af Grönland fra Arsuk til Holsteensborg.* (KBK Netpublikation DK003200), Copenhagen.

Briner, J.P., Stewart, H.A.M., Young, N.E., Philipps, W. & Losee, S. (2010). Using proglacial-threshold lakes to constrain fluctuations of the Jakobshavn Isbræ ice margin, western Greenland, during the Holocene. *Quaternary Science Reviews*, 29 (27–28), 3861–3874 (doi: 10.1016/j.quascirev.2010.09.005).

Bruun, D. (1917). Oversigt over Norburuiner i Godthåb og Frederikshaab Distrikter. *Meddelelser om Grønland.* 56 (3), 55-147.

Buch, E., & Hansen, H.H. (1988). Climate and cod fishery at West Greenland.*Longterm changes in marine fish populations. Vigo, Spain: Instituto Investigaciones Marinas*, 345-364.

Cappelen, J. (2012). Greenland-DMI Historical Climate Data Collection 1873-2011*Technical Report 12-04.* Copenhagen ISSN: 1399-1388.

Carr, J.R., Vieli, A., & Stokes, C. (2013a). Influence of sea ice decline, atmospheric warming, and glacier width on marine-terminating outlet glacier behavior in northwest

Greenland at seasonal to interannual timescales. *Journal of Geophysical Research: Earth Surface*, *118*(3), 1210-1226 (doi:10.1002/jgrf.20088).

Carr, J.R., Stokes, C.R., & Vieli, A. (2013b). Recent progress in understanding marine-terminating Arctic outlet glacier response to climatic and oceanic forcing: Twenty years of rapid change. *Progress in Physical Geography*, *37*(4), 436-467 (doi: 10.1177/0309133313483163).

Chauché, N., Hubbard, A., Gascard, J.-C., Box, J.E., Bates, R., Koppes, M., Sole, A., & Patton, H. (2013). Ocean properties, ice–ocean interactions, and calving front morphology at two major west Greenland glaciers, *Cryosphere Discussions*, 7, 5579-5611, (doi:10.5194/tcd-7-5579-2013).

Chandler, D.M., Wadham, J.L., Lis, G.P., Cowton, T., Sole, A., Bartholomew, I., Telling, J., Nienow, P., Bagshaw, E., Mair, D., Vinen, S. & Hubbard, A. (2013). Evolution of the subglacial drainage system beneath the Greenland Ice Sheet revealed by tracers. *Nature Geoscience*, *6*(3), 195-198 (doi:10.1038/ngeo1737).

Christoffersen, P., Mugford, R.I., Heywood, K.J., Joughin, I., Dowdeswell, J.A., Syvitski, J.P.M., Luckman, A., & Benham, T.J. (2011). Warming of waters in an East Greenland fjord prior to glacier retreat: mechanisms and connection to large-scale atmospheric conditions. *Cryosphere*, *5*(3), 701-714 (doi:10.5194/tc-5-701-2011).

Church, J.A., Clark, P.U., Cazenave, A., Gregory, J.M., Jevrejeva, S., Levermann, A., & Unnikrishnan, A.S. (2013). Sea-Level Rise by 2100.*Science*, *342*(6165), 1445.

Colgan, W., Pfeffer, W.T., Rajaram, H., & Abdalati, W. (2012). Monte Carlo ice flow modeling projects a new stable configuration for Columbia Glacier, Alaska, by c.2020. *Cryosphere*, *6* (2), 893-930 (doi: 10.5194/tcd-6-893-2012).

Cook, S., Zwinger, T., Rutt, I.C., O'Neel, S., & Murray, T. (2012). Testing the effect of water in crevasses on a physically based calving model. *Annals of Glaciology*, *53* (60), 90-96 (doi: 10.3189/2012AoG60A107).

Cook, S., Rutt, I.C., Murray, T., Luckman, A., Selmes, N., Goldsack, A., & Zwinger, T. (2013). Modelling environmental influences on calving at Helheim Glacier, East Greenland. *Cryosphere Discussions*, *7* (5) (doi: 10.5194/tcd-7-4407-2013).

Cowton, T., Nienow, P., Sole, A., Wadham, J., Lis, G., Bartholomew, I., Mair, D. & Chandler, D. (2013). Evolution of drainage system morphology at a land-terminating Greenlandic outlet glacier. *Journal of Geophysical Research: Earth Surface*, *118*(1), 29-41 (doi:10.1029/2012JF002540).

Crantz D. (1820). *The history of Greenland including an account of the mission carried on by the united brethren in that country: from the German of David Crantz*, 2 vols. Longman, Hurst, Rees, Orme and Brown, London.

Csatho, B., Schenk, T., Van der Veen, C.J., & Krabill, W.B. (2008). Intermittent thinning of Jakobshavn Isbræ, West Greenland, since the Little Ice Age. *Journal of Glaciology*, *54* (184), 131-144 (doi: 10.3189/002214308784409035).

Cuffey, K.M. & Paterson, W.S.B. (2010). *The physics of glaciers*, 4th edn., Butterworth-Heinemann, Oxford.

D'Andrea, W.J., Huang, Y., Fritz, S.C. & Anderson, N.J. (2011). Abrupt Holocene climate change as an important factor for human migration in West Greenland. *Proceedings of the National Acadamy of Science (PNAS)*, 108 (24), 9765–9769 (doi: 10.1073/pnas.1101708108).

Das, S.B., Joughin, I., Behn, M.D., Howat, I.M., King, M.A., Lizarralde, D., & Bhatia, M.P. (2008). Fracture propagation to the base of the Greenland Ice Sheet during supraglacial lake drainage. *Science*, *320*(5877), 778-781 (doi:10.1126/science.1153360).

Dietrich, R., Maas, H.G., Baessler, M., Rülke, A., Richter, A., Schwalbe, E., & Westfeld, P. (2007). Jakobshavn Isbræ, West Greenland: Flow velocities and tidal interaction of the front area from 2004 field observations. *Journal of Geophysical Research: Earth Surface*, *112*(F3), F03S21, (doi:10.1029/2006JF000601).

Dugmore, A.J., McGovern, T.H., Vésteinsson, O., Arneborg, J., Streeter, R., & Keller, C. (2012). Cultural adaptation, compounding vulnerabilities and conjunctures in Norse Greenland. *Proceedings of the National Academy of Sciences*, *109*(10), 3658-3663, (doi: 10.1073/pnas.1115292109)

Egede, H. (1741). *Det gamle Grönlands nye Perlustration, eller Naturel-historie, og Beskrivelse over det gamle Grönlands, Temperament og Beskaffenhed*, Copenhagen.

Enderlin, E.M. & Howat, I.M. (2013). Submarine melt rate estimates for floating termini of Greenland outlet glaciers (2000–2010) *Journal of Glaciology,* 59 (213), 67–75 (doi: 10.3189/2013JoG12J049).

Enderlin, E.M., Howat, I.M. & Vieli, A. (2013). The sensitivity of flowline models of tidewater glaciers to parameter uncertainty. *Cryosphere*, 7 (5), 1579–1590 (doi: 10.5194/tc-7-1579-2013).

Enderlin, E.M., Howat, I.M., Jeong, S., Noh, M.J., Angelen, J.H., & Broeke, M.R. (2014). An Improved Mass Budget for the Greenland Ice Sheet.*Geophysical Research Letters*, 41, 866–872, (doi:10.1002/2013GL059010).

Ettema, J., van den Broeke, M.R., van Meijgaard, E., van de Berg, W.J, Bamber, J.L., Box, J.E. and Bales, R.C. (2009). Higher surface mass balance of the Greenland ice sheet revealed by high-resolution climate modeling, *Geophysical Research Letters*, 36, L12501, (doi:10.1029/2009GL038110).

Favier, L., Durand, G., Cornford, S.L., Gudmundsson, G.H., Gagliardini, O., Gillet-Chaulet, F., Zwinger, T., Payne, A.J., & Le Brocq, A.M.. (2014). Retreat of Pine Island Glacier controlled by marine ice-sheet instability. *Nature Climate Change*. (doi:10.1038/nclimate2094).

Fettweis, X., Tedesco, M., van den Broeke, M., & Ettema, J. (2011). Melting trends over the Greenland ice sheet (1958–2009) from spaceborne microwave data and regional climate models *Cryosphere*, *5* (2), 359-375 (doi: 10.5194/tc-5-359-2011).

Fowler, A.C. (2010). Weertman, Lliboutry and the development of sliding theory *Journal of Glaciology*, 56 (200), 965–972 (doi: 10.3189/002214311796406112).

Fujisada, H., Urai, M., & Iwasaki, A. (2012). Technical methodology for ASTER Global DEM. *Geoscience and Remote Sensing, IEEE Transactions on*, *50*(10), 3725-3736.

Giesecke, K.L. (1910). Mineralogisches Reisejournal uber Grønland 1806–13 *Meddelelser om. Grønland*, 35.

Gladstone, R.M., Lee, V., Rougier, J., Payne, A.J., Hellmer, H., Le Brocq, A., Shepherd, A., Edwards, T.L., Gregory, J., & Cornford, S. L. (2012). Calibrated prediction of Pine Island Glacier retreat during the 21st and 22nd centuries with a coupled flowline model. *Earth and Planetary Science Letters*, *333*, 191-199 (doi: 10.1126/science.1153360).

Glen, J. W. (1955). The creep of polycrystalline ice. *Proceedings of the Royal Society of London. Series A. Mathematical and Physical Sciences*, *228*(1175), 519-538.

Gogineni, S., Tammana, D., Braaten, D., Leuschen, C., Akins, T., Legarsky, J., Kanagaratnam, P., Stiles, J, Allen, C., & Jezek, K. (2001). Coherent radar ice thickness measurements over the Greenland ice sheet. *Journal of Geophysical Research: Atmospheres*, *106* (D24), 33761-33772 (doi: 10.1029/2001JD900183).

Gudmundsson, G.H. (2003). Transmission of basal variability to a glacier surface. *Journal of Geophysical Research: Solid Earth*, *108*(B5), 2253, (doi:10.1029/2002JB002107).

Gudmundsson, G.H. (2006). Fortnightly variations in the flow velocity of Rutford Ice Stream, West Antarctica. *Nature*, *444*(7122), 1063-1064 (doi:10.1038/nature05430).

Gudmundsson, G.H., Krug, J., Durand, G., Favier, L., & Gagliardini, O. (2012). The stability of grounding lines on retrograde slopes. *Cryosphere Discussions*, *6*(4), 2597-2619.

Hanna, E., & Cappelen, J. (2003). Recent cooling in coastal southern Greenland and relation with the North Atlantic Oscillation, *Geophysical Research Letters*, 30, 1132, (doi:10.1029/2002GL015797, 3).

Hanna, E., Huybrechts, P., Steffen, K., Cappelen, J., Huff, R., Shuman, C., Irvine-Flynn, T., Wise S., & Griffiths, M. (2008). Increased Runoff from Melt from the Greenland Ice Sheet: A Response to Global Warming. *Journal of Climate, 21*(2), 331-341 (doi: 10.1175/2007JCLI1964.1).

Hanna, E., Cappelen, J., Fettweis, X., Huybrechts, P., Luckman, A., Ribergaard, M.H. (2009). Hydrologic response of the Greenland ice sheet: the role of oceanographic warming. *Hydrological Processes, 23* (1), 7-30 (doi: 10.1002/hyp.7090).

Hoffman, M.J., Catania, G.A., Neumann, T.A., Andrews, L.C. & Rumrill, J.A. (2011). Links between acceleration, melting, and supraglacial lake drainage of the western Greenland Ice Sheet, *Journal of Geophysical Research, 116*, F04035, (doi:10.1029/2010JF001934).

Holland, D.M., Thomas, R.H., De Young, B., Ribergaard, M.H. & Lyberth, B. (2008). Acceleration of Jakobshavn Isbræ triggered by warm subsurface ocean waters. *Nature Geoscience,* 1 (10), 659–664 (doi: 10.1038/ngeo316).

Howat, I.M., & Eddy, A. (2011). Multi-decadal retreat of Greenland's marine-terminating glaciers. *Journal of Glaciology, 57* (203), 389-396 (doi: 10.3189/002214311796905631).

Howat, I.M., Box, J.E., Ahn, Y., Herrington, A., & McFadden, E.M. (2010). Seasonal variability in the dynamics of marine-terminating outlet glaciers in Greenland. *Journal of Glaciology, 56*(198), 601-613 (doi: 10.3189/002214310793146232)

Hvidegaard, S.M., Sorensen, L.S., & Forsberg, R. (2012). ASTER GDEM validation using LiDAR data over coastal regions of Greenland. *Remote Sensing Letters*, 3(1), 85–91, 2012. (doi: 10.1080/01431161.2010.527389).

Iken, A., & Bindschadler, R. A. (1986). Combined measurements of subglacial water pressure and surface velocity of Findelengletscher, Switzerland: conclusions about drainage system and sliding mechanism. *Journal of Glaciology, 32*(110), 101-119.

Iverson, N. R., Baker, R. W., Le B Hooke, R., Hanson, B., & Jansson, P. (1999). Coupling between a glacier and a soft bed: I. A relation between effective pressure and local shear stress determined from till elasticity. *Journal of Glaciology*, *45*(149), 31-40.

Jamieson, S.S.R., Vieli, A., Livingstone, S.J., Cofaigh, C.Ó., Stokes, C., Hillenbrand, C.D., & Dowdeswell, J.A. (2012). Ice-stream stability on a reverse bed slope. *Nature Geoscience, 5* (11), 799-802 (doi: 10.1038/ngeo1600).

Jamieson, S.S.R., Vieli, A., Ó'Cofaigh, C., Stokes, C.R., Livingstone, S.J., & Hillenbrand, C.-D. (2014). Understanding controls on rapid ice-stream retreat during the last deglaciation of Marguerite Bay, Antarctica, using a numerical model, *Journal of Geophysical Research: Earth Surface*, 119, 247–263, (doi:10.1002/2013JF002934).

Jenkins, A. (2011). Convection-Driven Melting near the Grounding Lines of Ice Shelves and Tidewater Glaciers. *Journal of Physical Oceanography*, *41* (12) (doi: 10.1175/JPO-D-11-03.1).

Jensen, J.A.D. (1885). *Vestkysten af Grönland fra Arsuk til Holstensborg 61° til 67° N* KBK Netpublikation, DK003198. Copenhagen.

Johannessen, O.M., Babiker, M., & Miles, M.W. (2011). Petermann Glacier, North Greenland: massive calving in 2010 and the past half century. *Cryosphere Discussions*, *5*(1), 169-181 (doi:10.5194/tcd-5-169-2011).

Joughin, I., Howat, I.M., Fahnestock, M., Smith, B., Krabill, W., Alley, R.B., & Truffer, M. (2008a). Continued evolution of Jakobshavn Isbrae following its rapid speedup. *Journal of Geophysical Research: Earth Surface*, *113*(F4), F01004, (doi:10.1029/2007JF000837).

Joughin, I., Howat, I., Alley, R. B., Ekstrom, G., Fahnestock, M., Moon, T., & Tsai, V. C. (2008b). Ice-front variation and tidewater behavior on Helheim and Kangerdlugssuaq Glaciers, Greenland. *Journal of Geophysical Research: Earth Surface*, *113*(F1), F01004, (doi:10.1029/2007JF000837).

Joughin, I., Smith, B.E., Howat, I.M., Scambos, T., & Moon, T. (2010a). Greenland flow variability from ice-sheet-wide velocity mapping. *Journal of Glaciology*, *56* (197), 415-430 (doi: 10.3189/002214310792447734).

Joughin, I., Smith, B.E. & Holland, D.M. (2010b). Sensitivity of 21st century sea level to ocean-induced thinning of Pine Island Glacier, Antarctica. *Geophysical Research Letters*, 37 (20), L20502 (doi: 10.1029/2010GL044819).

Joughin, I., Alley, R.B., & Holland, D.M. (2012). Ice-sheet response to oceanic forcing. *Science*, *338*(6111), 1172-1176 (doi: 10.1126/science.1226481).

Kamenos, N.A., Hoey, T.B., Nienow, P., Fallick, A.E. & Claverie, T. (2012). Reconstructing Greenland ice sheet runoff using coralline algae. *Geology*, 40 (12), 1095–10098 (doi: 10.1130/G33405.1).

Kelley, S. E., Briner, J.P., & Young, N.E. (2013). Rapid ice retreat in Disko Bugt supported by ^{10}Be dating of the last recession of the western Greenland Ice Sheet. *Quaternary Science Reviews*, *82*, 13-22, (doi: 10.1016/j.quascirev.2013.09.018).

Kleinschmidt, S. (1859). *Godthåbs distrikt (hertil en Navneliste).* (Map No. KBK Netpublikation RI000074). Copenhagen.

Kobashi, T., Severinghaus, J.P., Barnola, J.M., Kawamura, K., Carter, T., & Nakaegawa, T. (2010). Persistent multi-decadal Greenland temperature fluctuation through the last millennium. *Climatic Change*, *100*(3-4), 733-756, (doi: 10.1007/s10584-009-9689-9).

Krug, J., Weiss, J., Gagliardini, O., & Durand, G. (2014). Combining damage and fracture mechanics to model calving. *Cryosphere Discussions*, *8*(1), 1111-1150 (doi:10.5194/tcd-8-1631-2014).

Lane, T.P., Roberts, D.H., Rea, B.R., Ó Cofaigh, C., Vieli, A., & Rodés, A. (2013). Controls upon the Last Glacial Maximum deglaciation of the northern Uummannaq Ice Stream System, West Greenland. *Quaternary Science Reviews*. (doi: 10.1016/j.quascirev.2013.09.013).

Larsen, N.K., Funder, S., Kjær, K.H., Kjeldsen, K.K., Knudsen, M.F., & Linge, H. (2013). Rapid early Holocene ice retreat in West Greenland. *Quaternary Science Reviews*. (doi: 10.1016/j.quascirev.2013.05.027).

Le Brocq, A.M., Ross, N., Griggs, J.A., Bingham, R.G., Corr, H.F., Ferraccioli, F., Jenkins, A., Jordan, T.A., Payne, A.J., Rippin, D., & Siegert, M. J. (2013). Evidence from ice shelves for channelized meltwater flow beneath the Antarctic Ice Sheet. *Nature Geoscience*, *6*(11), 945-948 (doi:10.1038/ngeo1977).

Lloyd, J., Moros, M., Perner, K., Telford, R.J., Kuijpers, A., Jansen, E., & McCarthy, D. (2011). A 100 yr record of ocean temperature control on the stability of Jakobshavn Isbrae, West Greenland. *Geology*, *39*(9), 867-870 (doi: 10.1130/G32076.1).

MacAyeal, D.R. (1989). Large-scale ice flow over a viscous basal sediment: Theory and application to ice stream B, Antarctica, *Journal of Geophysical Research*, 94, 4071–4088 (doi:10.1029/91JB02454).

McFadden, E.M., Howat, I.M., Joughin, I., Smith, B.E., & Ahn, Y. (2011). Changes in the dynamics of marine terminating outlet glaciers in west Greenland (2000–2009) *Journal of Geophysical Research: Earth Surface (2003–2012), 116* (F2) (doi: 10.1029/2010JF001757).

Meier, M.F., & Post, A. (1987). Fast tidewater glaciers. *Journal of Geophysical Research: Solid Earth (1978–2012)*, *92*(B9), 9051-9058 (doi: 10.1126/science.1143906).

Meier, M.F., Dyurgerov, M.B., Rick, U.K., O'Neel, S., Pfeffer, W.T., Anderson, R.S., & Glazovsky, A. F. (2007). Glaciers dominate eustatic sea-level rise in the 21st century. *Science*, *317*(5841), 1064-1067.

Mercer, J.H. (1961). The estimation of the regimen and former firn limit of a glacier *Journal of Glaciology*, 3 (30), 1053–1062.

Møller, H.P.C. (1840) *Kort over den Deel af Godthaabs District, som antages fornemmelig at have udgjort De Gamles Vesterbygd*, (KBK Netpublikation, DK003820), Copenhagen

Moon T., & Joughin I. (2008). Changes in ice front position on Greenland's outlet glaciers from 1992 to 2007. *Journal of Geophysical Research: Earth Surface, 113* (F2) (doi: 10.1029/2007JF000927).

Moon, T., Joughin, I., Smith, B. & Howat, I. (2012). 21st-century evolution of Greenland outlet glacier velocities. *Science*, 336 (6081), 576–578 (doi: 10.1126/science.1219985).

Morlighem, M., Rignot, E., Seroussi, H., Larour, E., Ben Dhia, H., & Aubry, D. (2011). A mass conservation approach for mapping glacier ice thickness. *Geophysical Research Letters*, *38* (19) (doi: 10.1029/2011GL048659).

Mortensen, J., Lennert, K., Bendtsen, J., & Rysgaard, S. (2011). Heat sources for glacial melt in a sub-Arctic fjord (Godthåbsfjord) in contact with the Greenland Ice Sheet. *Journal of Geophysical Research: Oceans, 116* (C1) (doi: 10.1029/2010JC006528).

Mortensen, J., Bendtsen, J., Motyka, R.J., Lennert, K., Truffer, M., Fahnestock, M., & Rysgaard, S. (2013). On the seasonal freshwater stratification in the proximity of fast-flowing tidewater outlet glaciers in a sub-Arctic sill fjord. *Journal of Geophysical Research: Oceans*, *118* (3), 1382-1395 (doi: 10.1002/jgrc.20134).

Mottram, R. H., & Benn, D. I. (2009). Testing crevasse-depth models: a field study at Breiðamerkurjökull, Iceland. *Journal of Glaciology*, *55*(192), 746-752 (doi: 10.3189/002214309789470905).

Motyka, R.J., Hunter, L., Echelmeyer, K. A., & Connor, C. (2003). Submarine melting at the terminus of a temperate tidewater glacier, LeConte Glacier, Alaska, USA. *Annals of Glaciology*, *36*(1), 57-65 (doi: 10.3189/172756403781816374).

Murray, T., Scharrer, K., James, T.D., Dye, S.R., Hanna, E., Booth, A.D., Selmes, N., Luckman, A., Hughes, A.L.C., Cook, S., & Huybrechts, P. (2010). Ocean regulation hypothesis for glacier dynamics in southeast Greenland and implications for ice sheet mass

changes. *Journal of Geophysical Research: Earth Surface, 115* (F3) (doi: 10.1029/2009JF001522).

Nansen F (1890). *The first crossing of Greenland* Longmans, London.

Nick, F.M., Vieli, A., Howat, I.M. & Joughin, I. (2009). Large-scale changes in Greenland outlet glacier dynamics triggered at the terminus. *Nature Geoscience,* 2 (2), 110–114 (doi: 10.1038/ngeo394).

Nick, F.M., Van der Veen, C.J., Vieli, A., & Benn, D.I. (2010). A physically based calving model applied to marine outlet glaciers and implications for the glacier dynamics. *Journal of Glaciology, 56* (199), 781-794 (doi: 10.3189/002214310794457344).

Nick, F.M., Luckman, A., Vieli, A., Van der Veen, C.J., Van As, D., Van de Wal, R.S.W., Pattyn, F., Hubbard, A.L., & Floricioiu, D. (2012). The response of Petermann Glacier, Greenland, to large calving events, and its future stability in the context of atmospheric and oceanic warming. *Journal of Glaciology, 58* (208), 229-239 (doi: 10.3189/2012JoG11J242).

Nick, F.M., Vieli, A., Andersen, M.L., Joughin, I., Payne, A., Edwards, T.L., Pattyn, F. & van de Wal, R.S. (2013). Future sea-level rise from Greenland's main outlet glaciers in a warming climate. *Nature*, *497*(7448), 235-238. (doi: 10.1038/nature12068).

Nienow, P., Sharp, M., & Willis, I. (1998). Seasonal changes in the morphology of the subglacial drainage system, Haut Glacier d'Arolla, Switzerland. *Earth Surface Processes and Landforms*, *23*(9), 825-843.

Nye, J.F. (1957). The distribution of stress and velocity in glaciers and ice-sheets. *Proceedings of the Royal Society London, Series A,* 239 (1216), 113–133 (doi: 10.1098/rspa.1957.0026).

Nye, J.F. (1965). The flow of a glacier in a channel of rectangular, elliptic or parabolic cross-section. *Journal of Glaciology*, *5*, 661-690.

O'Leary, M. & Christoffersen, P. (2013). Calving on tidewater glaciers amplified by submarine frontal melting, *Cryosphere*, 7, 119-128, (doi:10.5194/tc-7-119-2013, 2013).

O'Neel, S., Echelmeyer, K.A., & Motyka, R.J. (2003). Short-term variations in calving of a tidewater glacier: LeConte Glacier, Alaska, USA. *Journal of Glaciology*, *49*(167), 587-598 (doi: 10.3189/172756503781830430).

Oerlemans, J., Jania, J., & Kolondra, L. (2011). Application of a minimal glacier model to Hansbreen, Svalbard. *The Cryosphere*, *5*(1), 1-11 (doi: 10.5194/tc-5-1-2011).

Otero, J., Navarro, F.J., Martin, C., Cuadrado, M.L., & Corcuera, M.I. (2010). A three-dimensional calving model: numerical experiments on Johnsons Glacier, Livingston Island, Antarctica. *Journal of Glaciology*, *56*(196), 200-214 (doi: 10.3189/002214310791968539).

Pattyn, F., Schoof, C., Perichon, L., Hindmarsh, R.C.A., Bueler, E., de Fleurian, B., Durand, G., Gagliardini, O., Gladstone, R., Goldberg, D., Gudmundsson, G.H., Lee, V., Nick, F.M., Payne, A.J., Pollard, D., Rybak, O., Saito, F., & Vieli, A. (2012). Results of the Marine Ice Sheet Model Intercomparison Project, MISMIP, *Cryosphere Discussions*, 6, 267-308, (doi:10.5194/tcd-6-267-2012, 2012).

Phillips, T., Rajaram, H., & Steffen, K. (2010). Cryo-hydrologic warming: A potential mechanism for rapid thermal response of ice sheets. *Geophysical Research Letters*, *37*(20), L20503, (doi:10.1029/2010GL044397).

Pfeffer, W.T. (2007). A simple mechanism for irreversible tidewater glacier retreat. *Journal of Geophysical Research: Earth Surface*, 112, F03S25, (doi:10.1029/2006JF000590).

Podrasky, D., Truffer, M., Fahnestock, M., Amundson, J.M., Cassotto, R., & Joughin, I. (2012). Outlet glacier response to forcing over hourly to interannual timescales, Jakobshavn Isbræ, Greenland. *Journal of Glaciology*, *58*(212), 1212 (doi: 10.3189/2012JoG12J065).

Poulsen, J. (1860). *Godthåb commune* (KBK Netpublikation RI000059), Copenhagen.

Pralong, A., & Funk, M. (2005). Dynamic damage model of crevasse opening and application to glacier calving. *Journal of Geophysical Research: Solid Earth*, *110*, B01309, (doi:10.1029/2004JB003104).

Rahmstorf, S. (1995). Bifurcations of the Atlantic thermohaline circulation in response to changes in the hydrological cycle. *Nature*, *378*(6553), 145-149.

Rayner, N.A., Parker, D.E., Horton, E.B., Folland, C.K., Alexander, L.V., Rowell, D.P., Kent, E.C., & Kaplan, A. (2003). Global analyses of sea surface temperature, sea ice, and night marine air temperature since the late nineteenth century. *Journal of Geophysical Research: Atmospheres, 108* (D14) (doi: 10.1029/2002JD002670).

Rea, B.R., & Evans, D.J. (2007). Quantifying climate and glacier mass balance in north Norway during the Younger Dryas. *Palaeogeography, Palaeoclimatology, Palaeoecology*, *246*(2), 307-330 (doi: 10.1016/j.palaeo.2006.10.010).

Rea, B.R., & Evans, D.J. (2011). An assessment of surge-induced crevassing and the formation of crevasse squeeze ridges. *Journal of Geophysical Research: Earth Surface*, *116*, F04005, (doi:10.1029/2011JF001970).

Rignot, E., & Kanagaratnam, P. (2006). Changes in the velocity structure of the Greenland Ice Sheet. *Science, 311*(5763), 986-990 (doi: 10.1126/science.1121381).

Rignot, E., & Steffen, K. (2008). Channelized bottom melting and stability of floating ice shelves. *Geophysical Research Letters*, *35*, L02503, (doi:10.1029/2007GL031765).

Rignot, E., Koppes, M. & Velicogna, I. (2010). Rapid submarine melting of the calving faces of West Greenland glaciers. *Nature Geoscience*, 3 (3), 141–218 (doi: 10.1038/ngeo765).

Rignot, E., Fenty, I., Menemenlis, D., & Xu, Y. (2012). Spreading of warm ocean waters around Greenland as a possible cause for glacier acceleration. *Annals of Glaciology*, *53* (60), 257-266 (doi: 10.3189/2012AoG60A136).

Rink, H. (1856). *Sydgrønlands nordlige distrikter* (KBK Netpublikation RI000095), Copenhagen.

Rink, H. (1866). *Kyststrækning fra Frederikshåb i syd til Napasaq i nord.* (KBK Netpublikation RI000029), Copenhagen.

Roberts, D.H., Rea, B.R., Lane, T.P., Schnabel, C., & Rodés, A. (2013). New constraints on Greenland ice sheet dynamics during the last glacial cycle: evidence from the Uummannaq ice stream system. *Journal of Geophysical Research: Earth Surface*, *118*(2), 519-541 (doi: 10.1002/jgrf.20032).

Roussell, A. (1941). Farms and Churches of the Medieval Norse Settlement in Greenland. *Meddelelser om Grønland*, 89 (1).

Schild, K.M., & Hamilton, G.S. (2013). Seasonal variations of outlet glacier terminus position in Greenland. *Journal of Glaciology*, *59*(216), 759-770 (doi: 10.3189/2013JoG12J238).

Schoof, C. (2005). The effect of cavitation on glacier sliding. *Proceedings of the Royal Society A: Mathematical, Physical and Engineering Science,461*(2055), 609-627 (doi: 10.1098/rspa.2004.1350).

Schoof, C. (2007). Marine ice-sheet dynamics. Part 1. The case of rapid sliding. *Journal of Fluid Mechanics*, *573*, 27-55 (doi: 10.1017/S0022112006003570).

Sciascia, R., Straneo, F., Cenedese, C., & Heimbach, P. (2013). Seasonal variability of submarine melt rate and circulation in an East Greenland fjord. *Journal of Geophysical Research: Oceans*, *118* (5), 2492-2506 (doi: 10.1002/jgrc.20142).

Shepherd, A., Hubbard, A., Nienow, P., King, M., McMillan, M., & Joughin, I. (2009). Greenland ice sheet motion coupled with daily melting in late summer.*Geophysical Research Letters, 36*, L01501, (doi:10.1029/2008GL035758).

Smed, J. (1978). Fluctuations in the temperature of the surface water in areas of the northern North Atlantic, 1876 to 1975. *On Climate Changes and Related Problems. p 205-210(SEE N 80-27009 17-47).*

Sole, A.J., Mair, D.W.F., Nienow, P.W., Bartholomew, I.D., King, M.A., Burke, M.J., & Joughin, I. (2011). Seasonal speedup of a Greenland marine-terminating outlet glacier forced by surface melt–induced changes in subglacial hydrology. *Journal of Geophysical Research: Earth Surface, 116* (F3) (doi: 10.1029/2010JF001948).

Sole, A.J., Payne, A.J., Nienow, P.W., Christoffersen,P., Cottier, F.R., & Inall, M.E. (2012). Increased glacier runoff enhances the penetration of warm Atlantic water into a large Greenland fjord. *Cryosphere Discussions, 6,* 4861-4896 (doi:10.5194/tcd-6-4861-2012).

Sole, A., Nienow, P., Bartholomew, I., Mair, D., Cowton, T., Tedstone, A., & King, M. A. (2013). Winter motion mediates dynamic response of the Greenland Ice Sheet to warmer summers. *Geophysical Research Letters*, *40*(15), 3940-3944 (doi:10.1002/grl.50764).

Stocker, T.F., Dahe, Q., & Plattner, G.K. (2013). Climate Change 2013: The Physical Science Basis. *Working Group I Contribution to the Fifth Assessment Report of the Intergovernmental Panel on Climate Change. Summary for Policymakers (IPCC, 2013).*

Stommel, H. (1961). Thermohaline convection with two stable regimes of flow, *Tellus,* 2, 224–230.

Straneo, F., & Heimbach, P. (2013). North Atlantic warming and the retreat of Greenland's outlet glaciers. *Nature, 504* (7478), 36-43 (doi: 10.1038/nature12854).

Straneo, F., Hamilton, G.S., Sutherland, D.A., Stearns, L.A., Davidson, F., Hammill, M.O., Stenson, G.B. & Rosing-Asvid, A. (2010). Rapid circulation of warm subtropical waters in

a major glacial fjord in East Greenland. *Nature Geoscience, 3*(3), 182-186. (doi: 10.1038/ngeo764).

Straneo, F., Curry, R.G., Sutherland, D.A., Hamilton, G.S., Cenedese, C., Våge, K., & Stearns, L.A. (2011). Impact of fjord dynamics and glacial runoff on the circulation near Helheim Glacier. *Nature Geoscience*, *4*(5), 322-327 (doi: doi:10.1038/ngeo1109).

Straneo, F., Sutherland, D.A., Holland, D., Gladish, C., Hamilton, G.S., Johnson, H.L., Rignot, E. & Koppes, M. (2012). Characteristics of ocean waters reaching Greenland's glaciers. *Annals of Glaciology, 53*(60), 202-210. (doi: 10.3189/2012AoG60A059)

Straneo, F., Heimbach, P., Sergienko, O., Hamilton, G., Catania, G., Griffies, S., Hallberg, R., Jenkins, A., Joughin, I., Motyka, R., Pfeffer, T.W., Price, S.F., Rignot E., Scambos, T., Truffer, M., & Vieli, A. (2013). Challenges to understanding the dynamic response of Greenland's marine terminating glaciers to oceanic and atmospheric forcing. *Bulletin of the American Meteorological Society*, 94, 1131–1144 (doi:10.1175/BAMS-D-12-00100.1).

Sundal, A.V., Shepherd, A., Nienow, P., Hanna, E., Palmer, S., & Huybrechts, P. (2011). Melt-induced speed-up of Greenland ice sheet offset by efficient subglacial drainage. *Nature, 469*(7331), 521-524 (doi:10.1038/nature09740).

Tachikawa, T., Hato, M., Kaku, M., & Iwasaki, A. (2011). Characteristics of ASTER GDEM version 2. In *Geoscience and Remote Sensing Symposium (IGARSS), 2011 IEEE International* (pp. 3657-3660). IEEE.

Taurisano, A., Bøggild, C.E., & Karlsen, H.G. (2004). A century of climate variability and climate gradients from coast to ice sheet in West Greenland. *Geografiska Annaler: Series A, Physical Geography, 86* (2), 217-224 (doi: 10.1111/j.0435-3676.2004.00226.x).

Tedstone, A.J., & Arnold, N.S. (2012). Automated remote sensing of sediment plumes for identification of runoff from the Greenland ice sheet. *Journal of Glaciology*, *58*(210), 699-712 (doi: 10.3189/2012JoG11J204).

Tedstone, A.J., Nienow, P.W., Sole, A.J., Mair, D.W., Cowton, T.R., Bartholomew, I.D., & King, M.A. (2013). Greenland ice sheet motion insensitive to exceptional meltwater forcing. *Proceedings of the National Academy of Sciences, 110*(49), 19719-19724 (doi:10.1073/pnas.1315843110).

Thomas, R.H. (2004). Force-perturbation analysis of recent thinning and acceleration of Jakobshavn Isbræ, Greenland. *Journal of Glaciology*, 50 (168), 57–66 (doi: 10.3189/172756504781830321).

Thorhallesen, E. (1776). *Efterretning om rudera eller levninger af de gamle nordmoends og isloenderes bygninger paa Grønlands vester-side, tilligemed et anhang om deres undergang sammesteds*Trykt hos A.F. Stein, Copenhagen.

Van Angelen, J.H., van den Broeke, M.R., Wouters, B., & Lenaerts, J.T.M. (2013). Contemporary (1960–2012) evolution of the climate and surface mass balance of the Greenland ice sheet, *Surveys of Geophysics*. (doi: 10.1007/s10712-013-9261-z).

Van As, D., Hubbard, A.L., Hasholt, B., Mikkelsen, A.B., Van den Broeke, M.R. & Fausto, R.S. (2012). Large surface meltwater discharge from the Kangerlussuaq sector of the Greenland ice sheet during the record-warm year 2010 explained by detailed energy balance observations. *Cryosphere*, 6 (1), 199–209 (doi: 10.5194/tc-6-199-2012).

Van As, D., Andresen, M.L., Petersen, D., Fettweis, X., van Angelen, J.G., Lenearts, J.T.M., van den Broeke, M.R., Lea, J.M., Bayou, N., Bøggild, C.E., Ahlstrøm, A.P., & Steffen, K. (2014). Increasing meltwater discharge from the Nuuk region of the Greenland ice sheet and implications for mass balance (1960-2012) *Journal of Glaciology* 220 (60), 314-322 (doi: 10.3189/2014JoG13J065).

van den Broeke, M., Bamber, J., Ettema, J., Rignot, E., Schrama, E., van de Berg, W.J., van Meijgaard, E., Velicogna, I., & Wouters, B. (2009). Partitioning recent Greenland mass loss. *Science*, *326* (5955), 984-986 (doi: 10.1126/science.1178176).

Van der Veen, C.J. (2002). Calving glaciers. *Progress in Physical Geography*,*26*(1), 96-122 (doi: 10.1191/0309133302pp327ra).

Van der Veen CJ & Whillans IM (1996). Model experiments on the evolution and stability of ice streams. *Annals of Glaciology,* 23, 129–137.

Vaughan, D.G. (1995). Tidal flexure at ice shelf margins. *Journal of Geophysical Research: Solid Earth*, *100*(B4), 6213-6224 (doi:10.1029/94JB02467).

Vieli, A., & Nick, F.M. (2011). Understanding and modelling rapid dynamic changes of tidewater outlet glaciers: issues and implications. *Surveys in Geophysics, 32* (4-5), 437-458 (doi: 10.1007/s10712-011-9132-4).

Vieli, A., Jania, J., & Kolondra, L. (2002). The retreat of a tidewater glacier: observations and model calculations on Hansbreen, Spitsbergen. *Journal of Glaciology*, *48*(163), 592-600 (doi: 10.3189/172756502781831089).

Vinther, B.M., Andersen, K.K., Jones, P.D., Briffa, K.R., & Cappelen, J. (2006). Extending Greenland temperature records into the late eighteenth century. *Journal of Geophysical Research: Atmospheres, 111* (D11) (doi: 10.1029/2005JD006810).

Walter, J.I., Box, J.E., Tulaczyk, S., Brodsky, E.E., Howat, I.M., Ahn, Y., & Brown, A. (2012). Oceanic mechanical forcing of a marine-terminating Greenland glacier. *Annals of Glaciology*, *53*(60), 181-192 (doi: 10.3189/2012AoG60A083).

Warren, C.R. (1992). Iceberg calving and the glacioclimatic record. *Progress in Physical Geography*, *16*(3), 253-282 (doi: 10.3189/172756403781816446).

Warren, C., Benn, D., Winchester, V., & Harrison, S. (2001). Buoyancy-driven lacustrine calving, Glaciar Nef, Chilean Patagonia. *Journal of Glaciology*,*47*(156), 135-146 (doi: 10.3189/172756501781832403).

Weidick, A. (1959). Glacial variations in West Greenland in historical time Part I: South West Greenland. *Bulletin of the Greenland Geological Survey.* 18.

Weidick, A. (1968). Observations on some Holocene glacier fluctuations in West Greenland. *Meddelelser om Grønland* 165 (6).

Weidick A, & Citterio M (2011). The ice-dammed lake Isvand, West Greenland, has lost its water. *Journal of Glaciology*, *57* (201), 186-188 (doi: 10.3189/002214311795306600).

Weidick, A., Bennike, O., Citterio, M., & Nørgaard-Pedersen, N. (2012). .*Neoglacial and historical glacier changes around Kangersuneq fjord in southern West Greenland.* Geological Survey of Denmark and Greenland. Copenhagen (ISBN: 978-87-7871-347-6).

Weijer, W., Maltrud, M.E., Hecht, M.W., Dijkstra, H.A., & Kliphuis, M.A. (2012). Response of the Atlantic Ocean circulation to Greenland Ice Sheet melting in a strongly-eddying ocean model. *Geophysical Research Letters*, 39, L09606, (doi:10.1029/2012GL051611).

Woodruff, S.D., Slutz, R.J., Jenne, R.L., & Steurer, P.M. (1987). A comprehensive ocean-atmosphere data set. *Bulletin of the American Meteorological Society*, *68*(10), 1239-1250 (doi: 10.1175/1520-0477).

Xu, Y., Rignot, E., Menemenlis, D., & Koppes, M. (2012). Numerical experiments on subaqueous melting of Greenland tidewater glaciers in response to ocean warming and enhanced subglacial discharge. *Annals of Glaciology*, *53* (60), 229-234 (doi: 10.3189/2012AoG60A139).

Xu, Y., Rignot, E., Fenty, I., Menemenlis, D., & Mar Flexas, M. (2013). Subaqueous melting of Store Glacier, west Greenland from three-dimensional, high-resolution numerical modeling and ocean observations, *Geophysical Research Letters*, 40, 4648-4653 (doi:10.1002/grl.50825).

Appendix 1

Appendix 2